

Type of noise into ECG signal, described both from mathematical and theoretical pOV.

ResearchGate

Denoising using numerical filters and wavelets (just theory)

Expected shape of ECG spectrum and components

See discussions, stats, and author profiles for this publication at: <https://www.researchgate.net/publication/367162966>

# Denoising and Artifact Removal of the Electrocardiogram, Electrodermal Activity and Accelerometry for Continuous Ambulatory Monitoring of Epileptic Seizures with Wearable Devices

Technical Report · February 2022

DOI: 10.13140/RG.2.2.10053.12004

---

CITATIONS

0

3 authors:



João Saraiva

Instituto Superior Técnico

7 PUBLICATIONS 2 CITATIONS

[SEE PROFILE](#)

READS

604

281 PUBLICATIONS 3,059 CITATIONS

[SEE PROFILE](#)



Hugo Plácido da Silva

Institute of Telecommunications

University of Lisbon

346 PUBLICATIONS 6,666 CITATIONS

[SEE PROFILE](#)



Ana L. N. Fred

University of Lisbon

346 PUBLICATIONS 6,666 CITATIONS

[SEE PROFILE](#)

# Denoising and Artifact Removal of the Electrocardiogram, Electrodermal Activity and Accelerometry for Continuous Ambulatory Monitoring of Epileptic Seizures with Wearable Devices

João Miguel Areias Saraiva<sup>1,2</sup>  
joaomiguel.saraiva@tecnico.ulisboa.pt

Supervised by Ana Luís Nobre Fred<sup>1,3</sup> and Hugo Plácido da Silva<sup>1,3</sup>

<sup>1</sup> Department of Bioengineering, IST, Lisboa

<sup>2</sup> Department of Computer Science and Engineering, IST, Lisboa

<sup>3</sup> Instituto de Telecomunicações, Lisboa

**Abstract.** Around the world, about 50 million people suffer from epilepsy, a disease characterised by recurrent and unprovoked seizures of abrupt cerebral activity. Epileptic seizures require a thorough diagnosis and follow-up for long and frequent hospitalisations, which demand a heavy workload to the clinical teams. It has been suggested that these studies should be transferred to the ambulatory care, so the patient can be continuously monitored. In order to the patients keep their mobility, and so that seizures can be documented in residential and work environments, it has been suggested the use of discreet and comfortable wearable devices, to continuously acquire peripheral biosignals, such as the electrocardiography (ECG), the electrodermal activity (EDA), and the accelerometry (ACC). However, owing to their intrinsic design, and to the different types of noise and artifacts typical of ambulatory conditions, the biosignals acquired by them usually present poor quality. For that reason, methods for real-time denoising and artifact removal are required to process automatically and efficiently these biosignals. In this project, ECG, EDA, ACC, and the types of noises that can contaminate them are studied, as well as the signal processing techniques to improve their quality. Based on a state-of-the-art revision of biosignal processing, a real-time solution to denoise and remove artifacts is proposed. This solution is meant to be integrated in a wearable seizure monitoring system in the future.

**Keywords:** Biosignal Processing · Biosignal Denoising · Artifact Removal · Electrocardiogram (ECG) · Electrodermal Activity (EDA) · Accelerometry (ACC) · Wearables.

**Resumo.** Mundialmente, cerca de 50 milhões de pessoas sofrem de epilepsia, uma doença caracterizada por crises recorrentes e espontâneas de atividade cerebral abrupta. As crises epilépticas exigem um diagnóstico e acompanhamento minuciosos durante longos e frequentes interamentos hospitalares, que representam uma grande carga de trabalho para a equipa clínica do doente. Tem vindo a ser sugerido que se transfira estes estudos para os cuidados ambulatórios, onde o doente possa ser continuamente monitorizado. Para que o doente mantenha a mobilidade e para que se tire partido da documentação de crises que ocorram no seu ambiente residencial e de trabalho, tem vindo a ser sugerido o uso de *wearables* discretos e confortáveis que adquiriram continuamente biosinais periféricos, tais como a electrocardiografia (ECG), a atividade electrodérmica (EDA) e a acelerometria (ACC). Contudo, devido ao formato dos *wearables* e à inerente exposição a diferentes ruídos e artefactos em meio ambulatório, os biosinais por estes adquiridos apresentam, geralmente, uma baixa qualidade. Por essa razão, são necessários métodos de atenuação de ruído e de remoção de artefactos, que possam processar automaticamente e eficientemente estes biosinais em tempo real. Neste projeto, são estudados o ECG, o EDA e o ACC, os tipos de ruído que podem degradar a qualidade destes biosinais, bem como as técnicas de processamento de sinal para melhorar a qualidade dos mesmos. Com base numa revisão do estado da arte do processamento destes biosinais, é proposta uma solução para a atenuação de ruído e remoção de artefactos em tempo real. Esta solução tem como propósito ser, no futuro, integrada num sistema *wearable* de monitorização de crises epilépticas.

**Keywords:** Processamento de Biosinais · Remoção de Ruído · Remoção de Artefactos · Eletrocardiograma (ECG) · Atividade Eletrodérmica (EDA) · Acelerometria (ACC) · Wearables.

## Table of Contents

<b>Acronyms</b> .....	iii
<b>Symbols</b> .....	vi
1 Introduction .....	1
1.1 Motivation .....	1
1.2 Understanding Epileptic Seizures .....	2
1.3 The Problem .....	2
1.4 The Solution and Goals of this Work .....	3
1.5 Outline .....	3
2 Background .....	3
2.1 Electrodes for Electrophysiological Signal Acquisition .....	3
2.2 Electrocardiography (ECG) .....	5
2.3 Electrodermal Activity (EDA) .....	6
2.4 Accelerometry (ACC) .....	7
2.5 Biosignal Denoising and Artifact Removal .....	7
2.6 Digital Signal Processing (DSP) .....	11
3 Related Work .....	13
3.1 ECG Denoising and Artifact Removal .....	13
3.2 EDA Denoising and Artifact Removal .....	17
3.3 ACC Denoising .....	19
4 Solution Proposal .....	19
4.1 Top-level Architecture .....	20
4.2 Preliminary Results .....	21
5 Empirical Evaluation .....	22
5.1 Performance Metrics .....	22
5.2 Datasets for Evaluation .....	23
6 Work Calendarization .....	23
7 Conclusion .....	23
<b>References</b> .....	24
Annex 1 .....	36
Annex 2 .....	42

## Acronyms

- A-fib** atrial fibrillation. 13, 23, 37  
**AC** alternate current. 6, 10, 11  
**ACC** accelerometer. ii, 1–3, 7, 11, 16, 18–23, 39, 40  
**Acc** accuracy. 36–40  
**ADC** analog-digital converter. 20  
**ADTF** adaptive dual threshold filter. 14, 15  
**AE** autoencoder. 17, 19, 40  
**ANS** autonomic nervous system. 2, 6  
**APA** artifact power reduction. 17, 22  
**AR** autoregressive. 41  
**ASM** anti-seizure medication. 1  
**AUC** area under the curve. 18, 41
- BVP** blood volume pressure. 18  
**BW** baseline wander. 8, 9, 13–17, 21, 36–41
- C** clinical-grade. 1, 2, 36–40  
**CC** cross-correlation. 36–38  
**CMRR** common mode rejection ratio. 8  
**CNN** convolutional neural network. 16, 40  
**CNS** central nervous system. 1, 2  
**CWT** continuous wavelet transform. 13, 15
- DAE** denoising autoencoder. 12, 14, 16, 19–22  
**DC** direct current. 6, 9, 10  
**DCT** discrete cosine transformation. 15  
**DFT** discreet Fourier transform. 14, 15  
**DSP** digital signal processing. ii, 11, 12  
**DWT** discrete wavelet transform. 13–15, 17, 20, 38, 41
- ECG** electrocardiography. ii, 1–3, 5, 6, 8–11, 13–16, 19–23, 36–40  
**EDA** electrodermal activity. ii, 1, 3, 6–11, 17–21, 23, 41  
**EDR** ECG derived respiration. 6  
**EEG** electroencephalography. 1, 2  
**EEMD** ensemble empirical mode decomposition. 12, 13  
**EKF** extended kalman filter. 13, 15, 16, 39  
**EMD** empirical mode decomposition. 12, 13, 15, 16, 38  
**EMG** electromyography. 1, 9, 13–16, 20, 22, 36–40  
**EN** electrode noise. 8, 14–16, 36–40  
**EPSP** excitatory postsynaptic potential. 2
- FFT** fast Fourier transform. 13–15, 36  
**FIR** finite impulse response. 12, 13, 19, 36  
**FN** false negative. 22  
**FP** false positive. 22  
**FWT** fractional wavelet transform. 38
- GMM** gaussian mixture model. 17
- HFN** high-frequency noise. 13–15, 19, 36–38  
**HR** heart rate. 6, 9, 13, 14, 16, 20, 21, 36, 38, 39  
**HSM** Hospital de Santa Maria. 2, 21–23
- IF** isolated forest. 41  
**IIR** infinite impulse response. 12, 13, 36, 38  
**ILAE** International League Against Epilepsy. 2

- IMF** intrinsic mode function. 12, 15, 38  
**IPSP** inhibitory postsynaptic potential. 2  
**IT** Instituto de Telecomunicações. 2
- kNN** k-nearest neighbours. 18, 21, 41
- LDA** linear discriminant analysis. 41  
**LF** low-frequency. 38  
**LI** linear interpolation. 13  
**LMS** least mean squares. 12, 13, 16, 20, 39
- MA** motion artifact. 8–11, 14, 16, 20, 21, 36–39, 41  
**MAE** mean absolute error. 22, 36  
**MAP** maximum *a posteriori* probability. 17  
**MCF** Monte Carlo filter. 16, 17  
**MDAN** multisource domain-adversarial network. 18  
**MEMS** microelectromechanical system. 7, 11  
**ML** machine learning. 12, 18, 21, 41  
**MLP** multilayer perceptron. 41  
**MSE** mean squared error. 12, 14–17, 22, 36–40
- NB** Naïve-Bayes. 18, 41  
**NC** non-clinical-grade. 2, 16, 36, 38, 39, 41  
**NLM** non-local means. 13–15  
**NLMS** normalized least mean squares. 16, 39  
**NMSE** normalized mean squared error. 17, 22, 41  
**NN** neural network. 12, 13, 40
- PCA** principal component analysis. 16, 39  
**PLI** power-line interference. 8, 9, 11, 13–17, 21, 36–40  
**PNS** peripheral nervous system. 1  
**PPG** photoplethysmography. 18, 23
- Q** quality of signal. 36–41  
**QOF** quality of life. 1  
**QRS** QRS complex. 5, 9–11, 13–15
- R-Sen** sensitivity to detect R-peaks. 36–38  
**RF** random forest. 18, 21, 41  
**RIA** respiration-induced artifact. 8, 11, 21  
**RIIV** respiratory induced intensity variation. 18, 21  
**RLS** recursive least squares. 12, 13, 16, 39  
**RMS** root-mean-square. 7  
**RMSE** root mean squared error. 16, 17, 22, 37, 38, 40  
**RRI** R-R peak interval. 6, 14, 21, 37
- S** simulated. 36–39  
**SCL** skin conductance level. 6, 7, 17, 18  
**SCR** skin conductance response. 6, 7, 9, 11, 17, 18  
**SER** signal error ratio. 22  
**SNR** signal-to-noise ratio. 2, 7, 14–16, 19, 22, 36, 38, 40  
**SNRI** signal-to-noise ratio improvement. 14–16, 22, 36–40  
**SpO<sub>2</sub>** oxygen saturation. 23  
**STFT** short time Fourier transform. 13, 15, 16, 40  
**SUDEP** sudden unexpected death in epilepsy. 1  
**SVM** support vector machine. 16, 18, 21, 41  
**SWT** stationary wavelet transform. 17, 41
- TN** true negative. 22  
**TP** true positive. 22, 37

**V-fib** ventricular fibrillation. 13, 36  
**vEEG** video-electroencephalography. 1  
**VFCDM** variable frequency complex demodulation. 41

**W** wearable. 36, 38–40  
**WHO** World Health Organization. 1

## Symbols

$x[n]$	Input noisy biosignal.
$\hat{y}[n]$	Output denoised biosignal. Estimation of $y$ .
$y[n]$	Ground-truth clean biosignal.
$\eta[n]$	Noise component of a signal.
$n$	Samples index in a discrete timeseries.
$N$	Number of samples in a discrete timeseries.
$L$	Filter length or order. Its number of coefficients.
$M$	Window length.
$f_s$	Sampling frequency of an acquisition.
$f_c$	Cutoff frequency of a filter.
$E, V$	Potential values (in Volt).
$R$	Resistance values (in Ohm).
$Z$	Impedance values (in Ohm).
$C$	Capacitance values (in Farad).
$P$	Power values (in Watt).
$A$	Amplitude values (in root-mean-square).
$e^-$	Electron charge.
$\bar{\cdot}$	Mean of an arbitrary timeseries.
$Var[\cdot]$	Variance of an arbitrary timeseries.
$O(\cdot)$	Big-O notation. The computational complexity of a process relative to its input.

## 1 Introduction

Epilepsy is a chronic neurological disorder of the central nervous system (CNS), characterised by an enduring predisposition to generate epileptic seizures and the associated cognitive, psychological and social consequences [1]. The World Health Organization (WHO) reports that there are approximately 50 million people diagnosed with some form of epilepsy worldwide [2], from which 50 thousand (0.1%) live in Portugal [3].

Appropriate medication, termed anti-seizure medication (ASM), can control, reduce, or even cease most epileptic seizures of patients, allowing them to live normal personal and professional lives. However, it is estimated that ASMs only work effectively in approximately 2/3 (two thirds) of all epileptic patients [2, 4]. For the other 1/3 (one third) of patients, epileptic seizures are still recurrent in their daily lives, which is clinically designated as refractory epilepsy, or drug-resistant epilepsy [5]. Only 7–8% of these patients still have surgery as an option to cease seizures [6].

Epileptic seizures may represent serious danger situations in the daily life of patients with refractory epilepsy. Seizures can result in convulsions, falls, unawareness, unresponsiveness, memory impairment, incontinence, among other events. After the outbreak, complications may also arise, such as physical injury of the patients or others around them, drowning in the sea or swimming pools, or car accidents when the patient is the driver [7]. In the worst case scenario, epileptic seizures can also lead to *status epilepticus*<sup>4</sup> [8], sudden unexpected death in epilepsy (SUDEP) [9], or death by injury [10]. Besides the danger associated with some of these events, epilepsy can impact negatively patient's quality of life (QOF) and require dependence on family or professional caregivers [11]. Social stigma, fear and misconceptions about epilepsy also lead to patients with epilepsy to be discriminated in daily life situations [12] and to develop a low self esteem and mental health disorders [2, 13].

### 1.1 Motivation

In epilepsy monitoring units, hospitalised patients are conventionally monitored by a system termed video-electroencephalography (vEEG). The vEEG usually records multiple channels of scalp electroencephalography (EEG) and one lead of electrocardiography (ECG) signals of high clinical-grade (C) quality. The goal at these monitoring units is to record seizure activity, in order to follow-up on the epilepsy condition of patients, to study the effect of ASMs on them, or to conduct pre-surgical evaluations. However, this hospitalised monitoring presents with four main disadvantages [14, 15]:

- vEEG studies require repeated measurements to accurately capture the dynamics of the disease process, which is a laborious task. Also, they imply long hospitalisations, because there is no way of predicting when and how many seizures will patients experience, and, consequently, be recorded, during their stay.
- vEEG studies are conducted in controlled environments that can mask clinically important features that would be evident in the daily life conditions of the patient.
- vEEG studies imply uncomfortable instrumentation attached to the patient body for long periods of time.
- Visits to the hospital remain inaccessible to some patients for geographical and socioeconomical factors.

One way to mitigate these disadvantages is to continuously monitor seizure activity in outpatient conditions. Since there is usually no clinical-grade instruments in outpatient conditions, and for patients to have mobility to continue with their personal and professional lives as usual, the solution clinicians are interested to explore is the use of wearable devices. Current opinion among neurologists is that there is a need for automated seizure documentation and seizure detection systems, if possible using mobile or wearable devices, and, if they show a good performance, they could in the future be brought to the clinical practice [15–17]. Hence, for patients with epilepsy, specially the ones that cannot control seizures with medication, wearable devices have been engineered to continuously monitor, detect, and predict epileptic seizures [18]. These wearable devices can acquire the electrical activity of the brain (EEG), part of the CNS, or the electrical activity of the heart (ECG), the muscles (electromyography (EMG)), the skin (electrodermal activity (EDA)), or even movement (accelerometer (ACC)), temperature and audio timeseries, to which we call non-EEG biosignals or peripheral biosignals, since they reflect the peripheral nervous system (PNS) control over the body. The

---

<sup>4</sup> *Status epilepticus* is a medical emergency involving one acute prolonged seizure for more than 5 minutes.

reason why peripheral biosignals can be used to monitor epileptic seizures is introduced ahead. Examples of these wearable devices are chest patches [19], wristbands [20, 21], armbands [22–26], and behind the ear devices [27, 28]. The idea of such devices is to continuously collect biosignals of patients 24/7 (24 hours a day, 7 days a week), some to create complete documentation of seizure activity, some to issue alerts to caregivers when detecting seizures, and some even to predict seizures. The group I have been working with at Instituto de Telecomunicações (IT) has developed a chest-abdomen band that acquires ECG, ACC and respiratory signals [29]. The wearable band is currently being tested in patients hospitalised at the epilepsy monitoring unit of Hospital de Santa Maria (HSM), along with a signal acquisition and processing unit, named EpiBOX [30], developed by one of the PhD students.

## 1.2 Understanding Epileptic Seizures

Epileptic seizures are periods of synchronised hyperexcitability, product of the dysfunction of any mechanism responsible for the CNS homeostasis. The International League Against Epilepsy (ILAE) classifies seizures by onset location of this dysfunction as focal, generalised or unknown. In focal seizures, this dysfunction originates in one or more localised regions of the brain; whereas **generalised** seizures originate from widespread regions on both hemispheres of the brain. Independently of which mechanism fails, a seizure is triggered by either excessive excitatory neurotransmitter synapses, or insufficient inhibitory neurotransmitter synapses [31]. Either way leads to **hyperexcitability**. Examples of these are excess of K<sup>+</sup> in the extracellular space [32], blockade of the sodium-potassium ATPases [33, 34], abnormal mutations in Na<sup>+</sup> channels [35], abnormalities in glutamatergic and/or GABA-ergic receptors [36–38], or abnormalities in glia functions [39, 40]. Much as an action potential is triggered if the **synchronised** net sum of all the excitatory postsynaptic potentials (EPSPs) and inhibitory postsynaptic potentials (IPSPs) reaches a threshold, on a larger scale, excessive discharges only trigger a seizure if synchronised as well. Once an abnormal discharge begins, and a few neurons become hyperexcitable, they will excessively release potassium to the extracellular medium, which in turn will further depolarise other neurons and themselves again and again, beginning a *vicious cycle* of abnormal discharges [31], making seizures last from seconds to a few minutes. These abnormal activity periods can be directly measured with EEG signals.

When the abnormal activity described above perturbs brain structures responsible for controlling the autonomic nervous system (ANS), such as the amygdala, the hypothalamus, or the insular cortex, inadequate function of the ANS is triggered, involving cardiorespiratory changes, sweating, piloerection, dilation of pupils, incontinence, and changes in gastrointestinal function and thermoregulation [41–49]. These changes can be quantified by peripheral biosignals, and that is why peripheral biosignals can be used to monitor epileptic seizures. Besides ANS dysfunction, seizures can also present motor semiologies, which include tonic, atonic, and clonic components, which, respectively, mean rigid muscle contractions, sudden muscle tone relaxation, and rapidly and rhythmic muscle contractions [41, 50, 51]. There are also myoclonic components which present with brief, involuntary muscle jerks [41]. Epileptic spasms present with sudden flexion and extension of muscles of limbs and trunk, that is usually more sustained than myoclonus, but not as sustained as a tonic seizure [41]. Hyperkinetic seizures present with sequential ballistic movements [41]. Seizures with automatisms present with unconscious behaviours such as lip smacking, chewing motions, swallowing, eyelid flutters, unpurposeful walking, and hand fidgeting, picking or rubbing [50].

## 1.3 The Problem

There has been an increasing offer in wearables for seizure monitoring. However, wearable devices can only do so far in solving the mobility problem. Wearables are designed to be worn on specific body sites where they can accurately record the intended biosignals. Complementary to that, for wearables to go unnoticed, some of these body sites are the same commonly used for everyday accessories, like the wrist. The size of the wearable also influences how eye-catching it can be, and how it can get in the way of everyday tasks, hence conditioning the surface area it will cover and the number of electrodes it will have, if any. So for that reason, wearables are being developed in small size formats that are discreet and comfortable. Owing to these design restrictions, wearables are intrinsically non-clinical-grade (NC) instruments, that is, the quality of raw signals they acquire is usually inferior to that of clinical-grade (C) equipment, both in terms of poorer signal-to-noise ratio (SNR), and in terms of not being valid complementary means of diagnosis. Furthermore, the electrodes and analogue electronic components used in wearables are usually different from those used in clinical setups, which eliminate noise coming from body internal structures differently. Secondly, often those electrodes are inserted on a piece of cloth that is susceptible to movements due to daily life activities,

which produces artifacts on the acquired signals. And thirdly, in the specific case where epileptic patients are the users, some seizures produce artifacts on some biosignals that should be removed, and, conversely, some physiological seizure-related abnormalities that are important biomarkers can be mistakenly removed by artifact cleaning algorithms. Adds to the complexity of this last argument that epileptic seizures are extremely individualised, hence epileptic activity denoising should be dealt with in a patient-specific manner.

In order to the processing unit of a wearable to be able to run algorithms for annotation, detection and prediction of epileptic seizures, clean and reliable data needs to be provided. Since these algorithms are meant to run in real-time – and come later in the signal processing pipeline – denoising and artifact removal needs to run at the same pace if they are meant to deliver clean biosignals. For decades now, many signal processing methods for biosignal denoising and artifact removal have been proposed, but the vast majority of them is meant to analyse signals retrospectively. Moreover, real-time biosignal processing, however developed for clinical infrastructures, where computational power is not limited, is more scarce in the literature for mobile applications. Also, very few approaches have been proposed for real-time denoising specific for epilepsy monitoring.

#### 1.4 The Solution and Goals of this Work

The ultimate goal of the to-be-written dissertation is to develop novel real-time efficient denoising and artifact removal algorithms for low-quality biosignals acquired from wearables used by patients with epilepsy, which are inherently exposed to a variety of environmental noise and artifacts. In order to fulfil that, this intermediate project serves as a literature review on this topic, and a stepping stone to recall some signal processing methods known to be adequate for ambulatory low-quality biosignals. Hence, the goals to be achieved in this first project are to:

- Grasp the different modalities for acquiring peripheral biosignals of epileptic seizures.
- Study which environmental factors can contribute to deteriorate the quality of those biosignals.
- Understand how different types of epileptic seizures influence those biosignals.
- Review the state-of-the-art methods to denoise low-quality ambulatory biosignals.
- Based on what was learnt, propose a system for cleaning wearable biosignals of patients with epilepsy that can be used in a real-time seizure monitoring device.

#### 1.5 Outline

This document begins in Section 2 by exposing the necessary background on how to acquire and process peripheral biosignals associated with epileptic seizures. Section 3 reviews the state-of-the-art of approaches attempted to date to clean low-quality peripheral biosignals acquired in ambulatory conditions. Section 4 propose a real-time algorithm to denoise those peripheral biosignals, and Section 5 details how it will be evaluated. It ends with a plan dividing this work throughout the months to follow and some conclusions in Sections 6 and 7, respectively.

## 2 Background

This Section introduces the biosignals we are interested in studying and the noises that can affect their measurements. Before that, some formalisms should be made clear. In signal theory, signals are said to be generated by a process, which produces energy in some form, which can be measured as a variable [52]. The ECG and EDA measure, though electrodes, voltage variables generated by electrical energy, hence they are called electrophysiological signals. Conversely, the ACC measures motion variables generated by a mechanical energy. In this work, these are our variables of interest, which are known to be generated by nonlinear and nonstationary processes [53].

### 2.1 Electrodes for Electrophysiological Signal Acquisition

In an acquisition system, electrodes are the interface between the analog circuit and the skin, to which biopotentials reach. Electrodes are often made of conductive metals in order to transduce ionic electrochemical reactions into electric current, that can later be converted to the digital domain. By placing two electrodes of non-inert metals on the electrolyte solution of skin, there is a slight exchange of metal atoms

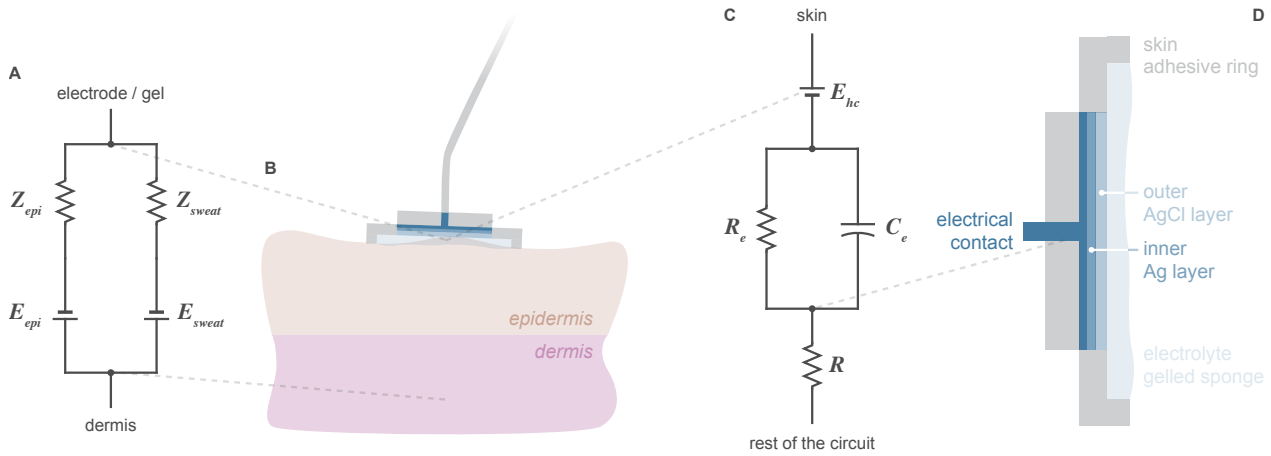
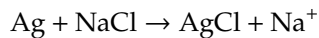


**Fig. 1.** Electrode-skin interface illustrations. A) Equivalent circuit of the electric nature of skin. B) Electrode-skin coupling with gel electrolyte. C) Equivalent circuit of the electric nature of electrodes in contact with skin. D) Material schematics of an Ag-AgCl electrode. Drawings inspired from [54].

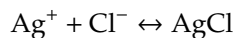
with the solution in each of them – a redox reaction – creating an **electrochemical cell**. The potential created due to this exchange in each electrode is called a half-cell potential. In theory, since the metal composition and temperature of both electrodes is the same, the individual half-cell potentials should be the same as well, but air exposure, oxidation and use degradation make that untrue, although the differences should be negligible. If they are not, electrode offset potentials will contaminate the signal. Equation 1 shows how the electrochemical cell potential,  $E_{cell}$ , can be computed with both individual half-cell potentials,  $E_{hc1}$  and  $E_{hc2}$ , with respect to a common reference [54].

$$E_{cell} = E_{hc1} - E_{hc2} \quad (1)$$

Electrodes are usually made of electrochemical reversible materials, to avoid electrode polarisation with time<sup>5</sup>, such as metals coated with their metallic salts, usually chlorides, that facilitate the redox reaction. The most widely used combination is a silver base coated with silver chloride. Silver-silver chloride (Ag-AgCl) electrodes are the general-purpose electrodes to acquire different types of biosignals, since they can be designed with low electrochemical noise, low drift, and low offset potentials. The silver reacts with the skin saline solution by the spontaneous reaction [54]:



And current can reversibly flow across the electrode by the two-stage chemical reaction [54]:



The transduced electrochemical reactions occur at the skin interface with the electrode surface – the **electrode-skin interface**. [54]. More accurately, the charge transfer occurs at the electrode-electrolyte layer of this interface, where the electrolyte is the saline environment of skin. However, this reaction usually requires some activation energy, causing the interface to offer some electrical resistance,  $R_e$ , in the order of  $10^6 \Omega$ , depending on the surface area and composition. This  $R_e$  is much smaller than the rest of the circuit resistance,  $R$  ( $R_e \ll R$ ). Moreover, the charge transfer and its storage in the electrode is equivalent to a capacitance,  $C_e$ , in the order of  $10^1 - 10^2 \mu\text{F}/\text{cm}^2$  [54]. Figure 1 depicts the electrical equivalent circuit of an electrode-electrolyte interface. Both  $R_e$  and  $C_e$  make up the **electrode impedance**. This impedance value decreases with frequency increase of the measured signal, which can be an issue, but that can be fixed with amplifiers of high input impedance [54].

<sup>5</sup> Metal polarisation occurs when it tends to oxidise more than to reduce. Eg.: Iron in iron-saline solutions.

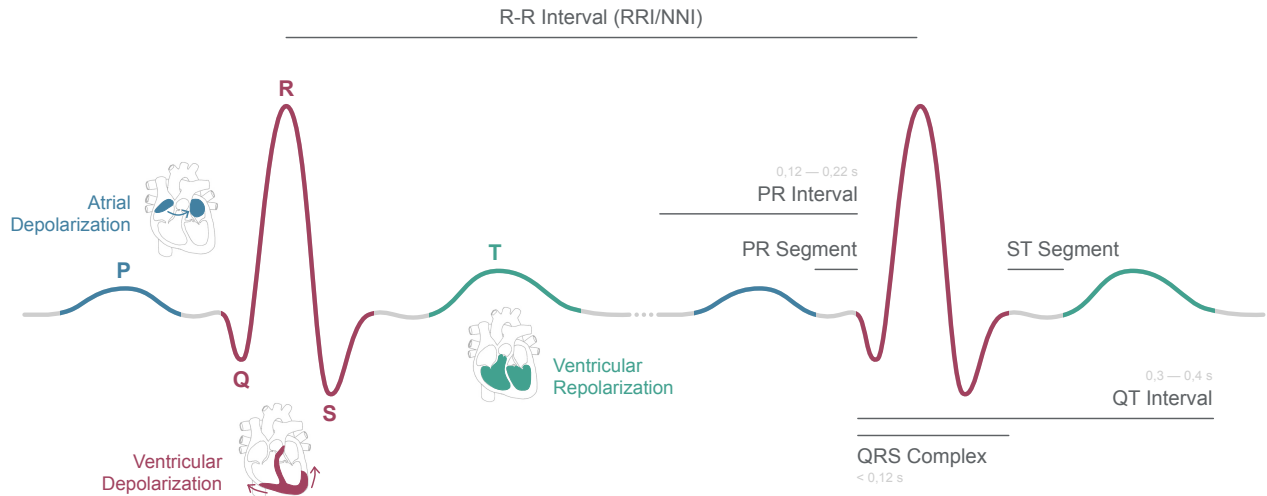


**Fig. 2.** Typical ECG waveform produced by the human heart as consequence of the depolarisation-repolarisation cycle of the heart chambers. Waves P, Q, R, S and T are the most important curves in each cycle. The QRS complex (in red) refers to the Q, R and S curves together. The PR interval is the time between the first deflection of the P wave and the first deflection of the QRS. The ST interval is the time between the end of the QRS and the start of the T wave.

The corneum is a layer of dead and dehydrated cells at the epidermis surface above the dermis. This layer presents significant electrical impedance,  $Z_{epi}$  in the range of  $10^6 \Omega$ , and it generates some electrical potential,  $E_{epi}$ , as well – see Figure 1. For that reason, in clinical-grade acquisitions, physicians often clean the skin with sandpaper and alcohol, and prepare the electrodes with some chloride-bearing gel, which hydrates the skin and reduces the  $Z_{epi}$  below  $5 \times 10^3 \Omega$  [54]. If the electrodes already come with the gel, we call them wet electrodes, if not we call them dry electrodes. One should note that, this preparation is not common practice with wearables made of dry electrodes. There is also another type of electrodes, called non-contact electrodes, which, as the name suggests, do not touch the skin, increasing the capacitance in the interface [54].

## 2.2 Electrocardiography (ECG)

The electrocardiography (ECG) is a technique to *directly* measure the heart electrical activity. It is said to be a *direct* measure because the recorded signals are the sum of voltage potentials generated by the cardiomyocytes' membrane depolarisation, together responsible for the coordinated heart depolarisation. The heart depolarisation is the orderly passage of electrical current through sequential regions of heart muscle. Each cardiac cycle is comprised of three stages: the atrial contraction, the inter-ventricular propagation, and the ventricular contraction [55]. In the absence of cardiac dysfunctions, the corresponding ECG signal presents a characteristic pattern, depicted in Figure 2. This pattern comprises five main waves – P, Q, R, S and T – that occur in the same temporal order of, and are produced by, those three stages [55]:

1. Firstly comes the P wave, which is a small upwards deflection caused by the atrial contraction, where the depolarisation is triggered at the sinoatrial node (SAN). Starting there, interventricular membrane depolarisation spreads across the atria until it reaches the atrioventricular node (AVN). After a short delay, the atrial contraction is completed.
2. Secondly, the membrane depolarisation spreads to the bundle of His and proceeds along two separate paths – the right branch and the left branch – until both waves reach the Purkinje fibres at the base of the heart. This depolarisation along with normal breathing produce the small and thin Q wave. Then comes the large R wave caused by the depolarisation of the main mass of the ventricles, and their final depolarisation at the base of the heart produce the S wave. These three waves are called the QRS complex, representing the complete ventricular depolarisation phenomenon. Atrial repolarization occurs during the QRS complex, but it gets *silenced* by it.
3. Thirdly, the electrical depolarisation spreads to the ventricular walls starting the ventricular contraction. The T wave is then produced by ventricular repolarization.

A clinical-grade ECG is acquired by attaching two to ten wet electrodes on the chest and limbs, which can provide one to twelve leads. These different leads acquire slightly different ECG traces, representing different

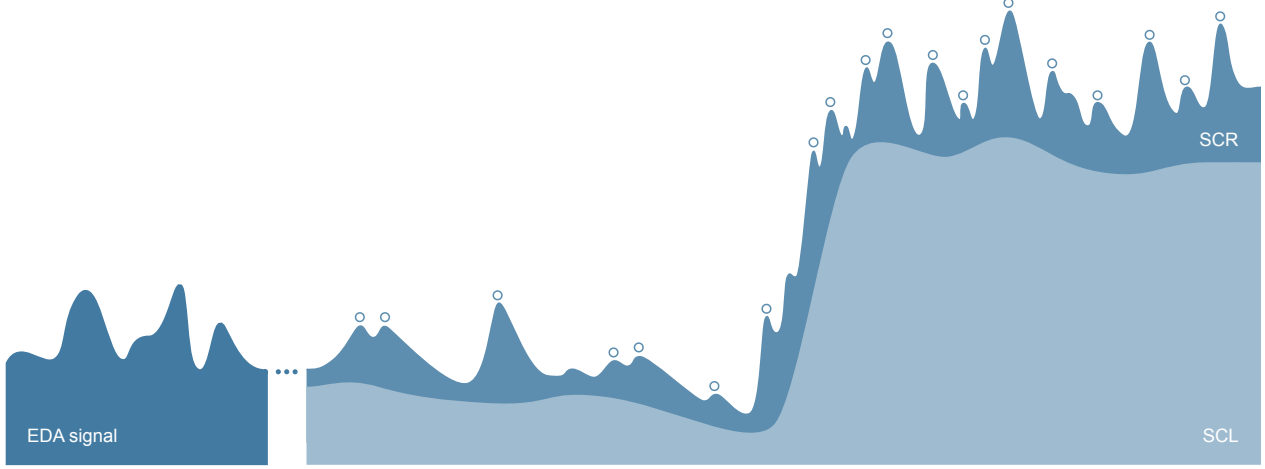


**Fig. 3.** Typical EDA signal. The signal can be separated into two components that superimpose each other: the SCL, which is of low-frequency, and the SCR, which is of high-frequency. The EDA peaks are identified with a dot on the SCR component. Merely illustrative drawing inspired in [56].

view angles and directions from which each electrode acquires the heart depolarisation. Depending on the lead angle and direction, at each timepoint, the ECG trace will present a positive deflection or a negative deflection if there is electrical activity, respectively, towards or away from the lead. Usually, depolarisation causes positive voltages and repolarization causes negative voltages, and the ECG trace is the net sum of all electrical activity at each timepoint [55]. However, epilepsy monitoring units and wearable devices usually do not acquire signals with twelve leads, but rather with just one or two on the chest, abdomen or left upper limbs. Also, wearables generally use dry electrodes, whereas in epilepsy monitoring units the staff uses wet electrodes.

From the ECG digital timeseries, besides the heart rate (HR), we can extract other common timeseries rich in information. One of them is the R-R peak interval (RRI) timeseries, in which each sample is the time difference (usually in milliseconds) between each consecutive pair of R peaks. Another one is the ECG derived respiration (EDR) timeseries, which can be computed from the interpolation of the amplitude of the R peaks.

### 2.3 Electrodermal Activity (EDA)

The electrodermal activity (EDA) can be measured by placing two electrodes on the epidermis. EDA signals are the product of the electrical impedance,  $Z_{\text{sweat}}$ , and the electrical potential,  $E_{\text{sweat}}$ , generated by the accumulation of sweat produced by sweat glands. As previously schemed on Figure 1,  $Z_{\text{sweat}}$  and  $E_{\text{sweat}}$  can be modelled as parallel components, together called **skin battery** [57]. Capillary vasodilatation and variations in sweat duct activity, controlled by the sympathetic branch of the ANS, lead to changes in the secretion of sweat [58]. Sweat is a fluid full of electrolytes, therefore its secretion changes the impedance across the skin battery, which in turn can be captured in the measured signal amplitude. This phenomenon became known as skin potential response (SPR) or galvanic skin response (GSR) [57, 59].

Usually, electrodes are placed in the hands, wrist or feet, because these are the body sites with more eccrine glands – the major sweat glands in the body. Measurements can be performed in two distinct approaches: endosomatic or exosomatic. Endosomatically, the device measures only the skin potential (SP). Exosomatically, a low external direct current (DC) or alternate current (AC) current is applied to the skin and electrical changes are recorded. When DC current is applied, we can measure [60]:

- Skin Conductance (SC) changes, by keeping voltage constant.
- Skin Resistance (SR) changes, by keeping the current constant.

When AC current is applied, we can measure [60]:

- Skin Impedance (SZ) changes, by keeping voltage constant.
- Skin Admittance (SY) changes, by keeping the current constant.

The EDA signal can be decomposed into tonic activity and phasic activity, as illustrated in Figure 3. The tonic activity, also known as SCL, comprises the slow electrical fluctuations (0–0.05 Hz) caused by normal physiological events, while the phasic activity, also known as SCR, incorporates the fast electrical fluctuations (0.05–2 Hz), generally in response to external and internal stimuli [61]. Both signals can be easily separated using bandpass filters [62].

The SCL signal represents a continuously moving baseline, with amplitude ranging from 2 to 20  $\mu\text{S}$ , varying for different patients, hence it is usually not analysed [63]. Regarding the SCR signal, it can be further divided into two components: the event related SCR (ER-SCR), which are true responses to stimuli, and the non-specific SCR (NC-SCR), which do not correspond to any event. When in response to a stimulus, the SCR signal presents a peak (0.1–1  $\mu\text{S}$ ) after some latency (1–3 seconds) [63]. This latency varies according to temperature and electrode placement. The time it takes the peak to drop to half its amplitude is called the half recovery time (2–10 seconds) [64]. The SCR signal is traditionally analysed by detecting the ER-SCR peaks' amplitude and latency [65], although more modern and robust methods have been developed [66,67].

## 2.4 Accelerometry (ACC)

Accelerometer sensors are cheap and small instruments capable of acquiring movement data that is simple to process. These sensors can convert movement into electrical voltage based on the gauge effect, capacitive, or piezoelectric physical phenomena. For human movement monitoring, usually microelectromechanical system (MEMS) sensors are used, which can record acceleration in meters per squared second ( $\text{m.s}^{-2}$ ), or g-force units ( $1g \approx 9.81\text{m.s}^{-2}$ ), according to Newton's second law of motion or Hooke's law [68]. Usually, three ACC channels are acquired, one per each of the three dimensions of the physical space [69–71], which allow us to extract translational and rotational information of movement. But there are also ACC devices with just one dimension [72]. Accelerometry can be acquired from any site of the body where movement is relevant. For seizure monitoring, ideally, the location would depend on the motor expression of each seizure type. For instance, for tonic and clonic seizures, irregular movements are detected in the upper limbs or wrists [70,71,73]; whereas epileptic spasms often express ballistic movements on the trunk [41].

## 2.5 Biosignal Denoising and Artifact Removal

When acquiring a biosignal of interest, contamination by background noise is inevitable. Generally speaking, noise in a signal is defined by *everything else that is not of our interest* [52]. Background noise,  $\eta$ , and signal of interest,  $y$ , are usually additive, which means that both components superimpose each other and may become indistinguishable in the acquired timeseries,  $x$ :

$$x[n] = y[n] + \eta[n] \quad (2)$$

Consequently, if physicians would look to the raw acquired signal,  $x$ , they would not make much of an interpretation. And the same can be said about most computer algorithms that have the goal of interpreting those signals. Therefore, denoising algorithms are necessary to *clean* the acquired signals, that is, to remove as much noise and artifacts as possible, while leaving the meaningful data unaltered. In engineering disciplines, it is common to use the SNR to quantify what amount of background noise is present in the acquired signal versus what amount of meaningful signal is present. Equation 3 mathematically defines SNR, where  $P_y$  is the power of meaningful input and  $P_\eta$  is the power of background noise or meaningless input. Alternately, the SNR can be defined by the ratio between the root-mean-square (RMS) amplitude of both components,  $A_y$  and  $A_\eta$ . The higher the SNR is, the less noise the signal has.

$$\text{SNR} = \frac{P_y}{P_\eta} = \left( \frac{A_y}{A_\eta} \right)^2 \quad (3)$$

The book of Semmlow and Griffel [52] divides background noise into four sources:

1. **Physiological variability:** Occurs when the variable of interest is indirectly measured.
2. **Environmental:** Other sources of similar form of energy.
3. **Artifacts:** Other sources of different form of energy.
4. **Electronic:** Thermal noise and shot noise.

Noise from source (1) can be present when we are indirectly measuring a variable, for instance respiration via ECG signal. This case will not be of our concern, since every biosignal will be measured directly. Noise from source (2) occurs when we measure an electrical variable with an electrode, that ends up acquiring other electrical variables. Electrodes capture electrical potentials, whatever they are, and do not distinguish between what truly is our signal of interest and everything else that is not. These sources can be further divided into internal or external:

- 1 - Internal: Source is the body. These include breathing, muscle, neuronal or cardiac noise and respiration-induced artifacts (RIAs), depending on what we are not interested in measuring.
- 2 - External: Source is not the body. These include power-line interference (PLI), surrounding electromagnetic noise, electrode noise (EN) due to loss of electrode contact, and others.

Noise from source (3) are called artifacts, and occur when, for instance, mechanical energy interferes with the measurement of an electrical variable. If this mechanical energy comes from body movements, we call these motion artifacts (MAs). It should be clear that, throughout this text, the terms noise and artifacts are not going to be used interchangeably like in this classification, but rather as separate concepts. In a general way, noise is random and obscures or hides features in the signal, whereas artifacts are structured signal components that look like physiological features, but really they are not. Noise from source (4) is produced by analogue electronics themselves, namely the resistance sources and the voltage barriers associated with semiconductor junctions. Electronic noise is the only noise source mathematically well-defined, whereas the other three noise sources are always unpredictable. Abstracting the mathematical definitions of electronic noise, it is sufficient to know that it is stationary, following a Gaussian distribution uniformly throughout a broad range of frequencies, hence we can model it as white noise [52]. Our main focuses will be sources (2) and (3), hence the next Subsections characterise each of their noises and artifacts in detail.

### Power-Line Interference (PLI)

Throughout the day, the patient can go around many environments exposed to different electromagnetic fields. To these fields contribute electrical wiring in buildings, radio-frequency appliances such as televisions, computers, cell phones, and even radio towers and atmospheric electricity, and they can induce electrical potential from millivolts to a few volts in the human body,  $V_{line}$ , that can be orders of magnitude larger than the biopotentials being acquired. These electric fields, between objects and the body, result in a capacitive coupling, with an air gap in between acting as a dielectric. Additionally, our bodies will also couple to the floor, or ground. Since we are closer to the floor than to those objects, the ground coupling can be 100 times higher. Both couplings act as a voltage divider, and result in an interference in the body called floating potential,  $V_{float}$  [54]:

$$V_{float} = V_{line} \cdot \frac{Z_{ground}}{Z_{line} + Z_{ground}} \quad (4)$$

where  $Z_{line}$  is the power-line impedance and  $Z_{ground}$  is the ground impedance. This floating potential can become very large, and can be boosted if the body is near metal objects. The power-line potential,  $V_{line}$ , can vary from object to object, but nearly all function at the same frequency, which is 50 Hz in Europe and 60 Hz in the United States. This induced floating potential in the body will superimpose to the biopotential we are trying to measure and, naturally, electrodes will record the sum of both – Equation 2. On ECG and EDA signals, we can notice the PLI as a continuous sinusoidal noise, predominant throughout all signal, with a fundamental frequency (50 or 60 Hz) and a number of odd harmonics, hence it approximates a linear process [74]. Therefore, the most traditional and simple method to remove PLI is to apply an analogue or digital notch filter, with a cutoff at 50 or 60 Hz. However, sometimes that is not enough if the PLI frequency varies in non-stochastic ways, or if we want high-resolution signals. Moreover, modern devices have a very high common mode rejection ratio (CMRR) to reduce PLI as much as possible [54].

### Baseline Wander (BW)

Improper electrode-skin impedance due to pressure, forces or movements cause transient millivolt-order changes in the skin-battery magnitude, which may induce an offset potential known as baseline wander (BW) or baseline drift [57]. On one example, pressure on the electrodes during acquisition will cause deformation of the skin and, consequently, variations in  $Z_{epi}$ , perturbing the recorded signal amplitude. On another example,

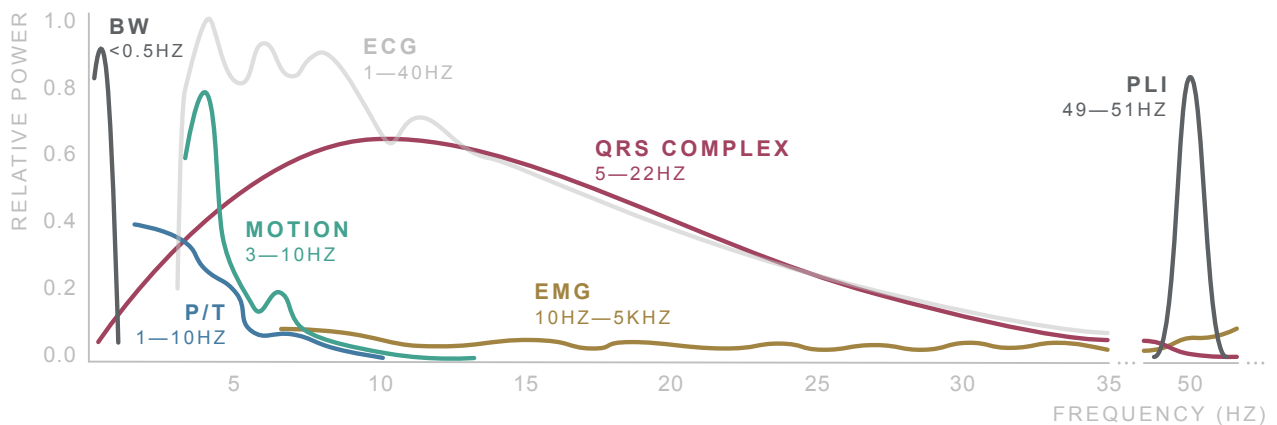


**Fig. 4.** Typical power spectrum of an ECG acquisition. The most salient morphology of the QRS complexes are predominantly under the red spectra, whereas the P and T waves predominantly occur under the blue spectra. EMG noise and MAs are indicated in yellow and green, respectively. BW and PLI are both identified in grey. Inspired in [76].

if electrodes are placed on the chest (e.g. in ECG), chest and diaphragm movement due to respiration and normal gating are sufficient to induce BW. Respiration movements of the rib cage produce a *wander* on chest ECG, that can cause T waves to be higher than R waves, which may end up being detected as false R peaks [54]. Besides respiration, in T-shirts and chestbands, BW may also be caused by gastrointestinal movements [75]. These induced potentials are inevitably captured by electrodes, and the base axis of the recorded trace will appear to *wander*, that is, to *move* up and down, rather than maintaining constant. This baseline wander frequency spectrum varies depending on what causes it, but it is usually lower than 0.5 Hz, as illustrated in Figure 4. For that reason, the most traditional and simple method to remove slow baseline wander is applying an analogue or digital highpass filter with a cutoff at 0.5 Hz or 1 Hz [54]. When BW presents with a quasi-sinusoidal morphology, we can model it as linear [74], but when it presents spiky or trendy structures, that is no longer the case. Moreover, BW comes from a nonstationary process [53], so, in complex environments, a highpass filter is usually a poor and naive strategy.

### Electrophysiological Noise

When trying to acquire only one type of electrophysiological signal, we will often record a sum of that biopotential of interest and other biopotentials that are not of interest. As an example, let us suppose one acquires an ECG signal. The meaningful data would be solely the electrical potentials produced by the sinus node and those propagated across the remaining cardiac muscle. Every other tissue that may produce an electrical biopotential and that is recorded by the electrodes is said to be noise, hence it must be removed. The same analogy is valid for EDA signal regarding every other biopotential that is not the galvanic skin response. Let us study two types of these noises:

- **Myogenic Noise:** When acquiring ECG or EDA, the electrodes will also record myogenic potentials, or EMG, in the background. Myogenic potentials are biopotentials generated by skeletal muscle activity. Since they are not of interest, they are considered background noise [54]. Fortunately, these different biopotentials can have somewhat different spectra, which is useful to separate them in the frequency domain. The EMG typically ranges from 10 Hz to 5 kHz [54] – see Figure 4. The ECG typically ranges from 0.05 Hz to 100 Hz [54], however the QRS power spectra usually ranges from 5 Hz to 22 Hz [77], and the power of P and T waves goes up to 10 Hz [78], although these frequencies may change from subject to subject, and according to HR. And the SCR component of EDA typically ranges from 0.05 Hz to 2 Hz [61]. The most simple and naive methods apply bandpass filters, where the passband is one of these typical known frequencies of the biopotential of interest. Since EMG is a nonstationary and nonlinear biopotential [53,74], usually it dynamically intersects the frequencies of ECG and EDA, in which case a bandpass filter is often an insufficient effort.
- **Electrodermal Noise:** When acquiring ECG, if sweat excretion increases, there will be a resistance change that shunts the skin battery and changes its magnitude. Specifically, accumulation of sweat under the electrodes changes the electrical impedance,  $Z_{sweat}$ , and the electrical potential,  $E_{sweat}$ , of the electrode-skin interface (Figure 1) in a pressure, temperature, hydration, and time dependent manner. In turn, the recorded ECG trace will be superimposed by slow drifts in the DC amplitude, called electrodermal noise or EDA noise, which are difficult to remove in low-frequency signal segments [54].

## Motion Artifacts (MA)

In daily life activities, limbs and trunk movements or normal gating can create artifacts in ECG and EDA, that look like physiological features, although they are not. This kind of movements can be seen as a nonstationary and nonlinear process [53, 74], which produces high-amplitude artifacts [79]. In ambulatory EDA it is particularly challenging to detect and remove MAs caused by movement of electrodes during daily life activities. In ECG, since it is a repetitive regular pattern, MAs are generally more easy to discriminate from *normal* segments.

Dry contact electrodes are particularly prone to MAs, because upon motion there is a high probability the electrode stops touching directly the skin for a few moments, creating an air gap, which translates into an increased capacitance in the interface in the order of  $10^1 - 10^2$  pF. By recalling Figure 1, we can infer that an additional capacitance of that order in series with the rest of the model will result in an increased impedance up to a factor of 1000 [80], i.e., a motion artifact. Conversely, non-contact electrodes already present this extra capacitance due to their insulating layer and air gap, so impedance variations due to motion will be in the same order as the impedance values prior to motion, which constitutes an advantage relatively to dry contact electrodes [80]. As for wet contact electrodes, the gel helps to minimise impedance variations caused by MAs.

One traditional technique to prevent MAs is to increase the input impedance of the circuit to extremely high values (e.g.  $> 1T\Omega$ ) [80–82]. Despite this guaranteeing almost no loss of AC signal, it does not eliminate large DC drifts caused by MAs. Large DC voltage differences at the electrode-skin interface increase the current that goes through it by several orders of magnitude higher than the signals of interest, which is even further multiplied by the high input impedance that was designed to fix this issue in the first place. The result are large slow drifts on top of the recorded signals [80]. So, other techniques (analogue or digital) need to tackle the MAs problem.

## Discriminating Artifacts in ECG

Given an algorithm to detect artifacts in ECG segments, there is a panoply of patterns to consider. For starters, a P wave should always be present before every QRS complex. If it is not, the patient might not be under the sinus rhythm, i.e., it is not the sinoatrial node marking the pace, or the recorded signal might come from other electrical source [55]. Whatever the reason is, that segment should not be used in subsequent analyses. Also, the QRS complexes should always be identifiable, and, if they are not, even after denoising, the segment can be discarded as well. Then, when detecting artifacts in ECG, it is important to understand that abnormalities can be:

1. Artifacts, which indeed must be removed. (E.g. a motion artifact.)
2. Typical phenomena of seizures, which should not be removed, since they are crucial for an accurate seizure classification, as well as interpretation by physicians. (E.g. inverted T waves.)
3. Caused by cardiovascular comorbidities or normal differences, and some should be removed, since they may be wrongly classified and interpreted as seizures. (E.g. arrhythmias.)

Discriminating case (1) from cases (2) and (3) is a highly patient-specific task. Case (2) because seizure semiology is extremely individualised and differs with type of seizure. Case (3) because each patient has their own diagnoses of cardiovascular disorders, if any, or have their characteristic lifestyles or belong to an ethnicity characterised by unusual ECG features. Hence being so important a patient-specific approach when removing artifacts, otherwise segments with important biomarkers might be wrongfully discarded. Discriminating between cases (2) and (3) is also a very individualised task. Let us exemplify this with three possibly benign abnormalities:

- A wide or broader QRS complex usually represents bundle branch block, which is a delay in the electric conduction during the interventricular depolarisation [55] (Figure 2). Left bundle branch block is common in patients with high blood pressure and more predominant in older adults, and right bundle branch block can also occur in healthy individuals [83]. However, 30% of patients with focal seizures of impaired awareness show bundle-branch block during seizures [84].

- Young patients and athletes can show a more than usual elevation of the ST segment, and inversion of the T wave is common in some ethnicities [55]. In these groups of people, these are normal phenomena. However, elevation and depression of the ST segment, and inverted or biphasic T waves have been observed in the ECG of patients with focal and generalised seizures [45, 84–86].
- The absence of P waves and irregularly spaced and narrow QRS complexes is the hallmark of atrial fibrillation [55], which is common in patients with high blood pressure, atherosclerosis, congenital heart defect, among other heart conditions [87]. However, some patients show atrial fibrillation during focal and generalised seizures [84, 88].

### Respiration-induced Artifacts in EDA

Irregular respiration can *indirectly* induce artifacts on the EDA signal. Common examples of irregular respiration are deep breaths or coughing. We say they *indirectly* induce artifacts, because these phenomena increase adrenaline in circulation that, in turn, stimulate eccrine glands to produce sweat [79]. These sweat releases can be rather sudden, therefore creating peak artifacts in the SCR signal [89]. Although this is a response of the sympathetic nervous system, it is caused by irregular respiration, which we are not interested in measuring, hence, preferably, it should be removed. Respiration-induced artifacts<sup>6</sup> (RIAs) are much more predominant in signals acquired in ambulatory settings, particularly by wearables, since while monitoring patients continuously during their normal physical activities, some of these naturally imply irregular respiration [90]. Respiration has a similar frequency band to that of EDA, therefore the two activities are indiscernible in the frequency domain, which can make the denoising process difficult.

### Enhancing Quality of ACC

Accelerometry signals acquired from MEMS may present with external and internal noise. Environmental mechanical and electrical vibrations may displace the MEMS pieces, contributing this to external noise, as well as PLI if powered by AC current. These types of external noise can be neglected when ACC is being used as a biosignal, since the measured acceleration is usually of low-frequency [91]. Internal noise can be electronic noise, from circuit components (e.g. amplifiers), and thermo-mechanical noise, from molecular agitation of mechanical pieces, also known as Brownian noise. These types of internal noise can be attenuated with analogue preconditioning and good circuitry design practices.

Contrarily to electrophysiological signals, the concept of MAs does not exist in ACC signals, since the variable of interest is, indeed, motion. However, ACC signals collected from the wrist may present with noise from motion itself, such as low-amplitude natural tremors caused by shaky hands, or even high-amplitude handshakes. The natural tremors are usually randomly distributed, hence they can be seen as Gaussian noise, and the ACC trace can be easily stabilised by applying fairly simple smoothing techniques. There can also occur artifacts caused by displacements of the sensor, for instance, when it is embedded in a piece of cloth, that do not correspond to a motion of a body part. These artifacts should be removed as well, or at least ignored, but they are very difficult to distinguish from body motion.

### Coloured Noise

As a last note, some authors refer to stochastic noise with different power spectra with different colours. White noise, as aforementioned, shows a uniform power spectral density, i.e., it shows similar power throughout *all* frequencies. Pink, blue, and violet noise power densities change, respectively, -10 dB, +3.01 dB, and +6.02 dB per frequency decade [92].

## 2.6 Digital Signal Processing (DSP)

Before diving into the state-of-the-art, let us recapitulate which types of techniques exist for DSP, their advantages and limitations. A DSP method can be classified into several classes according to the following properties: (a) linearity; (b) stationarity; (c) causality; (d) whether it is parametric or nonparametric; (e) the domain in which the operations are performed, i.e. time, frequency or both; (f) the operations can be correlations, convolutions, or other types; (g) whether the output is the denoised signal, or, instead, an

---

<sup>6</sup> This term should not be confused with breathing that causes baseline wander in chest ECG.

action follows, such as thresholding, elimination or subtraction; (h) whether it uses other timeseries as noise references or not; (i) adaptability; (j) optimality; and (k) class of computational complexity. Table 1 summarises some of these properties (*a*, *b*, *e*, *i*, and *k*) for some methods and operations of DSP.

Regarding properties (*a*) and (*b*), a method is linear if it outputs a result that complies with the homogeneity properties, and it may or may not be suitable to denoise stationary processes, i.e., processes with time-invariant distributions. As aforementioned, some types of noise and artifacts are produced by nonlinear and nonstationary processes, but we can make the assumption these behave as linear and stationary, if we process their timeseries in segments (or blocks), under the assumption they approximate to linear and stationary processes only during those segments [52]. Assumptions like this allow us to harness the power of the vast majority of DSP methods, which assume linear and stationary conditions. Although we should be aware that, as these are approximations, the denoising task might be incomplete. Moreover, denoising segment-by-segment can create artifacts or ringing effects on the edge of segments, depending on the method. Padding techniques may help to overcome that.

Regarding property (*g*), hereinafter, we will refer to **actions** as what is done with the output of operations. In the sense that: these methods might output a denoised signal directly, or an action must subsequently be performed to reconstruct the signal. An action might be a **threshold** or an **elimination** of some components extracted by an operation. A **subtraction** of some component from the signal can also reconstruct the signal. The method can also output a reconstructed signal or extract and output **features** of it. These different actions make up different strategies in which DSP methods might be used in. Regarding property (*h*), some techniques use information from other biosignals to denoise the biosignal of interest, something that has been coined as noise references [93]. Property (*k*) is perhaps the most important to this work, since it quantifies how much time a technique takes to run on a machine. In this text, we will use the Big-O notation to compare techniques in terms of time complexity classes: polynomial, linear, quadratic, logarithmic, etc. [94].

Most of the methods that are reviewed in Section 3 involve finite impulse response (FIR) and infinite impulse response (IIR) filters. On one hand, the former are always stable and do not distort the signal, however they require more computations than the latter. On the other hand, IIR filters can achieve the same output with less coefficients, shorter latency, and less memory, for they are recursive, however their design needs to be more rigorous to ensure stability and avoid phase distortions and time delays [95]. In the time-domain, median and average filters can show similar filtering characteristics. These methods traverse the signal with a sliding window and compute the median or average of all the samples inside the window at each timestep, and can either deliver an output directly or extract a component that is latter subtracted from the signal. Wavelet-based methods have the advantage of capturing time and frequency features by *stretching* the signal to fit a predefined waveform, however choosing the mother wavelet and the number of decomposition levels can be a hard design choice [96]. Actions like thresholding or elimination of specific wavelet coefficients are usually performed after decomposition. Empirical mode decomposition (EMD) and other intrinsic mode function (IMF) decomposition techniques are also usually employed. Conversely to wavelets, EMD generally does not attenuate the signal's amplitude, however it shows a higher time complexity (Table 1). Additionally, EMD lacks robustness to small perturbations. Ensemble empirical mode decomposition (EEMD) can solve that issue, although at the cost of even higher time complexity [97].

Wiener filters are optimal filters that define the coefficients in order to minimise the mean squared error (MSE) between the output and the ground truth. The least mean squares (LMS) and recursive least squares (RLS) algorithms are also said to be optimal, for they minimise a specific cost function, but they are also adaptive, that is, they adapt their model parameters or coefficients in real-time in order to minimize that cost function. The LMS algorithm, although the fastest one, shows slow convergence rate, is very sensitive to its stepsize parameters, and can show some unstable behaviour [96, 98]. The RLS algorithm shows higher computational cost, and may display some numerical instabilities as well [98]. Moreover, due to its intrinsic memorisation, the RLS performance can get severely hindered in situations where the noise keeps changing patterns [53]. Kalman filters are also adaptive, although they are restricted to the Gaussian space [96]. In fact, by definition, any algorithm can be adaptive by segment or by sample if it has a strategy for that. Neural networks (NNs) and other machine learning (ML) methods are, by nature, also adaptive. The particular case of denoising autoencoders (DAEs) is commonly used to denoise nonlinear and nonstationary processes. DAEs are divided into an encoder and a decoder. On a first stage, the encoder translates the signal to a lower dimensional space, and on a second stage the decoder reconstructs back the signal. These models are trained to receive noisy signals and learn to output their denoised versions, or they can learn to output directly a representation of features to be used on some subsequent analysis. ML detectors can also be used to identify

**Table 1.** Comparison of different methods employed in digital signal processing.

Operation	Linearity	Stationarity	Domain	Adaptation	Time Complexity
IIR/FIR	Linear	Stationary	Frequency	None	$O(N)$ , $O(N^2)$ zero-phase
FFT	Linear	Stationary	Frequency	None	$O(N \log N)$
STFT	Linear	Stationary	Time-Frequency	None	$O(N \log M)$ , $O(NM)^*$
S-transform	Linear	Stationary	Time-Frequency	None	$O(N^2 \log N)$ , $O(N \log N)^{**}$
DWT/CWT	Linear	Stationary	Time-Frequency	None	$O(N)^*$
Wiener	Linear	Stationary	Frequency	None	$O(L^3)$
RLS	Linear	Nonstationary	n.a.	By sample	$O(L^2)$
LMS	Linear	Nonstationary	n.a.	By sample	$O(L)$
Kalman/EKF	Linear	Nonstationary	Time	By sample	$O(4N^3)$
EMD	Nonlinear	Nonstationary	Time-Frequency	Intrinsically	$O(N \log N)$
EEMD	Nonlinear	Nonstationary	Time-Frequency	Intrinsically	$O(EN \log N)$
NN	Nonlinear	Nonstationary	n.a.	Intrinsically	Architecture-dependent
NLM	Nonlinear	Stationary	Time	None	$O(NM)$
Median	Nonlinear	Nonstationary	Time	None	$O(N^2)$ , $O(N)^{**}$
Average	Linear	Stationary	Time	None	$O(N)$
LI	Linear	Stationary	Time	None	$O(N)$

$N$ , number of samples.  $L$ , filter length.  $E$ , number of ensembles. \* Filter banks implementation. \*\* The fastest version.

artifact segments to be discarded. These detectors usually binarily classify segments in *artifact* and *not-artifact* classes, from a set of features extracted from them.

### 3 Related Work

In this Section, the state-of-the-art of denoising and artifact removal of the three biosignals studied is presented and compared using the metrics described in Section 5. The goal of this Section is not only to summarise the most recent advances in cleaning these biosignals, but also to give a clear picture of what were, and still are, the more traditional methods to do so, without getting into much technicality. Refer to Annex 1 for technical details of the approaches here reviewed. From the three biosignals studied, the denoising of ECG has received the most attention throughout the years, in many applications such as HR, arrhythmias, atrial fibrillation (A-fib), ventricular fibrillation (V-fib), stress, and fall detection, or simply ambulatory monitoring, hence we start with the ECG.

#### 3.1 ECG Denoising and Artifact Removal

**Frequency-domain Filtering.** Lowpass, highpass, bandpass and notch filters are still the most common and straightforward way of filtering ECG, both analogically and digitally. Lowpass filters have been designed to suppress EMG noise [99–102], PLI [95, 103, 104], or any other high-frequency noise (HFN) [96, 105–108] (including high-frequency white noise [109]). They can also be used to remove fluctuations caused by respiratory sinus arrhythmia [110]. While the majority display cutoff frequencies of around 30–40 Hz, some opt for lower frequencies when only some waves are relevant for their specific analysis, and some opt for higher frequencies if high-resolution signals are required. Highpass filters, on the other hand, have been designed to reject most of BW noise [95, 99–102, 104, 108, 111–113], the majority with a cutoff around 0.05–0.50 Hz, higher if P and T waves can be attenuated. Bandpass filters can intersect the passbands of these two types of filters [75, 114–118]. To highlight QRS complexes while attenuating P and T waves, [15, 25] Hz or [6, 22] Hz passbands have been recommended [119, 120], whereas to not attenuate any wave, [1, 12] Hz

passbands are preferred [121], although these approaches will distort the signal. Notch filters are designed almost exclusively to reject the PLI frequency [99, 101, 102, 122, 123]. Our confidence in these filters relies on assuming the signal of interest and the background noise do not share overlapping frequencies, however we know that not to be true. Annex Table 2 shows a technical summary of these filters.

**Average and Median Windows.** To avoid the computational complexity of operations in the frequency-domain, some methods have been proposed to behave similarly to frequency filters. Moving average [124, 125] and median [107, 112, 126] filters can extract and isolate BW in a separate timeseries, which can then be subtracted from the ECG to correct its baseline. Average and median filters output a result equivalent to that of a realisation of a lowpass filter. Subtracting that result from the raw input makes the whole process equivalent to the realisation of a highpass filter. The window length,  $M$ , of these filters can be played with to simulate different cutoff frequencies,  $f_c$ , of the highpass filter intended to resemble, through the relationship  $f_c = f_s/(2M)$  [127]. Windows of 150–200 ms have showed to suppress the P and QRS waves, and windows of 600 ms to suppress T waves, and in some works two sequential median filters, each with one of these lengths, have been applied to isolate BW [103, 107, 128]. An *et al.* (2020) showed on the MIT-BIH arrhythmia dataset that a moving average of  $M = 1$ s yields higher signal-to-noise ratio improvement (SNRI) and slightly lower MSE than a median filter of the same length [111]. Without the subtraction action, a median filter can also be used to suppress drifts while preserving sharp edges in RRI timeseries [110]. Annex Table 3 shows a technical summary of these types of filters.

**Interpolations and Other Time-domain Methods.** Since, depending on the sorting method, computing a median can become expensive, a cubic interpolation over some median points has been proposed to model BW [129]. However, cubic interpolation can introduce artifacts if the signal has ectopic heartbeats, slow HR, or pronounced BW [130]. To remove EMG noise, Shusterman *et al.* (2000) [130] proposed to subtract a "cutting line" dynamically computed with the maximum value and the standard deviation of each ECG segment. Subtraction of the spline interpolation of PQ segments (or PR segments [131]) has also been suggested to remove BW, although it performed poorer than a median filter [112]. Moreover, after highpass filtering to remove most of BW, linear interpolation, as a second step, is able to correct baseline to zero in a more refined way, and, in fact, in Holter acquisitions, this last step was sufficient to remove all BW in 75% of acquisitions [130]. However, if linear interpolation is used to remove BW with high-amplitude and high-frequency drifts, one should pay attention to potential distortions to the cardiac morphology [130]. In Annex Table 3 there is also a technical summary of some of these filters.

**Wavelets.** Some authors state that their developed wavelet methods outperform other conventional frequency filters, median filters and interpolations to remove BW [112, 113, 132], and even EMG and EN from the MIT stress dataset [100]. Moreover, a group argued that using the fractional wavelet transform, which accounts for signal rotation in the time-frequency distribution, yields 4 times less MSE than using the discrete wavelet transform (DWT). However, there is strong evidence from other groups that these same DWT methods are less robust than non-local means (NLM) [133, 134], frequency decomposition modulation [135–137], adaptive filters [111], DAEs [138, 139], or notch filters when it comes to PLI rejection [122]. Nonetheless, wavelet methods can complement other techniques, and contribute to improve the performance of denoising systems, particularly in the detection of MAs [99, 108]. By testing several mother wavelets, *db8* and *sym8* have been suggested to model white noise and to remove it with the lowest MSE [140], whereas to threshold and remove both BW and HFN the *sym2* yields lower MSE on the MIT-BIH arrhythmia dataset [141]. On the Physionet QT database, *sym3* is able to model sinusoidal BW, but for spiky and trendy BW the *meyer* wavelet was found to yield lower MSE [142]. The majority of authors [100, 113, 132, 141–147] agrees that, after wavelet decomposition, the first and second level detail coefficients (high-frequency) should be eliminated to suppress PLI, EMG, and HFN, whereas the last level approximation coefficients (low-frequency) should be eliminated to suppress BW. If the goal is to keep the morphology of the R wave, for HR detection or RRI computation, then only the relevant levels should be maintained [121]. For instance, in 5-level decomposition, the coefficients of levels 3 and 4 can be used to detect the QRS complex, levels 4 and 5 the T wave, and level 4 the P wave [147]. Some works, after elimination, also apply an adaptive dual threshold filter (ADTF), rather than just a single threshold, which further improves the output SNR [143]. Annex Table 4 shows a technical summary of wavelet-based filters.

**Fourier Transforms.** For high resolution ECG, it is common to dynamically find the PLI fundamental frequency and its harmonics in the Fourier domain. Such adaptive filters based on discreet Fourier transform (DFT) [148] or fast Fourier transform (FFT) [149, 150] can achieve double the SNRI and four time less MSE than a static notch filter, with estimation errors, respectively, of 0.01 Hz and 0.1 Hz. Singhal *et al.* (2020) [137]

suggested to apply the DFT or the discrete cosine transformation (DCT) in order to decompose the signal into orthogonal components, and simultaneously separate BW and PLI. Their method outperforms EMD, wavelet threshold, and extended kalman filter (EKF) approaches, achieving 10–24 dB of SNRI on the MIT-BIH arrhythmia dataset. The S-transform, which can be seen as a generalisation of the short time Fourier transform (STFT), and an extension of the continuous wavelet transform (CWT) without its disadvantages, has been proposed by Ari *et al.* (2013) [151] to attenuate HFN. This is achieved by removing any components above 200 Hz, and smoothing the boundaries around the QRS complexes, by keeping them intact with a time-domain mask. This strategy outperforms a simple lowpass filter, achieving a SNRI of 10.13 dB and 8.51 dB in removing BW and EMG noise, respectively, on the MIT-BIH arrhythmia dataset. In an investment to reduce the time complexity of computing FFT, Cuomo *et al.* (2015) [152] proposed a recursive linear kernel function in terms of frequency, without requiring to compute the FFT of the signal. Despite it taking only  $O(N)$  in time to run, the schema only removes noise of well-known frequencies bands  $[\mu - \sigma, \mu + \sigma]$ , where  $\mu$  is the central frequency of the noise to remove and  $\sigma$  determines the lower and upper boundaries. The group proved this method can remove stationary BW, achieving similar SNR in half the time the traditional FFT filtering, and superior SNR to lowpass filtering, median or moving average filtering.

**Frequency Complex Demodulation.** Still in the high-resolution paradigm, Hossain *et al.* (2021) [135] experimented a variable frequency complex demodulation (VFCDM), based on the Hilbert transform, into 12 non-overlapping bands from 0 to 180 Hz ( $f_s/2$ ), each with a 15 Hz range, and only keeps the ones that most contribute to the biopotential typical morphology, while rejecting the others. The 1<sup>st</sup> band contained the P and T waves and was kept as is. From the 2<sup>nd</sup> to the 4<sup>th</sup> bands, the QRS complexes were isolated with a Tukey mask, then being added to the first band, the result being the reconstructed signal. The 5<sup>th</sup> band and onwards ( $> 75$  Hz) were considered noise, and were therefore eliminated. Their algorithm outperformed DWT, NLM and EMD conventional approaches in every aspect, including 4–11 dB SNR improvement in signals with added Gaussian white noise, 5–29 dB SNR improvement in signals with added PLI, and 5–18, 0.5–7.6 and 5–23 dB SNR improvement in signals with added blue, pink and violet noise, respectively. Regarding real BW, EMG and EN contaminated armband signals, their algorithms achieved SNR improvements of 4–22, 4–14, 4–10 dB, respectively. The Hilbert transform is computed usually based on its relation with the FFT, hence it inherits its time complexity of  $O(N \log(N))$ .

**Decomposition into IMFs.** Zhang *et al.* (2020) [153] decomposed ECG with EMD, discarded the residue, and sorted the IMFs by frequency. The ones of lower frequency are discarded as noise, based on the assumption of presenting less local maxima than the number of R peaks in the ECG. The ones of higher frequency are recursively thresholded, meaning the local maxima and minima of these IMFs are recursively set to zero if lower than a threshold, until there are no more maxima and minima. The processed IMFs are then reconstructed. This method achieves an SNRI of 11–21 dB in removing BW from the MIT-BIH arrhythmia dataset, however a poorer 0–7 dB improvement in removing EMG and EN [153]. Rakshit *et al.* (2018) [154] use EMD to decompose the signal and apply wavelet (*sym7*) soft thresholding on the detail coefficients of IMFs 1 to 3, aiming at reducing HFNs, while preserving QRS complexes. Then, an adaptive switching mean filter is applied to further improve signal quality on non-QRS regions. This requires R peak correction after, for they get attenuated. On the MIT-BIH arrhythmia dataset, with EMG, PLI, and white noise, this approach achieves minimal MSE (0.0005–0.01) and SNRI of 5.7–9.3 dB, 7.1–14.2 dB, and 5.9–10.3 dB, respectively, outperforming wavelet with and without ADTF, and EKF [154]. Kumar *et al.* (2018) [133] use a standard deviation measure to quantify noise in the signal, and, using EMD, decompose the signal into a number of IMFs proportional to that measure. The QRS boundaries are identified in an IMF, and a Tukey window is used to isolate them, while eliminating other components, the result of which is then added to the other IMFs. This preserves the QRS complexes and attenuates some white noise in other regions. Finally a NLM filter is applied to the EMD output, with a window also proportional to that standard deviation measure, completing the denoising process. On white and coloured Gaussian noises added to the MIT-BIH arrhythmia dataset, both techniques together (EMD + NLM) add up to an SNRI of 4 dB higher, and a MSE half of that when used alone. The strategy slightly outperformed wavelet thresholding form other authors [133]. Another work with white noise on the same dataset also achieved lower MSE with NLM than with wavelet thresholding, and EMD with wavelet thresholding [134]. Bing *et al.* (2020) [155] also decompose the noisy signal into a set of IMFs, but with high-order synchrosqueezing transform (FSSTH), an extension of the STFT, instead of EMD, eliminates the ones considered noisier, and filters the remaining ones with a NLM filter. This strategy proves to achieve a SNRI of 2–2.5 dB higher than without the IMFs preselection, although with an execution time 4–5 times higher. It also achieves a SNRI 5–7.5 dB higher than that of traditional STFT thresholding [155].

**Adaptive Algorithms.** Several approaches to model different types of noise using the RLS [53, 111, 156, 157] and LMS [53, 98, 157, 158] algorithms, or improved versions of them, have been proposed. Annex Table 5 shows a technical summary of these filters. An adaptive RLS filter achieved almost double of SNRI and half of MSE than EMD, wavelet thresholding, average and median filters, and highpass filters in removing BW and MAs from the MIT-BIH arrhythmia dataset [111]. Besides, when it comes to abnormal ECG signals, the adaptive RLS filter was the only one that did not cause distortions on the signals when correcting them. Some works developed EKF to remove EMG and MAs [159], although their performance was overall worst than EMD and wavelet methods in the MIT-BIH arrhythmia dataset [154]. Lazaro *et al.* (2020) were able to compute HR from a wearable armband with 0.08 bpm bias, by removing EMG noise with normalized least mean squares (NLMS) using an estimation of EMG extracted using principal component analysis (PCA) from one of the electrodes [158]. Their system also included an artifact detector, discussed below. Subtraction of the LMS estimated BW, EMG, EN, and white noise yields lower MSEs than subtracting those estimated by RLS, however RLS estimates for static PLI yield lower MSEs [53]. Conversely, in another work, when PLI frequency drifts  $\pm 1$  Hz, an LMS algorithm yielded higher SNRI than RLS [157]. To reject PLI, EKF has proved more effective in its frequency and amplitude estimation than RLS, both in the MIT-BIH arrhythmia dataset and in NC dynamic conditions [156]. Javed *et al.* (2020) proved that using a variable stepsize and a regularization factor in LMS yields lower deviation from the clean ECG without PLI [98]. Lee and Chung (2009) experimented an adaptive filter on stress ECG (while running) collected from a T-shirt, that used ACC as noise reference of BW and MAs and, although it showed visually good quality outputs, it was not quantitatively evaluated [160]. Also on a T-shirt, other group, Lee and Kim (2016), showed that BW and MAs could be better estimated using Quadratic Variation (QV), and their subtraction from the signal improves R peak detection from 85% to almost 100% compared to adaptive filtering using ACC as noise reference [161].

**Denoising Autoencoders.** Annex Table 6 summarises various architectures of DAEs, usually with convolutional layers, that improve the SNR of ECGs from the MIT-BIH arrhythmia dataset, contaminated with noises from the MIT-BIH stress database [139, 162, 163]. With a simple 2-layer DAE, Xiong *et al.* (2015) [139] achieved at least 4 times higher SNRI and ten times lower MSE than a wavelet soft thresholding method, in denoising BW, EMG, and EN. Instead of taking raw ECG, Xia *et al.* (2018) [103] method first subtracts two median filters (200 ms, 600 ms) to correct baseline, the product being then fed to the DAE. This strategy worked impeccably in arrhythmia classification. Abecassis *et al.* (2018) [138] developed a DAE that takes ACC as noise reference to completely remove EMG noise. Their results outperformed with distinction EMD and wavelet-based methods from other authors. For a wearable armband, Reljin *et al.* (2020) [164] proposed a DAE that uses STFT images of raw ECG with various coloured noise, which improves the detection of R peaks in 30.7%.

**Motion Detection.** After wavelet decomposition, a moving integration window applied to the lowest-frequency coefficients has been successfully proposed to detect motion artifacts in stress (running) ECG, with a false detection rate and miss rate both of 0.83% [74]. When multiple ECG channels are available, it has been suggested to look for disturbances to be correlated in all channels, and to classify them as artifacts [108], however this most likely will not be our case. Nonetheless, correlations with ACC channels contribute to the detection of motion artifacts. Based on the first derivative of ACC chest signals, a change in position while sleeping can be useful to discard ECG segments as artifacts [165]. Instead of using ACC as reference, another group suggests to find correlations between the electrode-skin impedance signal and the potential of the ECG signal, and if correlation is absent by a certain threshold, then the segment must be an artifact [166]. Machine learning techniques have also been successful. For their wearable armband, Lazaro *et al.* (2020) [158] develops a support vector machine (SVM) to discriminate between normal and artifact segments, based on ECG features like entropy, kurtosis, skweness, auto-correlation, and frequency power, which attained a sensitivity and specificity, respectively, of 92.05% and 90.00%. An A-fib convolutional neural network (CNN) fusion classifier proposed by Zhang *et al.* (2020) [167] is also able to identify noisy segments using STFT images of the signal, for which it attains a remarkable F1-score of 1.00. Pawar *et al.* (2007) [168] use PCA to learn different heartbeats, as observations represented as eigenvectors, and sort them according to their eigenvalues, on the assumption that the ones with the highest eigenvalues represent motion artifacts, and should, therefore, be discarded. The group trained different classifiers for different activities, having one of them achieved a mean 92.44% accuracy in detecting artifacts caused by arm movements, walking, and climbing up and down stairs. Banerjee *et al.* (2021) [96] also use PCA to extract features of five consecutive clean heartbeats that occur before each corrupted heartbeat. Here, the eigenvector with the highest variance is classified as MA, and a Monte Carlo filter (MCF) achieving a 0.033–0.051 root mean squared error (RMSE) on the MIT-BIH arrhythmia dataset is also proposed to attenuate the MAs, instead of discarding the segment.

MCFs are a type of particle filter able to predict a clean sample based on a noisy observation, and they work very well in nonlinear and non-Gaussian conditions [96].

### 3.2 EDA Denoising and Artifact Removal

**Traditional Filtering.** The predominant frequency of EDA is [0.017, 0.25] Hz, hence removing PLI, electrode instability, myogenic potentials, and other high-frequency components is fairly straightforward with a lowpass filter at 0.25 Hz, a moving average filter, or exponential smoothing [79, 169, 170]. To remove baseline wander and slow drifts induced by changes in temperature and humidity, a highpass filter at 0.05 Hz has proven effective [171, 172]. Traditional methods for artifact correction consist also of lowpass filtering [173], exponential smoothing [174], moving average filtering [172, 175], and Kalman filtering [176]. These techniques present limitations or are incomplete at denoising: some are unable to correct high-amplitude artifacts; some indiscriminately filter the whole signal, ending up distorting segments without artifacts; some assume noise is stationary and are not suitable for unpredictable environments; and some are only suited for offline analysis, for they demand a high computational power [177, 178].

**White Noise.** Tronstad *et al.* (2015) [176] developed an extended Kalman filter that removes white noise from palmar EDA with similar RMSE (0.27) to that of a lowpass filter, although it is better at removing artifacts, caused by brief losses of electrode contact, than a simple lowpass filter. Kalman filters are intended to model signals and reconstruct their original morphology, and for that reason the authors reported the filter needed more than half a minute to obtain stable state estimates for its parameters, which makes them unsuitable for online denoising. Thiam *et al.* (2020) [179] experimented three autoencoder (AE) strategies to remove white noise from finger's EDA for posterior classification. Their models are able to remove the white noise of EDA with an average MSE of 0.041–0.051.

**Wavelets.** Four groups have proposed wavelet thresholding algorithms to remove motion artifacts from EDA signals, and the specifications of them are summarised in Table 7. All of them prefer to decompose the signals with stationary wavelet transform (SWT) rather than with DWT. The computed wavelet coefficients that show a high variance when fitted to well-known distributions are removed, for being considered artifacts. Chen *et al.* (2015) [180] decompose each segment in 8 levels using the *haar* wavelet, and fit the wavelet coefficients to two Gaussian distributions: one representing the SCL activity, one representing the SCR activity. This is known as a gaussian mixture model (GMM). To make this modeling, the limiting computation of this method becomes the use of expectation-maximisation to estimate the Gaussian parameters for each of the eight levels, for which we know it takes  $O(N+2N^2)$  in time [181]. Lowast and Veerabhadrappa (2020) [182] experimented a similar approach with two Daubechies wavelets, *db4* and *db14*, and also *brior3.5* and *sym4*. No differences in denoising BW were found. Shukla *et al.* (2018) [177] fit the highest level wavelet coefficients, i.e., the detail coefficients that represent noise, with a Laplace distribution of zero mean,  $\mathcal{L}(0, b)$ , using maximum-likelihood to estimate the scale parameter,  $b$ . A threshold on high variations in the distribution is also applied. The group achieved a better performance when using *haar* as mother wavelet, than when using *db3*. Moreover, this approach takes only  $O(N)$  in time. Swangnetr and Kaber (2013) [183] experimented a similar approach, where it was shown that when using *db1* and *db5* a higher MSE is obtained than with *db3*. As summarised in Table 7, in tests conducted by [177], with the same dataset, on the same machine, we can infer that the approach followed by Swangnetr and Kaber showed a lower artifact power reduction (APA) than the remaining works, nonetheless in terms of normalized mean squared error (NMSE) it is significantly better than the other alternatives ( $p < 0.001$ ). Furthermore, the *haar* wavelets show slightly better APA than the other mother wavelets, and the *haar* version of Shukla *et al.* [177] significantly outperformed the one of Chen *et al.* (2015) [180] ( $p < 0.001$ ). Additionally, the Shukla *et al.* (2018) approach comes with a very cheap time complexity: On the same empirical evaluation, the method of Shukla *et al.* (2018) with Laplacian distributions is about 863 times faster than the the one of Chen *et al.* (2015) with Gaussian distributions [177].

**Waveform fitting.** Other techniques relying on the EDA morphology, but not using wavelets, have also been proposed. Greco *et al.* (2016) [184] use quadratic programming<sup>7</sup> and maximum *a posteriori* probability (MAP) to estimate three parameters that model the SCL and SCR waveforms without noise. These techniques have limited  $O(N^3)$  time complexity [185]. Shukla *et al.* (2018) [177] compared this method on the same machine and same dataset as above, for which, although it yielded a somewhat similar performance (APA = 5.89 dB; NMSE = -1.89 dB), it run 1254 times slower than their own proposed method, and 1.5 times slower than

---

<sup>7</sup> Techniques to optimize multivariate quadratic functions.

the method of Chen *et al.* [180]. Kelsey *et al.* (2017) [170] proposed a curve fitting method from a dictionary they have created with artifact-free SCR waveforms and SCR waveforms with artifacts. The acquired signals were downsampled, as much as possible without aliasing, and an optimisation algorithm tried to minimise the difference between these sparse representations and the dictionary templates. In the fields of compressed sensing, this technique is called sparse recovery. Their model achieved 66–96% artifact detection accuracies (Table 8). These fitting techniques require to solve optimisation problems, which, in general, hinder the execution time.

**Motion detection.** Some authors have developed ML detectors of motion artifacts. Table 8 summarises the features, the family of classification models chosen, and their respective performance. Hossain *et al.* (2021) [186] algorithm computes a set of features from 5-second segments, from which the *best* ones were selected for each case by a random forest (RF), and, posteriorly, each segment was classified by a SVM model with an accuracy of 83.85%. The group also obtained a similar accuracy with a RF classification. Anusha *et al.* (2019) [169] also tested different models, the best accuracy of 97.83% having been achieved with a k-nearest neighbours (kNN) classifier. From the models tested, the group's Naïve-Bayes (NB) classifier also detected motion artifacts with a good accuracy of approximately 95%. Zhang *et al.* (2017) [187] also tested different models on 5-second segments, and the best detection sensitivity-specificity area under the curves (AUCs) of 0.937 and 0.935 were achieved by RF and logistic regression classifiers, respectively. An unsupervised model, called kNN distance also achieved an AUC of 0.930. Although, training and testing the models on different datasets showed higher performances on the kNN and SVM classifiers, with AUCs respectively of 0.946 and 0.944. Extracting the same set of features from ACC signals and feeding them together with EDA features to the models, yielded the logistic regression classifier a slightly higher AUC of 0.941. Taylor *et al.* (2015) [188] also presented an SVM model trained with features from 5-second segments, which achieved a 95.67% accuracy. In all these four works, the models were trained at least with features extracted from the raw or filtered signals, from their first and second derivatives, and from wavelet coefficients.

**How to spot artifacts or invalid segments.** Taylor *et al.* (2015) [188] collaborated with experts that agreed on a set of criteria to find artifact segments in EDA. Those are (i) an SCL below 0; (ii) a quantization error superior to 5% of amplitude; (iii) a sudden change in amplitude correlated with motion; and (iv) a peak without exponential decay. The third criterion should be considered wisely in our application: we cannot discard a segment simply because an ACC sensor shows abrupt motion, since some epileptic seizures present strong motor components. The fourth criterion can be valuable since we know SCR peaks present a decay exponential period, as introduced in Section 2. However if two peaks follow one another, the decay response of the first gets *silenced* by the second peak, which does not constitute an artifact. Zhang *et al.* (2017) [187] added a fifth criterion defending that, although EDA can suddenly increase due to sweat release, there is no physiological mechanism for a sudden EDA decrease, therefore: (v) a sudden drop of more than  $0.1\mu\text{S}$ . However, before 2013 there was not a consensus these quick increases and decreases could not be produced by human physiology, therefore segments presenting such slopes would be rejected [189–191]. Also other morphological features such as maximum and minimum amplitude, and minimum width of an SCR wave have been considered [190,191]. Kleckner *et al.* (2018) [192] proposed three rules to mark EDA segments as invalid for further processing. The first rule checks whether EDA amplitude is out of the normal range of 0.05 to  $60\mu\text{S}$ , since that could mean the electrode lost contact with the skin or that the circuit is overloaded. Human analysis used to follow this rule, as well as to check for a minimum width of SCR waves [190,191]. The second rule checks whether EDA amplitude changes too quickly, faster than  $\pm 10\mu\text{S.sec}^{-1}$ , which could represent high-frequency artifacts. The third rule checks – with a different sensor – whether the temperature is out of the normal range of 30 to  $40^\circ\text{C}$ , which could mean the sensor is not being worn. They proposed an algorithm that whenever one of these conditions holds, the segment and its surroundings are discarded, which showed an accuracy of 92% with inter-rater expert annotation.

**Respiration-induced artifacts.** Lee *et al.* (2020) [172] proposed to use photoplethysmography (PPG) as respiration noise reference to clean EDA from respiration-induced artifacts. The respiratory rate or volume of air breathed influences the intrathoracic blood volume pressure (BVP), and consequently the one that can be measured on the wrist by a PPG sensor [193,194]. Hence, irregular respiration is expressed as abnormalities in the PPG signal [195]. The group's algorithm extracts the respiratory induced intensity variation (RIIV) signal from the PPG, segments it in windows of 5 breaths (5 peaks), extracts eleven morphological features from each segment, and trains them in a multisource domain-adversarial network (MDAN) classifier, that detects respiration abnormalities with 84.9% accuracy. Following that, peak clusters are identified on the EDA signal, and the ones that are temporally aligned with the detected respiration abnormalities are corrected. This correction assumes the respiration abnormality and EDA are additive, hence the first is subtracted

from the second's amplitude. Although the authors do not individually evaluate the denoising component of their system, the overall algorithm, which was meant to detect high stress levels, performed better in computing stress metrics than the ones of Chen *et al.* (2015) and Greco *et al.* (2016). To our knowledge, this is the only method published that targets the removal of respiration-induced artifacts from EDA in wrist wearables. Other two studies were able to attenuate respiration-induced artifacts from respiration signals acquired from a belt sensor [195, 196].

### 3.3 ACC Denoising

**Time domain filtering.** The cheapest way to improve ACC signal quality is to smooth it with a median filter or a moving average filter [197, 198]. This process can come with a downsampling effect, or not, depending on the window overlap when traversing the signal. If it does, and one does not want to loose samples, oversampling should be performed prior to these filters being applied. These filters are excellent in removing noise that can be modelled as Gaussian, such as small vibrations cause by tremors, in removing sensor noise and variability, caused by sensor precision and sensibility, and in removing HFN spikes. In practical terms, they end up rejecting high frequencies, so this process reassembles the effect of lowpass filters. A Gaussian filter has also been experimented to attenuate high frequency components, ending up removing minor features and sharpening features like walking [199]. Kalman filters have also shown good results in attenuating measurement noise, tend components, and random white noises due to vibration, temperature, and electromagnetic interference [200–203].

**Frequency domain filtering.** Lowpass filtering at a cutoff superior to the bandwidth, or lower if one does not need higher frequencies, is also employed to clean ACC signals [204, 205]. Highpass filtering (e.g. > 0.05 Hz) may also reduce very slow components. One group has proposed to remove the gravitational acceleration component with a highpass FIR filter at 0.25 Hz [197]. Another group applies a 0.25–13 Hz bandpass filter in a system for detecting epileptic seizures [71]. Despite frequency-based techniques showing good empirical results, from a theoretical point of view, if we want to remove Gaussian noise that is *equally* distributed throughout *all* frequencies, any frequency-based technique is somewhat incomplete, for they do not remove noise present inside the passband. Besides, converting signals to the frequency domain adds more computational cost than processing them directly on the time domain, as median or average filters do. Hence, and since there is no need for high-resolution ACC signals, these methods can be excessive for our application.

**Wavelet thresholding.** Wavelet decomposition and subsequent coefficient thresholding to remove electronic noise and HFN of signals collected from a wearable capacitive ACC has been developed [91]. Wavelets have also been proposed to remove white noise and circuit electronic noise from industrial high-g ACC signals [206, 207], but, again, we will not be dealing with high-g signals.

**Total variation denoising.** Total variation (TV) methods have been employed to simplify 1D signals that keep varying between plateaus, by cleaning those while keeping sharp edges between transitions [208]. This method has shown greater SNR improvement than lowpass filters in removing circuit and environmental noise [205]. Since our ACC signals are to be acquired during everyday mobility, and not during *plateau-like* activities (e.g. lifting weights), these method could hide important features for seizure classification.

**Autoencoders.** In a strategy to get rid of noise and extract meaningful representations of movement all at once, DAEs have been widely used and successful in activity classification tasks in wearables [209–213]. This unsupervised approach to AEs is not trained to output clean signals, like some presented before for ECG, but rather to output meaningful tensors, that map inputs to useful intermediate representations, which, in turn, improve the accuracy of subsequent classification, therefore encompassing both denoising and feature extraction steps all in one model. Besides this advantage, running AEs online is usually cheap in time. Unsupervised AE techniques can also output the denoised signals rather than an intermediate feature representation, in which case we can directly evaluate the improvement in signal quality. Recently, a deep learning AE was shown to increase the SNR of wearable ACC signals by 30.2 dB, which lead to an increase in 55.3% in recognising locomotion activities [214]. This denoising process was better than a Kalman filter.

## 4 Solution Proposal

The goal of this work is to develop a biosignal digital denoising and artifact removal module to be integrated and be part of a larger system of seizure monitoring. To meet the needs of this larger system, this module

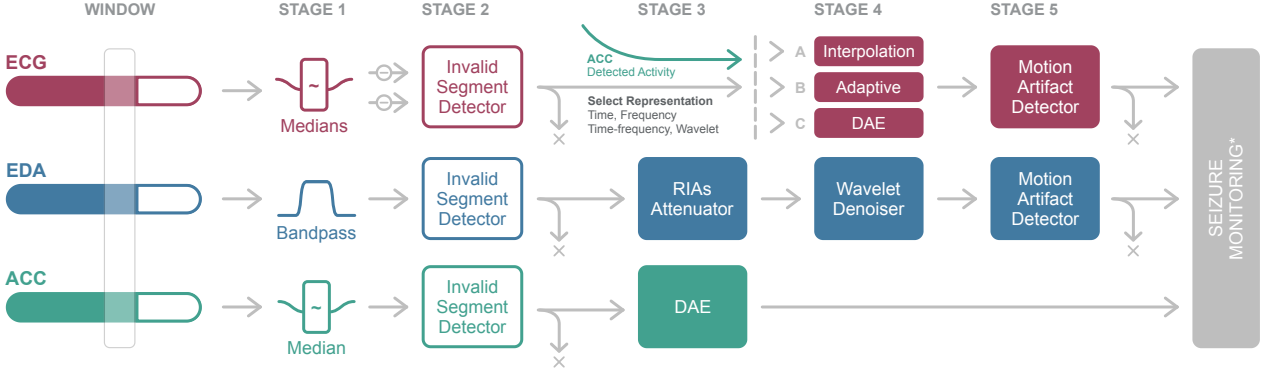


**Fig. 5.** Top-level architecture of the system to be developed. A moving window slides through the timeseries, each of which is processed individually in submodules. ECG pipeline is in red. EDA pipeline is in blue. ACC pipeline is in green. The \* grey block is to be included in the system, but to be developed in another work apart from this one.

is required to: (i) Be suitable to run online, presenting at most linear time complexity, and (ii) Be completely automatic, without the need of human intervention to continually adjust parameters.

#### 4.1 Top-level Architecture

With these requirements in mind, a solution of the module to be developed is here proposed, for which Figure 5 schemes its top-level architecture. The three biosignal timeseries – ECG, EDA, ACC – are given as input to the system in its raw form by the respective analog-digital converters (ADCs). Any conversions to meaningful units should be computed at this stage. A sliding window will segment the timeseries as they become available, and create individual segments (e.g. of 3 seconds) to be processed individually. This processing is done independently for each biosignal modality, in its respective submodule, each one comprising multiple processing stages. Let us analyse each processing submodule.

The **ECG submodule** will bandpass filter each segment, by subtracting two median filters, one with a 200 ms window, and the other with a 600 ms window, as suggested by [103, 107, 128]. These window lengths should, based on HR frequency changes, retroactively adapt through the course of acquisition, so that they correctly capture all waves. Next, invalid segments should be discarded, such as when there is no signal because electrodes have lost contact, or when the signal is saturated at the lower or upper amplitude limits. In the next stages, we should develop some different methods and draw a comparative analysis between them, not only in terms of signal enhancement versus computational complexity, but also in terms of their performance given the environmental conditions. The whole-system architecture will include some activity detector, based on the ACC signal, and that information shall be used to guide the ECG submodule to dynamically exchange between different models, if necessary, each of which specifically engineered to tackle denoising during those activities. A couple of examples should make this clearer. Let us say the patient can be sleeping, eating, or running. In the first scenario, most of the time the body should be motionless, except for the breathing motion of the rib cage, in the case our wearable stays on the chest, hence simple methods like interpolation are sufficient to complete denoising and correct baseline to zero [130]. In the second scenario, the patient will perform repetitive movements bringing cutlery near the mouth, along with other movements, so to be repetitively changing the model would hinder the system performance. Perhaps the system would consume more resources reasoning about which model to use, rather than using one. Therefore, an adaptive filtering algorithm like the LMS should be experimented to model different noise morphologies and remove them, as suggested by [98, 157, 158]. Moreover, the LMS algorithm presents a very low time complexity, as consistently demonstrated in the literature, nonetheless other adaptive schemes should be experimented as well. Wavelet thresholding will also be experimented to address MAs, given its proven effectiveness [99, 108]. If DWT is employed, a mother wavelet of the *sym* family should be our first choice [141], but to correct high-frequency drifts the *meyer* wavelet has proven more effective [142]. In the third scenario, when a patient is running, or in any other stress conditions, we can expect a highly degraded ECG signal, with different noise and artifact morphologies, and no clear pattern to distinguish them. As so, DAEs will be studied to enhance the signal as much as possible, or at least to allow the R peaks to be correctly identified. As reviewed in [103, 138, 139], DAEs can be extremely effective, compared to other techniques, in removing EMG noise and MAs in chaotic environments, and additionally they are

patient-specific. These strategies for these and other scenarios will be compared, as well as other models that may present as suitable along the research. Finally, a motion artifact detector should be included as the last processing stage, with the goal of discarding any segment that even after denoising is severely hindered by MAs, so that it does not influence the subsequent seizure monitoring stage. Some ML detectors here reviewed have proven to be suitable for this kind of classification [158, 167, 168]. All valid segments that are not discarded should be delivered for seizure monitoring, or we might think of other outputs to deliver in the cases that there is still too much noise, like, for instance, in the running scenario, where the DAE might directly extract ECG features, or in other scenarios where only the R peaks are visible and, therefore, only the RRI signal is delivered. This is of concern because discarding many segments may lead to overdeleting time intervals from which the extracted HR could still be of value. This matter will also be dependent on what the seizure monitoring module requests at each timepoint.

The **EDA submodule** will apply a bandpass filter (or separated lowpass and highpass filters) to each segment. In the works previously reviewed, we could see that bandpass filtering is effective and sufficient to remove very high and very low frequency noises. Next, just like in ECG, each segment should be discarded if invalid. An invalid EDA segment is one that matches some of the criteria indicated by [187, 188, 192], or its amplitude is saturated at the lower or upper amplitude limits. Valid segments then proceed to three processing stages. We should analyse if our datasets present a significant proportion of RIAs, and, if they do, the first stage should be their attenuation. This should be done using RIIV timeseries, which has proven to be a very effective proxy for RIAs [172], from which they can be detected and corrected, although its efficiency remains yet to be addressed. On the next stage, wavelet thresholding should be considered to attenuate BW and MAs. Wavelet methods have proven to be useful denoising methods [177, 180, 182, 183], that rely on prior knowledge of noise-free EDA morphology to compute the *differences* and find MAs. If employed, the *haar* window should be used, since it better captured sudden changes of MAs effectively. On the last stage, denoised segments that still present significant MAs should be discarded. Hard detection of artifacts should consider the indications of [187, 188]. For ML detection, RF, SVM and kNN classifiers have proven useful in the automatic detection of MAs [169, 187, 188], hence they will be compared and the one with highest performance should integrate the system. All valid segments should be delivered for seizure monitoring.

The **ACC submodule** should start by applying each segment a median filter to smooth its trace. Each segment should then be discarded if invalid. An invalid ACC segment would be one that its amplitude is saturated at the lower or upper amplitude limits, which, for instance, in Bitalino are  $\pm 3g$ . A DAE, like the ones introduced in Section 3 should be experimented, to compare if the subsequent seizure detection task is improved or not. If the cost-benefit relation would come to not be reasonably justified, the DAE should not be included. Roughly speaking, a case of that would be, for example, an increase of seizure detection accuracy in 2% with a cost of doubling the processing time. Either way, the smoothed valid segments or the DAE output representation should be delivered for seizure monitoring.

These stages of denoising and artifact removal, and their combinations, should all be evaluated in order to improve the metrics described ahead in Section 5. If the cost-benefit of one stage is not worth it, it should not be part of the system. Stages that are able to denoise multiple types of noise with a single algorithm are also preferred, since, as aforementioned, they constitute a serious advantage in reducing the execution time.

## 4.2 Preliminary Results

During this semester, the approaches proposed by Cuomo *et al.* (2015) [152], Chiang *et al.* (2019) [162], and Abecassis *et al.* (2018) [138] have been experimented on the ECG data of patients wearing our chest-abdomen band at HSM. The software implementations and conducted tests can be found in <https://github.com/jomy-kk/EpilepsyLab>.

The first approach, as reviewed in the previous Section, denoised PLI (50 Hz) well, assuming it is static, and it successfully removed BW as well. Despite the scheme being time efficient ( $O(N)$ ), it requires to know the BW frequency *a priori*. This is a disadvantage, firstly because these frequencies change with the environment and activities, and secondly because it is hard to guess these frequencies without making some spectral study. Besides, visual analysis revealed the method can introduce some artifacts, and it causes ringing effects on the edge of segments.

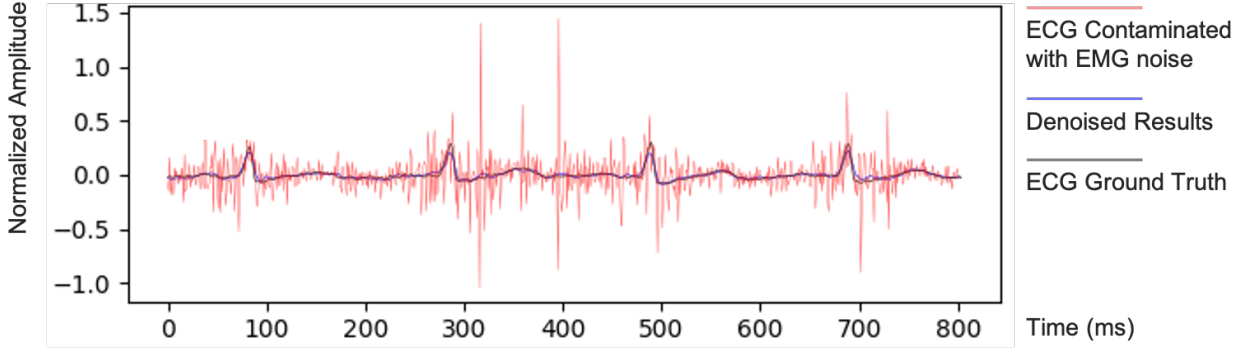


**Fig. 6.** Example of the denoising process of the DAE proposed by [138], on the ECG obtained from a patient with epilepsy in HSM, contaminated with real EMG noise added posteriorly. This is a result obtained with a model trained with 500 epochs with a termination loss of 0.0334.

The second approach is a DAE with 6 convolutional and 7 deconvolutional layers. Although, the authors report good results, in our dataset this DAE performed no better than a random model, hence we will not continue studying it. The third approach is also a DAE, with 2 convolutional and 3 deconvolutional layers, that, as aforementioned, uses ACC signals as a noise reference to achieve EMG denoising. This works under the premise that ACC signals encode movement information, which, in turn, is generated by muscle activity. We can think of it as the ACC channels being the observable variables, and the EMG noise as being the hidden variable. Testing on the MIT-BIH arrhythmia dataset, the results reported by the authors are confirmed: ECG signals severely polluted by EMG noise can be cleaned using the model. Testing on our HSM dataset, these results are also confirmed, specifically SNRIs of 6.44–7.87 dB are achieved for different EMG noise levels. Figure 6 shows an example of this remarkable denoising process. Moreover, the model has a linear execution time, and only requires 50 to 70 epochs of training to attain its optimal performance. Therefore, this model will continue to be studied in order to improve it in future versions.

## 5 Empirical Evaluation

### 5.1 Performance Metrics

Recall that, in our formalism defined in Section 2,  $\mathbf{x}$  stands for the noisy input signal to process,  $\hat{\mathbf{y}}$  stands for the output denoised signal, and  $\mathbf{y}$  stands for the ground truth clean signal. The methods to be developed in this work will be evaluated by the same metrics the methods here reviewed were, which are common practice in the signal processing community. Those are the SNR (dB), previously described in Equation 3, and, consequently, the  $SNRI = SNR(\hat{\mathbf{y}}) - SNR(\mathbf{x})$  (dB). Other measures in dB typically employed are the APA and signal error ratio (SER), defined below:

$$APA \text{ (dB)} = 10 \cdot \log_{10} \frac{Var[\mathbf{y}]}{Var[\hat{\mathbf{y}}]} , \quad SER \text{ (dB)} = 10 \cdot \log_{10} \frac{\hat{\mathbf{y}}^2}{(\hat{\mathbf{y}} - \mathbf{y})^2} ,$$

where  $Var[\cdot]$  is variance. Regarding error functions, usually the MSE, the RMSE, the mean absolute error (MAE), and the NMSE are employed, which are defined below:

$$MSE = \frac{(\mathbf{y} - \hat{\mathbf{y}})^2}{N} , \quad RMSE = \sqrt{MSE} , \quad MAE = \frac{|\mathbf{y} - \hat{\mathbf{y}}|}{N} , \quad NMSE \text{ (dB)} = 10 \cdot \log_{10} \frac{(\mathbf{y} - \hat{\mathbf{y}})^2}{(\mathbf{y} - \bar{\mathbf{y}})^2} ,$$

where  $\bar{\mathbf{y}}$  is the mean of  $\mathbf{y}$ . The sample indices of the signals are omitted for simplicity. Finally, when identification of some feature, or artifacts, is the performance metric, usually the accuracy,  $Acc$ , sensitivity,  $Sen$ , specificity,  $Spe$ , or F1-score,  $F1$ , are employed, which are defined below:

$$Acc (\%) = \frac{TP + TN}{TP + TN + FP + FN} , \quad Sen (\%) = \frac{TP}{TP + FN} , \quad Spe (\%) = \frac{TN}{TN + FP} , \quad F1 = \frac{2 \cdot TP}{2 \cdot TP + FP + FN} ,$$

where TP is the amount of true positives, TN is the amount of true negatives, FP is the amount of false positives, and FN is the amount of false negatives in the identification of a feature of interest, or artifacts, by some other algorithm applied after denoising.

## 5.2 Datasets for Evaluation

The system will be primarily tested on the data being acquired by the *PreEpiSeizures* group at HSM, but it is also planned to test it on datasets available from other hospitals. There are several open-access ECG datasets in Physionet, from which the MIT-BIH Arrhythmia dataset<sup>8</sup> and the MIT-BIH Noise Stress dataset<sup>9</sup> were extensively benchmarked in the literature here reviewed. There are other datasets there, with T-wave alternates<sup>10</sup>, ST depressions<sup>11</sup>, A-fib<sup>12</sup> and one dataset of ECG of patients with epileptic seizures<sup>13</sup>, that should be used in this work to make the models robust to a variety of scenarios. There is also one in Physionet with ECG with motion artifacts<sup>14</sup>, and another including simultaneous ECG, EDA, ACC and temperature signals<sup>15</sup>. We should also make use of the Australian SEER dataset<sup>16</sup> which include PPG, EDA, ACC, oxygen saturation (SpO<sub>2</sub>) and temperature long-term recordings acquired from a wristband worn by epilepsy patients. The Royal Melbourne Hospital has also collected ECG and respiration signals from epilepsy patients, which could be provided upon request to the group [215]. There is also a plan to acquire ECG, EDA, and ACC signals under stress activities with the wearable from the *PreEpiSeizures* group [29] and the Empatica E4 wristband [216]. A draft proposal for these acquisitions may be found in Annex 2.

## 6 Work Calendarization

The proposed solution should take six months to be developed. In March, a set of biosignals from patients with and without epilepsy, possibly from different institutes, will be gathered. The development of basic biosignal analysis and pre-processing tools will also be completed. In April, May, and June, different algorithms for, respectively, ECG, EDA, and ACC denoising and artifact removal will be separately developed and compared. In July, a battery of offline tests will be carried out, and, possibly, online tests with users may be conducted. The written dissertation document will be finalised by the end of October.

## 7 Conclusion

This review of the state-of-the-art led to the conclusion that real-time and efficient biosignal denoising and artifact removal are two very challenging problems, more so when acquired in uncontrolled environments with non-clinical-grade instruments. This project introduces the necessary knowledge to continue this research: it gives a general picture of the wearable devices for epilepsy monitoring; it introduces the operation principles of three different modalities for acquiring peripheral biosignals of epileptic seizures; and it presents a comprehensive mathematical framework of how those biosignals are susceptible to noise and artifacts. The proposed solution for the dissertation work is to be integrated in a larger system for real-time seizure monitoring, and it aims at three main contributions: a contribution to the patient, a contribution to clinicians, and a contribution to the field of signal processing:

- **Contribution to the patient:** Noise-robust wearable monitoring systems for patients with epilepsy will allow them to continuously be monitored at distance and more comfortably. Also, the disease progression will be able to be continuously accessed, as well as the follow-up on treatment effectiveness, adequacy, and side effects.
- **Contribution to clinicians:** Ambulatory monitoring systems for patients with epilepsy will release pressure from epilepsy monitoring units and disencumber long-term studies. They will also provide more complete and detailed data acquired in real environments.
- **Contribution to the field of signal processing:** Fast and energy-efficient algorithms capable of online biosignal denoising and artifact removal are transversal to many other application areas, making them a currently open problem in signal processing. Developing novel algorithms may help other researchers in their own applications.

<sup>8</sup> <https://physionet.org/content/mitdb/1.0.0/>

<sup>9</sup> <https://physionet.org/content/nstadb/1.0.0/>

<sup>10</sup> <https://physionet.org/content/twadb/1.0.0/>

<sup>11</sup> <https://physionet.org/content/edb/1.0.0/>

<sup>12</sup> <https://physionet.org/content/ltafdb/1.0.0/>

<sup>13</sup> <https://physionet.org/content/szdb/1.0.0/>

<sup>14</sup> <https://physionet.org/content/macecgdb/1.0.0/>

<sup>15</sup> <https://physionet.org/content/noneeg/1.0.0/>

<sup>16</sup> <https://seermedical.com/research-and-publications/>

## References

- [1] R. S. Fisher, C. Acevedo, A. Arzimanoglou, A. Bogacz, J. H. Cross, C. E. Elger, J. Engel Jr, L. Forsgren, J. A. French, M. Glynn, D. C. Hesdorffer, B. Lee, G. W. Mathern, S. L. Moshé, E. Perucca, I. E. Scheffer, T. Tomson, M. Watanabe, and S. Wiebe, "ILAE Official Report: A practical clinical definition of epilepsy," *Epilepsia*, vol. 55, no. 4, pp. 475–482, 2014, eprint: <https://onlinelibrary.wiley.com/doi/pdf/10.1111/epi.12550>. [Online]. Available: <https://onlinelibrary.wiley.com/doi/abs/10.1111/epi.12550>
- [2] WHO, "Epilepsy." [Online]. Available: <https://www.who.int/news-room/fact-sheets/detail/epilepsy>
- [3] J. Pimentel, "O doente epiléptico pode e deve ter uma vida normal," *Público*, Feb. 2020. [Online]. Available: <https://www.publico.pt/2020/02/10/impar/opiniao/doente-epileptico-vida-normal-1902967>
- [4] P. Kwan and M. J. Brodie, "Early Identification of Refractory Epilepsy," *New England Journal of Medicine*, vol. 342, no. 5, pp. 314–319, Feb. 2000. [Online]. Available: <http://www.nejm.org/doi/abs/10.1056/NEJM200002033420503>
- [5] P. Kwan, S. C. Schachter, and M. J. Brodie, "Drug-Resistant Epilepsy," *New England Journal of Medicine*, vol. 365, no. 10, pp. 919–926, Sep. 2011, publisher: Massachusetts Medical Society eprint: <https://doi.org/10.1056/NEJMra1004418>. [Online]. Available: <https://doi.org/10.1056/NEJMra1004418>
- [6] B. Litt and J. Echauz, "Prediction of epileptic seizures," *The Lancet Neurology*, vol. 1, no. 1, pp. 22–30, May 2002. [Online]. Available: <https://linkinghub.elsevier.com/retrieve/pii/S1474442202000030>
- [7] E. H. Al Zaid, "Prevalence of patients with epilepsy unfit to drive," *Journal of Family & Community Medicine*, vol. 26, no. 1, pp. 51–56, Apr. 2019.
- [8] R. Sutter, P. W. Kaplan, and S. Rueegg, "Outcome predictors for status epilepticus-what really counts," *NATURE REVIEWS NEUROLOGY*, vol. 9, no. 9, pp. 525–534, Sep. 2013.
- [9] C. M. DeGiorgio, A. Curtis, D. Hertling, and B. D. Moseley, "Sudden unexpected death in epilepsy: Risk factors, biomarkers, and prevention," *Acta Neurologica Scandinavica*, vol. 139, no. 3, pp. 220–230, Mar. 2019.
- [10] M. Nei and R. Bagla, "Seizure-related injury and death," *Current Neurology and Neuroscience Reports*, vol. 7, no. 4, pp. 335–341, Jul. 2007.
- [11] M. Tombini, G. Assenza, L. Quintiliani, L. Ricci, J. Lanzone, and V. Di Lazzaro, "Epilepsy and quality of life: what does really matter?" *Neurological Sciences*, vol. 42, no. 9, pp. 3757–3765, Sep. 2021, company: Springer Distributor: Springer Institution: Springer Label: Springer Number: 9 Publisher: Springer International Publishing. [Online]. Available: <https://link.springer.com/article/10.1007/s10072-020-04990-6>
- [12] F. M. C. Besag and M. J. Vasey, "Social cognition and psychopathology in childhood and adolescence," *Epilepsy & Behavior: E&B*, vol. 100, no. Pt B, p. 106210, Nov. 2019.
- [13] K. Eichenwald, *A Mind Unraveled: A Memoir*, 1st ed. New York: Ballantine Books, 2018.
- [14] G. D. Cascino, "Video-EEG Monitoring in Adults," *Epilepsia*, vol. 43, no. s3, pp. 80–93, 2002, eprint: <https://onlinelibrary.wiley.com/doi/pdf/10.1046/j.1528-1157.43.s.3.14.x>. [Online]. Available: <https://onlinelibrary.wiley.com/doi/abs/10.1046/j.1528-1157.43.s.3.14.x>
- [15] S. Beniczky and J. Jeppesen, "Non-electroencephalography-based seizure detection," *Current Opinion in Neurology*, vol. 32, no. 2, pp. 198–204, Apr. 2019. [Online]. Available: [https://journals.lww.com/co-neurology/Abstract/2019/04000/Non\\_electroencephalography\\_based\\_seizure\\_detection.5.aspx](https://journals.lww.com/co-neurology/Abstract/2019/04000/Non_electroencephalography_based_seizure_detection.5.aspx)
- [16] E. G. Gutierrez, N. E. Crone, J. Y. Kang, Y. I. Carmenate, and G. L. Krauss, "Strategies for non-EEG seizure detection and timing for alerting and interventions with tonic-clonic seizures," *Epilepsia*, vol. 59, no. S1, pp. 36–41, 2018, eprint: <https://onlinelibrary.wiley.com/doi/pdf/10.1111/epi.14046>. [Online]. Available: <https://onlinelibrary.wiley.com/doi/abs/10.1111/epi.14046>
- [17] S. Rheims, "Wearable devices for seizure detection: Is it time to translate into our clinical practice?" *Revue Neurologique*, vol. 176, no. 6, pp. 480–484, Jun. 2020. [Online]. Available: <https://www.sciencedirect.com/science/article/pii/S0035378720305208>
- [18] F. S. S. Leijten and t. D. T. Consortium, "Multimodal seizure detection: A review," *Epilepsia*, vol. 59, no. S1, pp. 42–47, 2018, eprint: <https://onlinelibrary.wiley.com/doi/pdf/10.1111/epi.14047>. [Online]. Available: <https://onlinelibrary.wiley.com/doi/abs/10.1111/epi.14047>
- [19] M. Zulqarnain, S. Stanzione, G. Rathinavel, S. Smout, M. Willegems, K. Myny, and E. Cantatore, "A flexible ECG patch compatible with NFC RF communication," *npj Flexible Electronics*, vol. 4, no. 1, pp. 1–8, Jul. 2020, bandiera\_abtest: a Cc\_license\_type: cc\_by Cg\_type: Nature Research Journals Number: 1 Primary\_atype: Research Publisher: Nature Publishing Group Subject\_term: Electrical and electronic

- engineering;Engineering Subject\_term\_id: electrical-and-electronic-engineering;engineering. [Online]. Available: <https://www.nature.com/articles/s41528-020-0077-x>
- [20] "Embrace2 Seizure Monitoring Device." [Online]. Available: <https://www.empatica.com/embrace2>
- [21] F. Onorati, G. Regalia, C. Caborni, M. Migliorini, D. Bender, M.-Z. Poh, C. Frazier, E. Kovitch Thropp, E. D. Mynatt, J. Bidwell, R. Mai, W. C. LaFrance Jr, A. S. Blum, D. Friedman, T. Loddenkemper, F. Mohammadpour-Touserkani, C. Reinsberger, S. Tognetti, and R. W. Picard, "Multicenter clinical assessment of improved wearable multimodal convulsive seizure detectors," *Epilepsia*, vol. 58, no. 11, pp. 1870–1879, 2017, eprint: <https://onlinelibrary.wiley.com/doi/pdf/10.1111/epi.13899>. [Online]. Available: <https://onlinelibrary.wiley.com/doi/abs/10.1111/epi.13899>
- [22] "NightWatch device." [Online]. Available: <https://www.nightwatchepilepsy.com>
- [23] J. Arends, R. D. Thijs, T. Gutter, C. Ungureanu, P. Cluitmans, J. V. Dijk, J. v. Andel, F. Tan, A. d. Weerd, B. Vledder, W. Hofstra, R. Lazeron, G. v. Thiel, K. C. B. Roes, F. Leijten, and a. t. D. T.-E. Consortium, "Multimodal nocturnal seizure detection in a residential care setting: A long-term prospective trial," *Neurology*, vol. 91, no. 21, pp. e2010–e2019, Nov. 2018, publisher: Wolters Kluwer Health, Inc. on behalf of the American Academy of Neurology Section: Article. [Online]. Available: <https://n.neurology.org/content/91/21/e2010>
- [24] "Brain Sentinel SPEAC device." [Online]. Available: <https://speacsystem.com/>
- [25] J. J. Halford, M. R. Sperling, D. R. Nair, D. J. Dlugos, W. O. Tatum, J. Harvey, J. A. French, J. R. Pollard, E. Faught, K. H. Noe, T. R. Henry, G. M. Jetter, O. V. Lie, L. C. Morgan, M. R. Girouard, D. P. Cardenas, L. E. Whitmire, and J. E. Cavazos, "Detection of generalized tonic-clonic seizures using surface electromyographic monitoring," *Epilepsia*, vol. 58, no. 11, pp. 1861–1869, 2017, eprint: <https://onlinelibrary.wiley.com/doi/pdf/10.1111/epi.13897>. [Online]. Available: <https://onlinelibrary.wiley.com/doi/abs/10.1111/epi.13897>
- [26] "Pulse Companion." [Online]. Available: <https://alert-it.co.uk/product/pulse-companion/>
- [27] M. A. Frankel, M. J. Lehmkuhle, M. Watson, K. Fetrow, L. Frey, C. Drees, and M. C. Spitz, "Electrographic seizure monitoring with a novel, wireless, single-channel EEG sensor," *Clinical Neurophysiology Practice*, vol. 6, pp. 172–178, 2021. [Online]. Available: <https://linkinghub.elsevier.com/retrieve/pii/S2467981X2100024X>
- [28] "Epitel Epilog seizure monitoring device." [Online]. Available: <https://www.epitel.com>
- [29] A. F. Manso, A. L. N. Fred, R. C. Neves, and R. C. Ferreira, "Real-Time Pervasive Monitoring System for Ambulatory Patients," in *2018 IEEE International Symposium on Medical Measurements and Applications (MeMeA)*, Jun. 2018, pp. 1–6.
- [30] A. S. Carmo, "EpiBOX: A Novel Approach to Long-Term Data Acquisition with Automatic Seizure Detection in Epilepsy," Master's thesis, Instituto Superior Técnico, Universidade de Lisboa, Jan. 2021. [Online]. Available: <https://fenix.tecnico.ulisboa.pt/cursos/mebiom/dissertacao/846778572212828>
- [31] H. E. Scharfman, "The Neurobiology of Epilepsy," *Current neurology and neuroscience reports*, vol. 7, no. 4, pp. 348–354, Jul. 2007. [Online]. Available: <https://www.ncbi.nlm.nih.gov/pmc/articles/PMC2492886/>
- [32] G. G. Somjen, "Ion regulation in the brain: implications for pathophysiology," *The Neuroscientist: A Review Journal Bringing Neurobiology, Neurology and Psychiatry*, vol. 8, no. 3, pp. 254–267, Jun. 2002.
- [33] C. Vaillend, S. E. Mason, M. F. Cuttle, and B. E. Alger, "Mechanisms of neuronal hyperexcitability caused by partial inhibition of Na<sup>+</sup>-K<sup>+</sup>-ATPases in the rat CA1 hippocampal region," *Journal of Neurophysiology*, vol. 88, no. 6, pp. 2963–2978, Dec. 2002.
- [34] T. Grisar, D. Guillaume, and A. V. Delgado-Escueta, "Contribution of Na<sup>+</sup>,K<sup>(+)</sup>-ATPase to focal epilepsy: a brief review," *Epilepsy Research*, vol. 12, no. 2, pp. 141–149, Jul. 1992.
- [35] M. H. Meisler, J. Kearney, R. Ottman, and A. Escayg, "Identification of epilepsy genes in human and mouse," *Annual Review of Genetics*, vol. 35, pp. 567–588, 2001.
- [36] V. I. Dzhala, D. M. Talos, D. A. Sdrulla, A. C. Brumback, G. C. Mathews, T. A. Benke, E. Delpire, F. E. Jensen, and K. J. Staley, "NKCC1 transporter facilitates seizures in the developing brain," *Nature Medicine*, vol. 11, no. 11, pp. 1205–1213, Nov. 2005.
- [37] B. S. Meldrum, "The role of glutamate in epilepsy and other CNS disorders," *Neurology*, vol. 44, no. 11 Suppl 8, pp. S14–23, Nov. 1994.
- [38] M. Barker-Haliski and H. S. White, "Glutamatergic Mechanisms Associated with Seizures and Epilepsy," *Cold Spring Harbor Perspectives in Medicine*, vol. 5, no. 8, p. a022863, Jun. 2015.
- [39] T. Fellin and P. G. Haydon, "Do astrocytes contribute to excitation underlying seizures?" *Trends in Molecular Medicine*, vol. 11, no. 12, pp. 530–533, Dec. 2005.
- [40] S. Duffy and B. A. MacVicar, "Modulation of neuronal excitability by astrocytes," *Advances in Neurology*, vol. 79, pp. 573–581, 1999.
- [41] W. T. Blume, H. O. Lüders, E. Mizrahi, C. Tassinari, W. Van Emde Boas, and J. Engel Jr., Ex-officio, "Glossary of Descriptive Terminology for Ictal Semiology: Report of the ILAE

- Task Force on Classification and Terminology," *Epilepsia*, vol. 42, no. 9, pp. 1212–1218, 2001, eprint: <https://onlinelibrary.wiley.com/doi/pdf/10.1046/j.1528-1157.2001.22001.x>. [Online]. Available: <https://onlinelibrary.wiley.com/doi/abs/10.1046/j.1528-1157.2001.22001.x>
- [42] C. Baumgartner, S. Lurger, and F. Leutmezer, "Autonomic symptoms during epileptic seizures," *Epileptic Disorders*, vol. 3, no. 3, pp. 103–16, Oct. 2001. [Online]. Available: [http://www.jle.com/fr/revues/epd/e-docs/autonomic\\_symptoms\\_during\\_epileptic\\_seizures\\_110095/article.phtml?tab=texte](http://www.jle.com/fr/revues/epd/e-docs/autonomic_symptoms_during_epileptic_seizures_110095/article.phtml?tab=texte)
- [43] F. Leutmezer, C. Schernthaner, S. Lurger, K. Pötzlberger, and C. Baumgartner, "Electrocardiographic changes at the onset of epileptic seizures," *Epilepsia*, vol. 44, no. 3, pp. 348–354, 2003.
- [44] K. Jansen and L. Lagae, "Cardiac changes in epilepsy," *Seizure*, vol. 19, no. 8, pp. 455–460, Oct. 2010. [Online]. Available: <https://www.sciencedirect.com/science/article/pii/S1059131110001573>
- [45] C. Opherk, J. Coromilas, and L. J. Hirsch, "Heart rate and EKG changes in 102 seizures: analysis of influencing factors," *Epilepsy Research*, vol. 52, no. 2, pp. 117–127, Dec. 2002. [Online]. Available: <https://www.sciencedirect.com/science/article/pii/S0920121102002152>
- [46] B. J. Dlouhy, B. K. Gehlbach, C. J. Kreple, H. Kawasaki, H. Oya, C. Buzzia, M. A. Granner, M. J. Welsh, M. A. Howard, J. A. Wemmie, and G. B. Richerson, "Breathing Inhibited When Seizures Spread to the Amygdala and upon Amygdala Stimulation," *The Journal of Neuroscience: The Official Journal of the Society for Neuroscience*, vol. 35, no. 28, pp. 10 281–10 289, Jul. 2015.
- [47] S. Sivathamboo, T. N. Constantino, Z. Chen, P. B. Sparks, J. Goldin, D. Velakoulis, N. C. Jones, P. Kwan, V. G. Macefield, T. J. O'Brien, and P. Perucca, "Cardiorespiratory and autonomic function in epileptic seizures: A video-EEG monitoring study," *Epilepsy & Behavior: E&B*, vol. 111, p. 107271, Oct. 2020.
- [48] C. J. Klein, M. H. Silber, J. R. Halliwill, S. A. Schreiner, G. A. Suarez, and P. A. Low, "Basal forebrain malformation with hyperhidrosis and hypothermia: variant of Shapiro's syndrome," *Neurology*, vol. 56, no. 2, pp. 254–256, Jan. 2001.
- [49] H. Yu, D. Yen, C. Yiu, W. Chung, J. Lirng, and M. Su, "Pilomotor seizures," *European Neurology*, vol. 40, no. 1, pp. 19–21, Jul. 1998.
- [50] O. Devinsky, A. Vezzani, T. J. O'Brien, N. Jette, I. E. Scheffer, M. de Curtis, and P. Perucca, "Epilepsy," *Nature Reviews Disease Primers*, vol. 4, no. 1, pp. 1–24, May 2018, bandiera\_abtest: a Cg\_type: Nature Research Journals Number: 1 Primary\_atype: Reviews Publisher: Nature Publishing Group Subject\_term: Diagnosis;Epilepsy;Therapeutics Subject\_term\_id: diagnosis;epilepsy;therapeutics. [Online]. Available: <https://www.nature.com/articles/nrdp201824>
- [51] R. S. Fisher, J. H. Cross, J. A. French, N. Higurashi, E. Hirsch, F. E. Jansen, L. Lagae, S. L. Moshé, J. Peltola, E. Roulet Perez, I. E. Scheffer, and S. M. Zuberi, "Operational classification of seizure types by the International League Against Epilepsy: Position Paper of the ILAE Commission for Classification and Terminology," *Epilepsia*, vol. 58, no. 4, pp. 522–530, 2017, eprint: <https://onlinelibrary.wiley.com/doi/pdf/10.1111/epi.13670>. [Online]. Available: <https://onlinelibrary.wiley.com/doi/abs/10.1111/epi.13670>
- [52] J. L. Semmlow and B. Griffel, *Biosignal and medical image processing*, third edition ed. Boca Raton: CRC Press, Taylor & Francis Group, CRC Press is an imprint of the Taylor & Francis Group, an Informa business, 2014.
- [53] F. Mohaddes, R. L. da Silva, F. P. Akbulut, Y. Zhou, A. Tanneeru, E. Lobaton, B. Lee, and V. Misra, "A Pipeline for Adaptive Filtering and Transformation of Noisy Left-Arm ECG to Its Surrogate Chest Signal," *Electronics*, vol. 9, no. 5, p. 866, May 2020, number: 5 Publisher: Multidisciplinary Digital Publishing Institute. [Online]. Available: <https://www.mdpi.com/2079-9292/9/5/866>
- [54] M. Kutz, *Biomedical Engineering and Design Handbook, Volumes I and II (2nd Edition)*. New York, USA: McGraw-Hill Professional Publishing, 2010, oCLC: 958553882. [Online]. Available: <http://public.ebookcentral.proquest.com/choice/publicfullrecord.aspx?p=4657812>
- [55] E. A. Ashley and J. Niebauer, *Conquering the ECG*. Remedica, 2004, publication Title: Cardiology Explained. [Online]. Available: <https://www.ncbi.nlm.nih.gov/books/NBK2214/>
- [56] B. Farnsworth, "What is EDA? And how does it work?" Jun. 2019. [Online]. Available: <https://imotions.com/blog/eda/>
- [57] R. Edelberg, "Biopotentials from the skin surface: the hydration effect," *Annals of the New York Academy of Sciences*, vol. 148, no. 1, pp. 252–262, Feb. 1968.
- [58] Y. Topoglu, J. Watson, R. Suri, and H. Ayaz, "Electrodermal Activity in Ambulatory Settings: A Narrative Review of Literature," Jan. 2020, pp. 91–102.
- [59] R. C. Wilcott, "Arousal sweating and electrodermal phenomena," *Psychological Bulletin*, vol. 67, no. 1, pp. 58–72, 1967, place: US Publisher: American Psychological Association.
- [60] M. Sharma, S. Kacker, and M. Sharma, "A Brief Introduction and Review on Galvanic Skin Response," *International Journal of Medical Research Professionals*, vol. 2, Dec. 2016.

- [61] T. Aslanidis, "Electrodermal activity: Applications in perioperative care," *International Journal of Medical Research and Health Sciences*, vol. 3, Jul. 2014.
- [62] D. R. Bach, K. J. Friston, and R. J. Dolan, "An improved algorithm for model-based analysis of evoked skin conductance responses," *Biological Psychology*, vol. 94, no. 3, p. 490, Dec. 2013, publisher: Elsevier. [Online]. Available: <https://www.ncbi.nlm.nih.gov/pmc/articles/PMC3853620/>
- [63] M. E. Dawson, A. M. Schell, and D. L. Filion, "The Electrodermal System," in *Handbook of Psychophysiology*, 4th ed., J. T. Cacioppo, L. G. Tassinary, and G. G. Berntson, Eds. Cambridge University Press, Dec. 2016, pp. 217–243. [Online]. Available: [https://www.cambridge.org/core/product/identifier/9781107415782%23CN-bp-10/type/book\\_part](https://www.cambridge.org/core/product/identifier/9781107415782%23CN-bp-10/type/book_part)
- [64] J. T. Cacioppo, L. G. Tassinary, and G. G. Berntson, Eds., *Handbook of psychophysiology*, 3rd ed, ser. Handbook of psychophysiology, 3rd ed. New York, NY, US: Cambridge University Press, 2007, pages: x, 898.
- [65] D. R. Bach, G. Flandin, K. J. Friston, and R. J. Dolan, "Time-series analysis for rapid event-related skin conductance responses," *Journal of Neuroscience Methods*, vol. 184, no. 2, pp. 224–234, Nov. 2009. [Online]. Available: <https://www.sciencedirect.com/science/article/pii/S0165027009004385>
- [66] D. M. Alexander, C. Trengove, P. Johnston, T. Cooper, J. P. August, and E. Gordon, "Separating individual skin conductance responses in a short interstimulus-interval paradigm," *Journal of Neuroscience Methods*, vol. 146, no. 1, pp. 116–123, Jul. 2005.
- [67] M. Benedek and C. Kaernbach, "Decomposition of skin conductance data by means of nonnegative deconvolution," *Psychophysiology*, vol. 47, no. 4, pp. 647–658, Jul. 2010. [Online]. Available: <https://www.ncbi.nlm.nih.gov/pmc/articles/PMC2904901/>
- [68] J. J. Kavanagh and H. B. Menz, "Accelerometry: A technique for quantifying movement patterns during walking," *Gait & Posture*, vol. 28, no. 1, pp. 1–15, Jul. 2008. [Online]. Available: <https://www.sciencedirect.com/science/article/pii/S0966636207002706>
- [69] G. Becq, P. Kahane, L. Minotti, S. Bonnet, and R. Guillemaud, "Classification of Epileptic Motor Manifestations and Detection of Tonic–Clonic Seizures With Acceleration Norm Entropy," *IEEE Transactions on Biomedical Engineering*, vol. 60, no. 8, pp. 2080–2088, Aug. 2013, conference Name: IEEE Transactions on Biomedical Engineering.
- [70] S. Beniczky, T. Polster, T. W. Kjaer, and H. Hjalgrim, "Detection of generalized tonic–clonic seizures by a wireless wrist accelerometer: A prospective, multicenter study," *Epilepsia*, vol. 54, no. 4, pp. e58–e61, 2013, .eprint: <https://onlinelibrary.wiley.com/doi/pdf/10.1111/epi.12120>. [Online]. Available: <https://onlinelibrary.wiley.com/doi/abs/10.1111/epi.12120>
- [71] D. Johansson, F. Ohlsson, D. Krysl, B. Rydenhag, M. Czarnecki, N. Gustafsson, J. Wipenmyr, T. McKelvey, and K. Malmgren, "Tonic-clonic seizure detection using accelerometry-based wearable sensors: A prospective, video-EEG controlled study," *SEIZURE-EUROPEAN JOURNAL OF EPILEPSY*, vol. 65, pp. 48–54, Feb. 2019. [Online]. Available: [https://www.seizure-journal.com/article/S1059-1311\(18\)30616-2/fulltext](https://www.seizure-journal.com/article/S1059-1311(18)30616-2/fulltext)
- [72] M. Velez, R. S. Fisher, V. Bartlett, and S. Le, "Tracking generalized tonic-clonic seizures with a wrist accelerometer linked to an online database," *Seizure - European Journal of Epilepsy*, vol. 39, pp. 13–18, Jul. 2016, publisher: Elsevier. [Online]. Available: [https://www.seizure-journal.com/article/S1059-1311\(16\)30025-5/fulltext](https://www.seizure-journal.com/article/S1059-1311(16)30025-5/fulltext)
- [73] S. Kusmakar, C. K. Karmakar, B. Yan, T. J. O'Brien, R. Muthuganapathy, M. Palaniswami, and IEEE, "Detection of Generalized Tonic-Clonic Seizures Using Short Length Accelerometry Signal," 2017, pp. 4566–4569.
- [74] F. Shi and X. Li, "Development of automatic motion artifact detection in mobile ECG monitor based on wavelet transform," in *2012 IEEE International Conference on Intelligent Control, Automatic Detection and High-End Equipment*, Jul. 2012, pp. 166–170.
- [75] J. Zhong, D. Hai, J. Cheng, C. Jiao, S. Gou, Y. Liu, H. Zhou, and W. Zhu, "Convolutional Autoencoding and Gaussian Mixture Clustering for Unsupervised Beat-to-Beat Heart Rate Estimation of Electrocardiograms from Wearable Sensors," *Sensors*, vol. 21, no. 21, p. 7163, Jan. 2021, number: 21 Publisher: Multidisciplinary Digital Publishing Institute. [Online]. Available: <https://www.mdpi.com/1424-8220/21/21/7163>
- [76] N. V. Thakor, J. G. Webster, and W. J. Tompkins, "Estimation of QRS Complex Power Spectra for Design of a QRS Filter," *IEEE Transactions on Biomedical Engineering*, vol. BME-31, no. 11, pp. 702–706, Nov. 1984, conference Name: IEEE Transactions on Biomedical Engineering.
- [77] Z. Zidemal, A. Amirou, M. Adnane, and A. Belouchrani, "QRS detection based on wavelet coefficients," *Computer Methods and Programs in Biomedicine*, vol. 107, no. 3, pp. 490–496, Sep. 2012. [Online]. Available: <https://www.sciencedirect.com/science/article/pii/S016926071100321X>

- [78] V. Afonso, W. Tompkins, T. Nguyen, and S. Luo, "ECG beat detection using filter banks," *IEEE Transactions on Biomedical Engineering*, vol. 46, no. 2, pp. 192–202, Feb. 1999, conference Name: IEEE Transactions on Biomedical Engineering.
- [79] W. Boucsein, *Electrodermal Activity*, 2nd ed. Springer US, 2012. [Online]. Available: <https://www.springer.com/gp/book/9781461411253>
- [80] A. Dabbaghian, T. Yousefi, S. Z. Fatmi, P. Shafie, and H. Kassiri, "A 9.2-g Fully-Flexible Wireless Ambulatory EEG Monitoring and Diagnostics Headband With Analog Motion Artifact Detection and Compensation," *IEEE Transactions on Biomedical Circuits and Systems*, vol. 13, no. 6, pp. 1141–1151, Dec. 2019, conference Name: IEEE Transactions on Biomedical Circuits and Systems.
- [81] n. Jiawei Xu, R. F. Yazicioglu, B. Grundlehner, P. Harpe, K. a. A. Makinwa, and C. Van Hoof, "A 160 W 8-Channel Active Electrode System for EEG Monitoring," *IEEE transactions on biomedical circuits and systems*, vol. 5, no. 6, pp. 555–567, Dec. 2011.
- [82] Y. Chi, S. Deiss, and G. Cauwenberghs, "Non-contact Low Power EEG/ECG Electrode for High Density Wearable Biopotential Sensor Networks," *2009 Sixth International Workshop on Wearable and Implantable Body Sensor Networks*, 2009.
- [83] "Bundle Branch Block," 2021. [Online]. Available: <https://www.cedars-sinai.org/health-library/articles.html>
- [84] M. Nei, R. T. Ho, and M. R. Sperling, "EKG abnormalities during partial seizures in refractory epilepsy," *Epilepsia*, vol. 41, no. 5, pp. 542–548, May 2000.
- [85] B. Blum, N. Kauli, E. Liban, and P. Levy, "Paroxysms of T-wave alterations in the ECG in experimental epilepsy due to foci in the pseudosylvian gyrus," *Life Sciences*, vol. 9, no. 4, pp. 219–225, Feb. 1970.
- [86] S. Tigaran, V. Rasmussen, M. Dam, S. Pedersen, H. Høgenhaven, and B. Friberg, "ECG changes in epilepsy patients," *Acta Neurologica Scandinavica*, vol. 96, no. 2, pp. 72–75, Aug. 1997.
- [87] NHS, "Atrial fibrillation - Causes," May 2018, section: conditions. [Online]. Available: <https://www.nhs.uk/conditions/atrial-fibrillation/causes/>
- [88] M. Herskovitz and Y. Schiller, "Atrial fibrillation associated with epileptic seizures," *Archives of Neurology*, vol. 69, no. 9, pp. 1197–1199, Sep. 2012.
- [89] S. Hygge and K. Hugdahl, "Skin conductance recordings and the NaCl concentration of the electrolyte," *Psychophysiology*, vol. 22, no. 3, pp. 365–367, May 1985.
- [90] H. Bradley and J. Esformes, "Breathing pattern disorders and functional movement," *International Journal of Sports Physical Therapy*, vol. 9, no. 1, pp. 28–39, Feb. 2014.
- [91] L. Rong, Z. Jianzhong, L. Ming, and H. Xiangfeng, "A Wearable Acceleration Sensor System for Gait Recognition," in *2007 2nd IEEE Conference on Industrial Electronics and Applications*, May 2007, pp. 2654–2659, iSSN: 2158-2297.
- [92] U. S. I. for Telecommunication Siccences, "Federal Standard 1037C - ITS," 2001. [Online]. Available: <https://www.its.blldrdoc.gov/research-topics/federal-standard-1037c.aspx>
- [93] B. Widrow, J. Glover, J. McCool, J. Kaunitz, C. Williams, R. Hearn, J. Zeidler, J. Eugene Dong, and R. Goodlin, "Adaptive noise cancelling: Principles and applications," *Proceedings of the IEEE*, vol. 63, no. 12, pp. 1692–1716, Dec. 1975, conference Name: Proceedings of the IEEE.
- [94] D.-Z. Du and K.-I. Ko, *Theory of Computational Complexity*. Hoboken, NJ, USA: John Wiley & Sons, Inc., Jun. 2014. [Online]. Available: <http://doi.wiley.com/10.1002/9781118595091>
- [95] N.-T. Bui and G.-s. Byun, "The Comparison Features of ECG Signal with Different Sampling Frequencies and Filter Methods for Real-Time Measurement," *Symmetry*, vol. 13, no. 8, p. 1461, Aug. 2021, number: 8 Publisher: Multidisciplinary Digital Publishing Institute. [Online]. Available: <https://www.mdpi.com/2073-8994/13/8/1461>
- [96] S. Banerjee and G. K. Singh, "Monte Carlo Filter-Based Motion Artifact Removal From Electrocardiogram Signal for Real-Time Telecardiology System," *IEEE Transactions on Instrumentation and Measurement*, vol. 70, pp. 1–10, 2021, conference Name: IEEE Transactions on Instrumentation and Measurement.
- [97] W. Jenkal, R. Latif, A. Toumanari, A. El Ouardi, H. Anas, and O. el B'Charri, "Real-time hardware architecture of the adaptive dual threshold filter based ECG signal denoising," *Journal of Theoretical and Applied Information Technology*, vol. 96, pp. 4649–4659, Jul. 2018.
- [98] S. Javed and N. A. Ahmad, "Optimal preconditioned regularization of least mean squares algorithm for robust online learning," *Journal of Intelligent & Fuzzy Systems*, vol. 39, no. 3, pp. 3375–3385, Jan. 2020, publisher: IOS Press. [Online]. Available: <https://content.iospress.com/articles/journal-of-intelligent-and-fuzzy-systems/ifs191728>
- [99] M. Zhang and D. Pi, "Data Aggregation and Analysis: A Fast Algorithm of ECG Recognition Based on Pattern Matching," in *Cloud Computing and Security*, X. Sun, A. Liu, H.-C. Chao, and E. Bertino, Eds., vol. 10040. Cham: Springer International Publishing, 2016, pp. 313–323, series Title: Lecture Notes in Computer Science. [Online]. Available: <http://link.springer.com/10.1007/978-3-319-48674-1-28>

- [100] V. Gupta, M. Mittal, and V. Mittal, "Performance Evaluation of Various Pre-Processing Techniques for R-Peak Detection in ECG Signal," *IETE Journal of Research*, vol. 0, no. 0, pp. 1–16, Aug. 2020, publisher: Taylor & Francis \_eprint: <https://doi.org/10.1080/03772063.2020.1756473>. [Online]. Available: <https://doi.org/10.1080/03772063.2020.1756473>
- [101] I. Jekova and V. Krasteva, "Real time detection of ventricular fibrillation and tachycardia," *Physiological Measurement*, vol. 25, no. 5, pp. 1167–1178, Aug. 2004, publisher: IOP Publishing. [Online]. Available: <https://sci-hub.se/10.1088/0967-3334/25/5/007>
- [102] A. H. Sodhro, A. K. Sangaiah, G. H. Sodhro, S. Lohano, and S. Pirbhulal, "An Energy-Efficient Algorithm for Wearable Electrocardiogram Signal Processing in Ubiquitous Healthcare Applications," *Sensors*, vol. 18, no. 3, p. 923, Mar. 2018, number: 3 Publisher: Multidisciplinary Digital Publishing Institute. [Online]. Available: <https://www.mdpi.com/1424-8220/18/3/923>
- [103] Y. Xia, H. Zhang, L. Xu, Z. Gao, H. Zhang, H. Liu, and S. Li, "An Automatic Cardiac Arrhythmia Classification System With Wearable Electrocardiogram," *IEEE Access*, vol. 6, pp. 16 529–16 538, 2018, conference Name: IEEE Access.
- [104] N. T. Bui, D. T. Phan, T. P. Nguyen, G. Hoang, J. Choi, Q. C. Bui, and J. Oh, "Real-Time Filtering and ECG Signal Processing Based on Dual-Core Digital Signal Controller System," *IEEE Sensors Journal*, vol. 20, no. 12, pp. 6492–6503, Jun. 2020, conference Name: IEEE Sensors Journal.
- [105] C. Lastre-Dominguez, Y. S. Shmalijy, O. Ibarra-Manzano, and M. Vazquez-Olguin, "Denoising and Features Extraction of ECG Signals in State Space Using Unbiased FIR Smoothing," *IEEE Access*, vol. 7, pp. 152 166–152 178, 2019. [Online]. Available: <https://ieeexplore.ieee.org/document/8873580/>
- [106] S. Liu, E. Zhan, J. Zheng, L. Yu, and T. Xue, "Real-time method for ecg r-peak detection combining automatic threshold and differentiation," *Journal of Mechanics in Medicine and Biology*, vol. 20, no. 08, p. 1950023, Oct. 2020, publisher: World Scientific Publishing Co. [Online]. Available: <https://www.worldscientific.com/doi/abs/10.1142/S0219519419500234>
- [107] S. Raj, "An Efficient IoT-Based Platform for Remote Real-Time Cardiac Activity Monitoring," *IEEE Transactions on Consumer Electronics*, vol. 66, no. 2, pp. 106–114, May 2020. [Online]. Available: <https://ieeexplore.ieee.org/document/9040609/>
- [108] J. Lilienthal and W. Dargie, "Extraction of Motion Artifacts from the Measurements of a Wireless Electrocardiogram using Tensor Decomposition," in *2019 22th International Conference on Information Fusion (FUSION)*, Jul. 2019, pp. 1–8. [Online]. Available: <https://ieeexplore.ieee.org/document/9011290>
- [109] S. R. Krishnan and C. S. Seelamantula, "On the Selection of Optimum Savitzky-Golay Filters," *IEEE Transactions on Signal Processing*, vol. 61, no. 2, pp. 380–391, Jan. 2013, conference Name: IEEE Transactions on Signal Processing.
- [110] X. Zhou, H. Ding, B. Ung, E. Pickwell-MacPherson, and Y. Zhang, "Automatic online detection of atrial fibrillation based on symbolic dynamics and Shannon entropy," *BioMedical Engineering OnLine*, vol. 13, no. 1, p. 18, Feb. 2014. [Online]. Available: <https://doi.org/10.1186/1475-925X-13-18>
- [111] X. An and G. K. Stylios, "Comparison of Motion Artefact Reduction Methods and the Implementation of Adaptive Motion Artefact Reduction in Wearable Electrocardiogram Monitoring," *Sensors*, vol. 20, no. 5, p. 1468, Jan. 2020, number: 5 Publisher: Multidisciplinary Digital Publishing Institute. [Online]. Available: <https://www.mdpi.com/1424-8220/20/5/1468>
- [112] G. Lenis, N. Pilia, A. Loewe, W. H. W. Schulze, and O. Dössel, "Comparison of Baseline Wander Removal Techniques considering the Preservation of ST Changes in the Ischemic ECG: A Simulation Study," *Computational and Mathematical Methods in Medicine*, vol. 2017, p. e9295029, Mar. 2017, publisher: Hindawi. [Online]. Available: <https://www.hindawi.com/journals/cmmm/2017/9295029/>
- [113] A. Malhotra and A. Chintanpalli, "A Real Time Wavelet Filtering for ECG Baseline Wandering Removal," in *2020 International Conference on Artificial Intelligence and Signal Processing (AISP)*, Jan. 2020, pp. 1–5, iSSN: 2640-5768.
- [114] R. Rodríguez-Jorge, I. De León-Damas, J. Bila, and J. Škvor, "Internet of things-assisted architecture for QRS complex detection in real time," *Internet of Things*, vol. 14, p. 100395, Jun. 2021. [Online]. Available: <https://www.sciencedirect.com/science/article/pii/S2542660521000391>
- [115] F. S. Butt, L. La Blunda, M. F. Wagner, J. Schäfer, I. Medina-Bulo, and D. Gómez-Ullate, "Fall Detection from Electrocardiogram (ECG) Signals and Classification by Deep Transfer Learning," *Information*, vol. 12, no. 2, p. 63, Feb. 2021, number: 2 Publisher: Multidisciplinary Digital Publishing Institute. [Online]. Available: <https://www.mdpi.com/2078-2489/12/2/63>
- [116] S. Zhang, T. Zhao, X. Wang, C. Peng, Q. Li, and X. Zhang, "Design and Implementation of A Novel Real Time P-QRS-T Waves Detection Algorithm," in *2020 IEEE 4th Information Technology, Networking, Electronic and Automation Control Conference (ITNEC)*, vol. 1, Jun. 2020, pp. 1109–1112.
- [117] V. P. Rachim and W.-Y. Chung, "Wearable Noncontact Armband for Mobile ECG Monitoring System," *IEEE Transactions on Biomedical Circuits and Systems*, vol. 10, no. 6, pp. 1112–1118, Dec. 2016, conference Name: IEEE Transactions on Biomedical Circuits and Systems.

- [118] Q. Zhang, X. Zeng, W. Hu, and D. Zhou, "A Machine Learning-Empowered System for Long-Term Motion-Tolerant Wearable Monitoring of Blood Pressure and Heart Rate With Ear-ECG/PPG," *IEEE Access*, vol. 5, pp. 10 547–10 561, 2017, conference Name: IEEE Access.
- [119] H. Xiong, M. Liang, and J. Liu, "A Real-Time QRS Detection Algorithm Based on Energy Segmentation for Exercise Electrocardiogram," *Circuits, Systems, and Signal Processing*, vol. 40, no. 10, pp. 4969–4985, Oct. 2021, company: Springer Distributor: Springer Institution: Springer Label: Springer Number: 10 Publisher: Springer US. [Online]. Available: <https://link.springer.com/article/10.1007/s00034-021-01702-z>
- [120] T. Sharma and K. K. Sharma, "QRS complex detection in ECG signals using locally adaptive weighted total variation denoising," *Computers in Biology and Medicine*, vol. 87, pp. 187–199, Aug. 2017. [Online]. Available: <https://www.sciencedirect.com/science/article/pii/S001048251730149X>
- [121] U. Orhan and A. Aydin, "Heart Rate Detection on Single-Arm ECG by Using Dual-Median Approach," *Arabian Journal for Science and Engineering*, vol. 45, no. 8, pp. 6573–6581, Aug. 2020, company: Springer Distributor: Springer Institution: Springer Label: Springer Number: 8 Publisher: Springer Berlin Heidelberg. [Online]. Available: <https://link.springer.com/article/10.1007/s13369-020-04574-8>
- [122] A. Slimane and A. Zaid, "Real-time fast fourier transform-based notch filter for single-frequency noise cancellation: Application to electrocardiogram signal denoising," *Journal of Medical Signals & Sensors*, vol. 11, no. 1, p. 52, 2021. [Online]. Available: <http://www.jmssjournal.net/text.asp?2021/11/1/52/308421>
- [123] C. Arsene, "Design of Deep Convolutional Neural Network Architectures for Denoising Electrocardiographic Signals," in *2020 IEEE Conference on Computational Intelligence in Bioinformatics and Computational Biology (CIBCB)*, Oct. 2020, pp. 1–8.
- [124] D. Pandit, L. Zhang, C. Liu, S. Chattopadhyay, N. Aslam, and C. P. Lim, "A lightweight QRS detector for single lead ECG signals using a max-min difference algorithm," *Computer Methods and Programs in Biomedicine*, vol. 144, pp. 61–75, Jun. 2017. [Online]. Available: <https://www.sciencedirect.com/science/article/pii/S0169260716302735>
- [125] H. Chen and S. Chen, "A moving average based filtering system with its application to real-time QRS detection," in *Computers in Cardiology, 2003*, Sep. 2003, pp. 585–588, iSSN: 0276-6547.
- [126] L. Keselbrener, M. Keselbrener, and S. Akselrod, "Nonlinear high pass filter for R-wave detection in ECG signal," *Medical Engineering & Physics*, vol. 19, no. 5, pp. 481–484, Jun. 1997. [Online]. Available: <https://www.sciencedirect.com/science/article/pii/S1350453397000131>
- [127] S. Canan, Y. Ozbay, and B. Karlik, "A method for removing low varying frequency trend from ECG signal," in *Proceedings of the 1998 2nd International Conference Biomedical Engineering Days*, May 1998, pp. 144–146.
- [128] A. Galli, G. Frigo, D. Chindamo, A. Depari, M. Gadola, and G. Giorgi, "Denoising ECG Signal by CSTFM Algorithm: Monitoring During Motorbike and Car Races," *IEEE Transactions on Instrumentation and Measurement*, vol. 68, no. 7, pp. 2433–2441, Jul. 2019, conference Name: IEEE Transactions on Instrumentation and Measurement.
- [129] U. Zalabarria, E. Irigoyen, R. Martinez, and A. Lowe, "Online robust R-peaks detection in noisy electrocardiograms using a novel iterative smart processing algorithm," *Applied Mathematics and Computation*, vol. 369, p. 124839, Mar. 2020. [Online]. Available: <https://www.sciencedirect.com/science/article/pii/S0096300319308318>
- [130] V. Shusterman, S. I. Shah, A. Beigel, and K. P. Anderson, "Enhancing the Precision of ECG Baseline Correction: Selective Filtering and Removal of Residual Error," *Computers and Biomedical Research*, vol. 33, no. 2, pp. 144–160, Apr. 2000. [Online]. Available: <https://www.sciencedirect.com/science/article/pii/S0010480900915398>
- [131] L. Burattini, W. Zareba, and R. Burattini, "Automatic detection of microvolt T-wave alternans in Holter recordings: Effect of baseline wandering," *Biomedical Signal Processing and Control*, vol. 1, no. 2, pp. 162–168, Apr. 2006. [Online]. Available: <https://www.sciencedirect.com/science/article/pii/S1746809406000188>
- [132] S. Sahoo, P. Biswal, T. Das, and S. Sabut, "De-noising of ECG Signal and QRS Detection Using Hilbert Transform and Adaptive Thresholding," *Procedia Technology*, vol. 25, pp. 68–75, Jan. 2016. [Online]. Available: <https://www.sciencedirect.com/science/article/pii/S2212017316304297>
- [133] S. Kumar, D. Panigrahy, and P. K. Sahu, "Denoising of Electrocardiogram (ECG) signal by using empirical mode decomposition (EMD) with non-local mean (NLM) technique," *Biocybernetics and Biomedical Engineering*, vol. 38, no. 2, pp. 297–312, Jan. 2018. [Online]. Available: <https://www.sciencedirect.com/science/article/pii/S0208521617303017>
- [134] B. H. Tracey and E. L. Miller, "Nonlocal Means Denoising of ECG Signals," *IEEE Transactions on Biomedical Engineering*, vol. 59, no. 9, pp. 2383–2386, Sep. 2012. [Online]. Available: <http://ieeexplore.ieee.org/document/6242391/>

- [135] M.-B. Hossain, S. K. Bashar, J. Lazaro, N. Reljin, Y. Noh, and K. H. Chon, "A robust ECG denoising technique using variable frequency complex demodulation," *Computer Methods and Programs in Biomedicine*, vol. 200, p. 105856, Mar. 2021. [Online]. Available: <https://www.sciencedirect.com/science/article/pii/S0169260720316898>
- [136] M.-B. Hossain, J. Lázaro, Y. Noh, and K. H. Chon, "Denoising Wearable Armband ECG Data Using the Variable Frequency Complex Demodulation Technique," in *2020 42nd Annual International Conference of the IEEE Engineering in Medicine Biology Society (EMBC)*, Jul. 2020, pp. 592–595, iSSN: 2694-0604.
- [137] A. Singhal, P. Singh, B. Fatimah, and R. B. Pachori, "An efficient removal of power-line interference and baseline wander from ECG signals by employing Fourier decomposition technique," *Biomedical Signal Processing and Control*, vol. 57, p. 101741, Mar. 2020. [Online]. Available: <https://www.sciencedirect.com/science/article/pii/S1746809419303222>
- [138] L. Abecassis, M. Ho, O. Tit-Lartey, W. Hwang, T. Gathmann, Z. Lum, N. Y. Loong, and J. Moo, "Machine Learning based Denoising of Electrocardiogram Signals from a Wearable ECG Monitor," Imperial College London, Department of Bioengineering, FINAL REPORT FOR IBSC AND MENG GROUP PROJECT, Dec. 2018. [Online]. Available: [https://woochan-hwang.github.io/assets/Machine\\_Learning\\_based\\_Denoising\\_of\\_Electrocardiogram\\_Signals\\_from\\_a\\_Wearable\\_ECG\\_Monitor.pdf](https://woochan-hwang.github.io/assets/Machine_Learning_based_Denoising_of_Electrocardiogram_Signals_from_a_Wearable_ECG_Monitor.pdf)
- [139] P. Xiong, H. Wang, M. Liu, and X. Liu, "Denoising Autoencoder for Eletrocardiogram Signal Enhancement," *Journal of Medical Imaging and Health Informatics*, vol. 5, no. 8, pp. 1804–1810, Dec. 2015. [Online]. Available: <https://sci-hub.se/10.1166/jmhi.2015.1649>
- [140] B. N. Singh and A. K. Tiwari, "Optimal selection of wavelet basis function applied to ECG signal denoising," *Digital Signal Processing*, vol. 16, no. 3, pp. 275–287, May 2006. [Online]. Available: <https://www.sciencedirect.com/science/article/pii/S1051200405001703>
- [141] G. Li, Z. Tan, W. Xu, F. Xu, L. Wang, J. Chen, and K. Wu, "A particle swarm optimization improved BP neural network intelligent model for electrocardiogram classification," *BMC Medical Informatics and Decision Making*, vol. 21, no. 2, p. 99, Jul. 2021. [Online]. Available: <https://doi.org/10.1186/s12911-021-01453-6>
- [142] C.-C. Chen and F. R. Tsui, "Comparing different wavelet transforms on removing electrocardiogram baseline wavers and special trends," *BMC Medical Informatics and Decision Making*, vol. 20, no. 11, p. 343, Dec. 2020. [Online]. Available: <https://doi.org/10.1186/s12911-020-01349-x>
- [143] W. Jenkal, R. Latif, A. Toumanari, A. Dliou, O. El B'charri, and F. M. Maoulainine, "An efficient algorithm of ECG signal denoising using the adaptive dual threshold filter and the discrete wavelet transform," *Biocybernetics and Biomedical Engineering*, vol. 36, no. 3, pp. 499–508, 2016. [Online]. Available: <https://linkinghub.elsevier.com/retrieve/pii/S0208521616300456>
- [144] I. Ara, M. N. Hossain, and S. M. Y. Mahbub, "Baseline Drift Removal and De-Noising of the ECG Signal using Wavelet Transform," *International Journal of Computer Applications*, vol. 95, pp. 15–17, Jun. 2014.
- [145] A. Karimipour and M. R. Homaeinezhad, "Real-time electrocardiogram P-QRS-T detection-delineation algorithm based on quality-supported analysis of characteristic templates," *Computers in Biology and Medicine*, vol. 52, pp. 153–165, Sep. 2014. [Online]. Available: <https://www.sciencedirect.com/science/article/pii/S001048251400167X>
- [146] H. Altaf, S. N. Ibrahim, and R. F. Olanrewaju, "Non Invasive Stress Detection Method Based on Discrete Wavelet Transform and Machine Learning Algorithms," in *2021 IEEE 11th IEEE Symposium on Computer Applications Industrial Electronics (ISCAIE)*, Apr. 2021, pp. 106–111.
- [147] M. Bahoura, M. Hassani, and M. Hubin, "DSP implementation of wavelet transform for real time ECG wave forms detection and heart rate analysis," *Computer Methods and Programs in Biomedicine*, vol. 52, no. 1, pp. 35–44, Jan. 1997. [Online]. Available: <https://www.sciencedirect.com/science/article/pii/S016926079701780X>
- [148] N. Razzaq, S.-A. A. Sheikh, M. Salman, and T. Zaidi, "An Intelligent Adaptive Filter for Elimination of Power Line Interference From High Resolution Electrocardiogram," *IEEE Access*, vol. 4, pp. 1676–1688, 2016, conference Name: IEEE Access.
- [149] F. Shirbani and S. K. Setarehdan, "ECG power line interference removal using combination of FFT and adaptive non-linear noise estimator," in *2013 21st Iranian Conference on Electrical Engineering (ICEE)*, May 2013, pp. 1–5, iSSN: 2164-7054.
- [150] B. Chen, Y. Li, X. Cao, W. Sun, and W. He, "Removal of Power Line Interference From ECG Signals Using Adaptive Notch Filters of Sharp Resolution," *IEEE Access*, vol. 7, pp. 150 667–150 676, 2019, conference Name: IEEE Access.
- [151] S. Ari, M. K. Das, and A. Chacko, "ECG signal enhancement using S-Transform," *Computers in Biology and Medicine*, vol. 43, no. 6, pp. 649–660, Jul. 2013. [Online]. Available: <https://www.sciencedirect.com/science/article/pii/S0010482513000668>

- [152] S. Cuomo, G. De Pietro, R. Farina, A. Galletti, and G. Sannino, "A Novel O(n) Numerical Scheme for ECG Signal Denoising," *Procedia Computer Science*, vol. 51, pp. 775–784, Jan. 2015. [Online]. Available: <https://www.sciencedirect.com/science/article/pii/S1877050915010066>
- [153] M. Zhang and G. Wei, "An integrated EMD adaptive threshold denoising method for reduction of noise in ECG," *PLOS ONE*, vol. 15, no. 7, p. e0235330, Jul. 2020, publisher: Public Library of Science. [Online]. Available: <https://journals.plos.org/plosone/article?id=10.1371/journal.pone.0235330>
- [154] M. Rakshit and S. Das, "An efficient ECG denoising methodology using empirical mode decomposition and adaptive switching mean filter," *Biomedical Signal Processing and Control*, vol. 40, pp. 140–148, Feb. 2018. [Online]. Available: <https://www.sciencedirect.com/science/article/pii/S174680941730229X>
- [155] P. Bing, W. Liu, Z. Wang, and Z. Zhang, "Noise Reduction in ECG Signal Using an Effective Hybrid Scheme," *IEEE Access*, vol. 8, pp. 160790–160801, 2020, conference Name: IEEE Access.
- [156] S. Tahir, M. M. Raja, N. Razzaq, A. Mirza, W. Z. Khan, S. W. Kim, and Y. B. Zikria, "Extended Kalman Filter-Based Power Line Interference Canceller for Electrocardiogram Signal," *Big Data*, Jul. 2021, publisher: Mary Ann Liebert, Inc., publishers. [Online]. Available: <https://www.liebertpub.com/doi/10.1089/big.2021.0043>
- [157] M. Tomasini, S. Benatti, B. Milosevic, E. Farella, and L. Benini, "Power Line Interference Removal for High-Quality Continuous Biosignal Monitoring With Low-Power Wearable Devices," *IEEE Sensors Journal*, vol. 16, no. 10, pp. 3887–3895, May 2016, conference Name: IEEE Sensors Journal.
- [158] J. Lazaro, N. Reljin, M.-B. Hossain, Y. Noh, P. Laguna, and K. H. Chon, "Wearable Armband Device for Daily Life Electrocardiogram Monitoring," *Ieee Transactions on Biomedical Engineering*, vol. 67, no. 12, pp. 3464–3473, Dec. 2020, place: Piscataway Publisher: Ieee-Inst Electrical Electronics Engineers Inc WOS:000591819700018. [Online]. Available: <https://gateway.webofknowledge.com/gateway/Gateway.cgi?GWVersion=2&SrcAuth=DynamicDOIArticle&SrcApp=WOS&KeyAID=10.1109%2FTBME.2020.2987759&DestApp=DOI&SrcAppSID=E48XxfDJUYJDbzYBdih&SrcJTitle=IEEE+TRANSACTIONS+ON+BIOMEDICAL+ENGINEERING&DestDOIRegistrantName=Institute+of+Electrical+and+Electronics+Engineers>
- [159] O. Ozkaraca and I. Guler, "Denoising and remote monitoring of ecg signal with real-time extended kalman filter in a wearable system," *Biomedical Engineering: Applications, Basis and Communications*, vol. 27, no. 01, p. 1550009, Feb. 2015, publisher: National Taiwan University. [Online]. Available: <https://www.worldscientific.com/doi/abs/10.4015/S101623721550009X>
- [160] Y.-D. Lee and W.-Y. Chung, "Wireless sensor network based wearable smart shirt for ubiquitous health and activity monitoring," *Sensors and Actuators B: Chemical*, vol. 140, no. 2, pp. 390–395, Jul. 2009. [Online]. Available: <https://www.sciencedirect.com/science/article/pii/S0925400509003724>
- [161] S. C. Lee and S. M. Kim, "Motion Artifact Reduction Algorithm in Wearable Healthcare System1," *Journal of Medical Devices*, vol. 10, no. 2, May 2016. [Online]. Available: <https://doi.org/10.1115/1.4033169>
- [162] H.-T. Chiang, Y.-Y. Hsieh, S.-W. Fu, K.-H. Hung, Y. Tsao, and S.-Y. Chien, "Noise Reduction in ECG Signals Using Fully Convolutional Denoising Autoencoders," *IEEE Access*, vol. 7, pp. 60806–60813, 2019, conference Name: IEEE Access.
- [163] S. Nurmaini, A. Darmawahyuni, A. N. Sakti Mukti, M. N. Rachmatullah, F. Firdaus, and B. Tutuko, "Deep Learning-Based Stacked Denoising and Autoencoder for ECG Heartbeat Classification," *Electronics*, vol. 9, no. 1, p. 135, Jan. 2020, number: 1 Publisher: Multidisciplinary Digital Publishing Institute. [Online]. Available: <https://www.mdpi.com/2079-9292/9/1/135>
- [164] N. Reljin, J. Lazaro, M. B. Hossain, Y. S. Noh, C. H. Cho, and K. H. Chon, "Using the Redundant Convolutional Encoder–Decoder to Denoise QRS Complexes in ECG Signals Recorded with an Armband Wearable Device," *Sensors*, vol. 20, no. 16, p. 4611, Jan. 2020, number: 16 Publisher: Multidisciplinary Digital Publishing Institute. [Online]. Available: <https://www.mdpi.com/1424-8220/20/16/4611>
- [165] Y. Kishimoto, Y. Kutsuna, and K. Oguri, "Detecting Motion Artifact ECG Noise During Sleeping by Means of a Tri-axis Accelerometer," in *2007 29th Annual International Conference of the IEEE Engineering in Medicine and Biology Society*, Aug. 2007, pp. 2669–2672, iSSN: 1558-4615.
- [166] J. Ottenbacher, M. Kirst, L. Jatobá, U. Großmann, and W. Stork, "An approach to reliable motion artifact detection for mobile long-term ECG monitoring systems using dry electrodes," in *IV Latin American Congress on Biomedical Engineering 2007, Bioengineering Solutions for Latin America Health*, ser. IFMBE Proceedings, C. Müller-Karger, S. Wong, and A. La Cruz, Eds. Berlin, Heidelberg: Springer, 2008, pp. 440–443.
- [167] J. Zhang, J. Tian, Y. Cao, Y. Yang, and X. Xu, "Deep time–frequency representation and progressive decision fusion for ECG classification," *Knowledge-Based Systems*, vol. 190, p. 105402, Feb. 2020. [Online]. Available: <https://www.sciencedirect.com/science/article/pii/S0950705119306422>

- [168] T. Pawar, S. Chaudhuri, and S. P. Duttagupta, "Body Movement Activity Recognition for Ambulatory Cardiac Monitoring," *IEEE Transactions on Biomedical Engineering*, vol. 54, no. 5, pp. 874–882, May 2007, conference Name: IEEE Transactions on Biomedical Engineering.
- [169] a. Anusha A., P. Sukumaran, V. Sarveswaran, S. Surees Kumar, S. Shyam, T. J. Akl, P. Preejith S., and M. Sivaprakasam, "Electrodermal Activity Based Pre-surgery Stress Detection Using a Wrist Wearable," *IEEE Journal of Biomedical and Health Informatics*, vol. 24, no. 1, pp. 92–100, Jan. 2020, conference Name: IEEE Journal of Biomedical and Health Informatics.
- [170] M. Kelsey, R. V. Palumbo, A. Urbaneja, M. Akcakaya, J. Huang, I. R. Kleckner, L. F. Barrett, K. S. Quigley, E. Sejdic, and M. S. Goodwin, "Artifact detection in electrodermal activity using sparse recovery," in *Compressive Sensing VI: From Diverse Modalities to Big Data Analytics*, vol. 10211. SPIE, May 2017, pp. 92–101. [Online]. Available: <https://www.spiedigitallibrary.org/conference-proceedings-of-spie/10211/102110D/Artifact-detection-in-electrodermal-activity-using-sparse-recovery/10.1117/12.2264027.full>
- [171] B. Choi, H. Jebelli, and S. Lee, "Feasibility analysis of electrodermal activity (EDA) acquired from wearable sensors to assess construction workers' perceived risk," *Safety Science*, vol. 115, pp. 110–120, Feb. 2019.
- [172] G. Lee, B. Choi, H. Jebelli, c. ahn, and S. Lee, "Noise Reference Signal-based Denoising Method for EDA Collected by a Multimodal Wearable Biosensor from Fields," *Journal of Computing in Civil Engineering*, Jul. 2020.
- [173] P. Mz, L. T. S. Nc, G. S, M. Jr, and P. Rw, "Continuous monitoring of electrodermal activity during epileptic seizures using a wearable sensor," in *Annual International Conference of the IEEE Engineering in Medicine and Biology Society. IEEE Engineering in Medicine and Biology Society. Annual International Conference*, vol. 2010, 2010, pp. 4415–4418, iSSN: 1558-4615. [Online]. Available: <https://pubmed.ncbi.nlm.nih.gov/21095760/>
- [174] J. Hernandez, R. R. Morris, and R. W. Picard, "Call Center Stress Recognition with Person-Specific Models," in *Affective Computing and Intelligent Interaction*. Springer, Berlin, Heidelberg, Oct. 2011, pp. 125–134. [Online]. Available: [https://link.springer.com/chapter/10.1007/978-3-642-24600-5\\_16](https://link.springer.com/chapter/10.1007/978-3-642-24600-5_16)
- [175] I.-V. Bornoiu and O. Grigore, "A study about feature extraction for stress detection," May 2013, journal Abbreviation: 2013 - 8th International Symposium on Advanced Topics in Electrical Engineering, ATEE 2013 Pages: 4 Publication Title: 2013 - 8th International Symposium on Advanced Topics in Electrical Engineering, ATEE 2013.
- [176] C. Tronstad, O. M. Staal, S. Sælid, and G. Martinsen, "Model- based filtering for artifact and noise suppression with state estimation for electrodermal activity measurements in real time," in *2015 37th Annual International Conference of the IEEE Engineering in Medicine and Biology Society (EMBC)*, Aug. 2015, pp. 2750–2753, iSSN: 1558-4615.
- [177] J. Shukla, M. Barreda-Ángeles, J. Oliver, and D. Puig, "Efficient wavelet-based artifact removal for electrodermal activity in real-world applications," *Biomedical Signal Processing and Control*, vol. 42, pp. 45–52, Apr. 2018. [Online]. Available: <https://www.sciencedirect.com/science/article/pii/S1746809418300090>
- [178] R. R. Coifman and D. L. Donoho, "Translation-Invariant De-Noising," *Wavelets and Statistics*, pp. 125–150, 1995, publisher: Springer, New York, NY. [Online]. Available: [https://link.springer.com/chapter/10.1007/978-1-4612-2544-7\\_9](https://link.springer.com/chapter/10.1007/978-1-4612-2544-7_9)
- [179] P. Thiam, H. Kestler, and F. Schwenker, "Multimodal Deep Denoising Convolutional Autoencoders for Pain Intensity Classification based on Physiological Signals." SciTePress, 2020, pp. 289–296. [Online]. Available: <https://www.scitepress.org/Link.aspx?doi=10.5220%2f0008896102890296>
- [180] W. Chen, N. Jaques, S. Taylor, A. Sano, S. Fedor, and R. W. Picard, "Wavelet-Based Motion Artifact Removal for Electrodermal Activity," *Conference proceedings : ... Annual International Conference of the IEEE Engineering in Medicine and Biology Society. IEEE Engineering in Medicine and Biology Society. Annual Conference*, vol. 2015, pp. 6223–6226, 2015. [Online]. Available: <https://www.ncbi.nlm.nih.gov/pmc/articles/PMC5413204/>
- [181] Z. Chen, S. Haykin, J. J. Eggermont, and S. Becker, "Appendix E: Expectation-Maximization Algorithm," in *Correlative Learning*. John Wiley & Sons, Ltd, 2007, pp. 384–386, eprint: <https://onlinelibrary.wiley.com/doi/pdf/10.1002/9780470171455.app5>. [Online]. Available: <https://onlinelibrary.wiley.com/doi/abs/10.1002/9780470171455.app5>
- [182] G. S. Lowast and S. T. Veerabhadrappa, "Denoising wrist pulse signals using variance thresholding technique," *Indian Journal of Science and Technology*, vol. 13, no. 40, pp. 4275–4286, Nov. 2020, publisher: The Indian Society of Education and Environment.
- [183] M. Swangnetr and D. Kaber, "Emotional state classification in patient-robot interaction using wavelet analysis and statistics-based feature selection," *IEEE Transactions on Human-Machine Systems*, vol. 43, no. 1, pp. 63–75, 2013.

- [184] A. Greco, G. Valenza, A. Lanata, E. P. Scilingo, and L. Citi, "cvxEDA: A Convex Optimization Approach to Electrodermal Activity Processing," *IEEE Transactions on Biomedical Engineering*, vol. 63, no. 4, pp. 797–804, Apr. 2016, conference Name: IEEE Transactions on Biomedical Engineering.
- [185] S. P. Boyd and L. Vandenberghe, *Convex optimization*. Cambridge, UK ; New York: Cambridge University Press, 2004.
- [186] M. B. Hossain, H. F. Posada-Quintero, Y. Kong, R. McNaboe, and K. Chon, "A Preliminary Study on Automatic Motion Artifacts Detection in Electrodermal Activity Data Using Machine Learning," Jul. 2021. [Online]. Available: <https://arxiv.org/abs/2107.07650v1>
- [187] Y. Zhang, M. Haghdan, and K. S. Xu, "Unsupervised motion artifact detection in wrist-measured electrodermal activity data," in *Proceedings of the 2017 ACM International Symposium on Wearable Computers*, ser. ISWC '17. New York, NY, USA: Association for Computing Machinery, Sep. 2017, pp. 54–57. [Online]. Available: <https://doi.org/10.1145/3123021.3123054>
- [188] S. Taylor, N. Jaques, W. Chen, S. Fedor, A. Sano, and R. Picard, "Automatic identification of artifacts in electrodermal activity data," in *2015 37th Annual International Conference of the IEEE Engineering in Medicine and Biology Society (EMBC)*, Aug. 2015, pp. 1934–1937, iSSN: 1558-4615.
- [189] R. Kocielnik, N. Sidorova, F. M. Maggi, M. Ouwerkerk, and J. H. D. M. Westerink, "Smart technologies for long-term stress monitoring at work," in *Proceedings of the 26th IEEE International Symposium on Computer-Based Medical Systems*, Jun. 2013, pp. 53–58, iSSN: 1063-7125.
- [190] H. Storm, A. Fremming, S. Ødegaard, G. Martinsen, and L. Mørkrid, "The development of a software program for analyzing spontaneous and externally elicited skin conductance changes in infants and adults," *Clinical Neurophysiology*, vol. 111, no. 10, pp. 1889–1898, Oct. 2000. [Online]. Available: <https://www.sciencedirect.com/science/article/pii/S1388245700004211>
- [191] E. B. E. B. Hedman, "In-situ measurement of electrodermal activity during occupational therapy," Thesis, Massachusetts Institute of Technology, 2010, accepted: 2011-04-04T17:47:38Z. [Online]. Available: <https://dspace.mit.edu/handle/1721.1/62116>
- [192] I. R. Kleckner, R. M. Jones, O. Wilder-Smith, J. B. Wormwood, M. Akcakaya, K. S. Quigley, C. Lord, and M. S. Goodwin, "Simple, Transparent, and Flexible Automated Quality Assessment Procedures for Ambulatory Electrodermal Activity Data," *IEEE Transactions on Biomedical Engineering*, vol. 65, no. 7, pp. 1460–1467, Jul. 2018, conference Name: IEEE Transactions on Biomedical Engineering.
- [193] A. Garde, W. Karlen, J. M. Ansermino, and G. A. Dumont, "Estimating Respiratory and Heart Rates from the Correntropy Spectral Density of the Photoplethysmogram," *PLOS ONE*, vol. 9, no. 1, p. e86427, Jan. 2014, publisher: Public Library of Science. [Online]. Available: <https://journals.plos.org/plosone/article?id=10.1371/journal.pone.0086427>
- [194] H. Ugnell and P. Öberg, "The time-variable photoplethysmographic signal; dependence of the heart synchronous signal on wavelength and sample volume," *Medical Engineering & Physics*, vol. 17, no. 8, pp. 571–578, Dec. 1995. [Online]. Available: <https://www.sciencedirect.com/science/article/pii/135045339500008B>
- [195] W. Schneider and J. Chein, "Controlled & automatic processing: behavior, theory, and biological mechanisms," *Cognitive Science*, vol. 27, pp. 525–559, May 2003.
- [196] J. C. Ksander, S. M. Kark, and C. R. Madan, "Breathe Easy EDA: A MATLAB toolbox for psychophysiology data management, cleaning, and analysis," F1000Research, Tech. Rep. 7:216, Dec. 2018, type: article. [Online]. Available: <https://f1000research.com/articles/7-216>
- [197] M. J. Mathie, A. C. F. Coster, N. H. Lovell, and B. G. Celler, "Detection of daily physical activities using a triaxial accelerometer," *Medical & Biological Engineering & Computing*, vol. 41, no. 3, pp. 296–301, May 2003. [Online]. Available: <http://link.springer.com/10.1007/BF02348434>
- [198] M. Ciman, M. Donini, O. Gaggi, and F. Aiolfi, "Stairstep recognition and counting in a serious Game for increasing users' physical activity," *Personal and Ubiquitous Computing*, vol. 20, no. 6, pp. 1015–1033, Nov. 2016. [Online]. Available: <http://link.springer.com/10.1007/s00779-016-0968-y>
- [199] H. Cho and S. M. Yoon, "Divide and Conquer-Based 1D CNN Human Activity Recognition Using Test Data Sharpening," *Sensors*, vol. 18, no. 4, p. 1055, Apr. 2018, number: 4 Publisher: Multidisciplinary Digital Publishing Institute. [Online]. Available: <https://www.mdpi.com/1424-8220/18/4/1055>
- [200] P. Zhang, J. Chang, B. Qu, and Q. Zhao, "Denoising and Trend Terms Elimination Algorithm of Accelerometer Signals," *Mathematical Problems in Engineering*, vol. 2016, pp. 1–9, 2016. [Online]. Available: <http://www.hindawi.com/journals/mpe/2016/2759092/>
- [201] Z. Zhang, L. Ji, Z. Huang, and J. Wu, "Multi-model adaptation for thigh movement estimation using accelerometers," *IET Signal Processing*, vol. 5, no. 8, p. 709, 2011. [Online]. Available: <https://digital-library.theiet.org/content/journals/10.1049/iet-spr.2010.0146>
- [202] C. Kownacki, "Optimization approach to adapt Kalman filters for the real-time application of accelerometer and gyroscope signals' filtering," *Digital Signal Processing*, vol. 21, no. 1, pp. 131–140, Jan. 2011. [Online]. Available: <https://linkinghub.elsevier.com/retrieve/pii/S1051200410001843>

- [203] J. He, M. Zhou, X. Wang, and Y. Han, "Application of Kalman filter and k-NN classifier in wearable fall detection device," in *2017 IEEE SmartWorld, Ubiquitous Intelligence & Computing, Advanced & Trusted Computed, Scalable Computing & Communications, Cloud & Big Data Computing, Internet of People and Smart City Innovation (SmartWorld/SCALCOM/UIC/ATC/CBDCom/IOP/SCI)*. San Francisco, CA: IEEE, Aug. 2017, pp. 1–7. [Online]. Available: <https://ieeexplore.ieee.org/document/8397482/>
- [204] T. Pulecchi, A. Manes, M. Lisignoli, and M. Giglio, "Digital filtering of acceleration data acquired during the intervention of a lift safety gears," *Measurement*, vol. 43, no. 4, pp. 455–468, May 2010. [Online]. Available: <https://linkinghub.elsevier.com/retrieve/pii/S0263224109002498>
- [205] R. Abbasi-Kesbi and A. Nikfarjam, "Denoising MEMS accelerometer sensors based on L2-norm total variation algorithm," *Electronics Letters*, vol. 53, no. 5, pp. 322–324, Mar. 2017. [Online]. Available: <https://onlinelibrary.wiley.com/doi/10.1049/el.2016.3811>
- [206] E. Ioana-Raluca, A. Felix-Constantin, O. Radu, R. Constantin, and G. Teodor Lucian, "Inertial Sensor Signals Denoising with Wavelet Transform," *INCAS BULLETIN*, vol. 7, no. 1, pp. 57–64, Mar. 2015. [Online]. Available: [http://bulletin.incas.ro/files/edu\\_all\\_vol\\_7\\_iss\\_1.pdf](http://bulletin.incas.ro/files/edu_all_vol_7_iss_1.pdf)
- [207] Y. Shi, J. Zhang, J. Jiao, R. Zhao, and H. Cao, "Calibration Analysis of High-G MEMS Accelerometer Sensor Based on Wavelet and Wavelet Packet Denoising," *Sensors*, vol. 21, no. 4, p. 1231, Feb. 2021. [Online]. Available: <https://www.mdpi.com/1424-8220/21/4/1231>
- [208] I. Selesnick, "Total variation denoising (an MM algorithm)," 2012. [Online]. Available: [https://www.semanticscholar.org/paper/Total-variation-denoising-\(an-MM-algorithm\)-Selesnick/5e80ff176bfae173ddc5788775fde6cbdac23bd6](https://www.semanticscholar.org/paper/Total-variation-denoising-(an-MM-algorithm)-Selesnick/5e80ff176bfae173ddc5788775fde6cbdac23bd6)
- [209] F. Gu, K. Khoshelham, S. Valaee, J. Shang, and R. Zhang, "Locomotion Activity Recognition Using Stacked Denoising Autoencoders," *IEEE Internet of Things Journal*, vol. 5, no. 3, pp. 2085–2093, Jun. 2018, conference Name: IEEE Internet of Things Journal.
- [210] Q. Wang, L. Ye, H. Luo, A. Men, F. Zhao, and Y. Huang, "Pedestrian Stride-Length Estimation Based on LSTM and Denoising Autoencoders," *Sensors*, vol. 19, no. 4, p. 840, Feb. 2019. [Online]. Available: <http://www.mdpi.com/1424-8220/19/4/840>
- [211] X. Gao, H. Luo, Q. Wang, F. Zhao, L. Ye, and Y. Zhang, "A Human Activity Recognition Algorithm Based on Stacking Denoising Autoencoder and LightGBM," *Sensors*, vol. 19, no. 4, p. 947, Jan. 2019, number: 4 Publisher: Multidisciplinary Digital Publishing Institute. [Online]. Available: <https://www.mdpi.com/1424-8220/19/4/947>
- [212] Q. Ni, Z. Fan, L. Zhang, C. D. Nugent, I. Cleland, Y. Zhang, and N. Zhou, "Leveraging Wearable Sensors for Human Daily Activity Recognition with Stacked Denoising Autoencoders," *Sensors*, vol. 20, no. 18, p. 5114, Jan. 2020, number: 18 Publisher: Multidisciplinary Digital Publishing Institute. [Online]. Available: <https://www.mdpi.com/1424-8220/20/18/5114>
- [213] M. H. Mohd Noor, "Feature learning using convolutional denoising autoencoder for activity recognition," *Neural Computing and Applications*, vol. 33, no. 17, pp. 10 909–10 922, Sep. 2021. [Online]. Available: <https://link.springer.com/10.1007/s00521-020-05638-4>
- [214] S. Mohammed and I. Tashev, "Unsupervised deep representation learning to remove motion artifacts in free-mode body sensor networks," in *2017 IEEE 14th International Conference on Wearable and Implantable Body Sensor Networks (BSN)*, May 2017, pp. 183–188, iSSN: 2376-8894.
- [215] Y. Liu, S. Sivathamboo, P. Goodin, P. Bonnington, P. Kwan, L. Kuhlmann, T. O'Brien, P. Perucca, Z. Ge, and Assoc Comp Machinery, "Epileptic Seizure Detection Using Convolutional Neural Network: A Multi-Biosignal study," 2020.
- [216] "E4 wristband." [Online]. Available: <https://www.empatica.com/research/e4>
- [217] R. W. Schafer, "On the frequency-domain properties of Savitzky-Golay filters," in *2011 Digital Signal Processing and Signal Processing Education Meeting (DSP/SPE)*, Jan. 2011, pp. 54–59.
- [218] D. Castells-Rufas and J. Carrabina, "Simple real-time QRS detector with the MaMeMi filter," *Biomedical Signal Processing and Control*, vol. 21, pp. 137–145, Aug. 2015. [Online]. Available: <https://www.sciencedirect.com/science/article/pii/S1746809415001032>
- [219] N. Tulyakova and O. Trofymchuk, "Real-time filtering adaptive algorithms for non-stationary noise in electrocardiograms," *Biomedical Signal Processing and Control*, vol. 72, p. 103308, Feb. 2022. [Online]. Available: <https://www.sciencedirect.com/science/article/pii/S1746809421009058>

## Annex 1: Summary Tables with the Technical Details of Denosing Methods

**Table 2.** Summary of FIR and IIR frequency-domain filters to clean ECG.

Cleaning	Type	Cutoff	Frequency Response	Order	Performance	Q	Ref
BW, MA	Highpass	0.5 Hz	FIR	1188	SNRI = 15.1–17.6 dB MSE = 0.0072	C†	[111]
		0.5 Hz	IIR zero-phase	2	SNRI = 15.1–18.1 dB MSE = 0.0064		
BW, PLI	Lowpass	35 Hz	IIR Elliptic	15	SNRI = 201.44 dB	C†	[95]
	Highpass	0.05 Hz	IIR Elliptic	7			
	Lowpass	35 Hz	FIR Equiripple	91	SNRI = 158.66 dB		
	Highpass	0.05 Hz	IIR Elliptic	7			
General	Bandpass	[2.5, 22.5] Hz	IIR Butterworth	1	Good quality	W	[114]
BW, PLI	Bandpass	n.d.	IIR Elliptic	6	Fall Acc = 98.44%	NC	[115]
BW	Highpass	0.5 Hz	IIR Butterworth	2	CC = 0.9851	C	[112]
PLI	Notch	⌚ by FFT	n.d.	n.d.	SNR = 70.9 dB	NC	[122]
		[49, 51] Hz	Butterworth	4	SNR = 69.4 dB		
BW, HFN	Bandpass	[16, 31] Hz	n.d.	n.d.	R-Acc = 99.67%	C†	[116]
HFN	Lowpass	n.d.	Butterworth	n.d.	R-Sen = 99.2%	C†	[106]
BW, EMG, EN	Lowpass + Highpass	[3, 13] Hz	IIR	2 + 1	SNR = 16.67 dB MSE = 0.7%	C‡	[100]
		–	FIR Savitzky Golay	3	SNR = 16.77 dB MSE = 0.9%		
BW	Highpass	0.05 Hz	IIR Butterworth	5	SNRI = 290 dB	C†	[104]
PLI	Lowpass	40 Hz	IIR Inverse Chebyshev	7			
BW, MA	Bandpass	[0.4, 10] Hz	IIR Butterworth	2	HR MAE = 0.67 bpm	W	[75]
White	Lowpass <sup>1</sup>	–	FIR Savitzky Golay	3	SNRI = 8.80 dB	S	[109]
				⌚	SNRI = 13.64 dB		
PLI	Notch	50 Hz	n.d.	n.d.	V-fib and		
BW	2 Highpass	1.4 Hz	IIR	1	Tachycardia	C	[101]
EMG	Lowpass	30 Hz	IIR Butterworth	2	Sen = 95.93%		
PLI	Notch	60 Hz	Bi-quad	2	Energy savings estimated about 35.5%	NC	[102]
BW	Highpass	0.67 Hz	n.d.	n.d.			
EMG	Lowpass	100 Hz	n.d.	n.d.			
Coarse BW	Highpass	⌚ in [0, 1] Hz	IIR zero-phase	2	SNRI = 19 dB	S	[130]
Fine BW	Linear interpolation to bring baseline to zero.			–			

**Legend:** † MIT-BIH Arrhythmia Dataset (not necessarily the only one). ‡ MIT-BIH Arrhythmia Dataset (for ECG) + MIT-BIH Noise Stress Test Dataset (for noises). ⌚ means dynamically computed. (1): Savitzky Golay smoothing filters act as lowpass filters [217]. n.d.: Not defined by the authors.

**Table 3.** Summary of window-based moving average, median, and interpolation filters to clean ECG.

Cleaning	Operation	Window	Action	Performance	Q	Ref
BW, MA	Average	1 s	Subtraction	SNRI = 14.9–15.8 dB MSE = 0.0108	C†	[111]
	Median	1 s	Subtraction	SNRI = 14.1–14.2 dB MSE = 0.0161		
BW PLI, EMG	Median	150 ms; 50% overlap	Subtraction	R-Sen = 99.54%	C†	[129]
	Cutting line	1 s; 50% overlap	Subtraction			
BW, EMG, EN	Bandpass <sup>1</sup> + Average	100 ms of Energy	–	R-Acc = 99.14%	C†	[119]
BW	2 Medians	400 ms + 2 s	Subtraction	CC = 0.9904	C	[112]
	Cubic Interpolation	PQ segments	Subtraction	CC = 0.9813		
BW	Median	200ms	Subtraction	n.d.	C	[107]
Outliers	Median	17 samples of RRI	–	A-fib Acc = 91–98%	C†	[110]
BW HFN	Average Squaring and Sum	5 samples 150ms	Subtraction –	R-peak TP = 99.5%	C†	[125]
BW Strange shape	Median	≈ 10 s	Subtraction	R RMSE = $7.4 \times 10^{-8}$ s R RMSE = $1.0 \times 10^{-8}$ s	S	[126]
BW	Average	≈ 500 ms	Subtraction	R-Sen = 99.66%	C†	[124]
BW, HFN	Average and amplitude of maximum and minimum	n.d.	Subtraction	R-Sen = 99.43%; Error = 0.88%	C†	[218]
BW	Cubic Interpolation	PR segments	Subtraction	n.d.	C	[131]

**Legend:** † MIT-BIH Arrhythmia Dataset (not necessarily the only one). [1]: Bandpass [15, 25] Hz suppress P and T waves (only QRS wanted). n.d.: Not defined by the authors.

**Table 4.** Summary of wavelet-based filters to clean ECG.

Cleaning	Transform (Wavelet)	Levels	Action	Performance	Q	Ref
BW	DWT ( <i>db6</i> )	10	Eliminate D1, D2, and A10.	MSE = 0.4; CC = 0.94	C†	[132]
BW, PLI, HFN	DWT ( <i>db4</i> )	8	Eliminate D1, D2, and A8. Remaining Dx filtered by soft threshold.	R-Sen = 99,83%	C†	[145]
HFN	DWT (Quadratic)	5	Eliminate D1 and D2.	R-Sen = 99,80%	C†	[147]
BW	DWT ( <i>db4</i> )	7	Eliminate A7.	Good quality results	C	[113]
BW	[1] + DWT ( <i>db2</i> )	2	Select only HR sub-band.	RMSE = 0.78	NC	[121]
BW, EMG, EN	DWT ( <i>db4</i> )	5	Eliminate D1, D2 and D3.	SNR = 17.65 dB; MSE = 0.4%	C‡	[100]
	FWT	5	Keep only 5 <sup>th</sup> level.	SNR = 24.81 dB; MSE = 0.099%		
Sinusoidal BW	DWT ( <i>db3</i> or <i>sym3</i> )		Eliminate A8 to A11.	MSE = 0.0044		
Step-trend BW	DWT ( <i>meyer</i> )	11	Eliminate A8 to A11.	MSE = 0.0274	C	[142]
Spikes BW	DWT ( <i>meyer</i> )		Eliminate A1,A2,A10,A11.	MSE = 0.0044		
BW, MA, PLI	DWT ( <i>symlet4</i> )	4	Eliminate D1 and D2.	Stress Acc = 96.67%	W	[146]
BW	DWT ( <i>db8</i> )	9	Eliminate all Ax of LF.	CC = 0.9928	C	[112]
	DWT ( <i>VH</i> )	9	IIR Highpass 0.5 Hz all Ax.	CC = 0.9672		
BW HFN	DWT ( <i>db6</i> )	8	Eliminate A8 and D8. Threshold D1 and D2.	Good quality results	C†	[144]
	DWT ( <i>sym2</i> )			SNR = 1.2–1.7 dB; MSE = 1.8–3.0 × 10 <sup>-5</sup>		
BW, HFN	DWT ( <i>db6</i> )	8	Eliminate D1 and D2 (HFN) and A8 (BW).	SNR = 0.9–1.4 dB; MSE = 1.9–2.2 × 10 <sup>-5</sup>	C†	[141]
	DWT ( <i>db4</i> )			SNR = 0.3–0.4 dB; MSE = 2.2–4.0 × 10 <sup>-5</sup>		
BW, MA	DWT ( <i>db8</i> )	9	Eliminate D9.	SNRI = 14.1–15.2 dB MSE = 0.0125	C†	[111]
PLI				SNR = 23.29 dB; MSE = 0.0015		
EMG	DWT ( <i>db6</i> )	3	Eliminate D1 and D2. Adaptive dual threshold on the remaining.	SNR = 15.59 dB; MSE = 0.0069	C†	[143]
White				SNRI = 9.17 dB		
PLI				SNRI ≈ 14.2–7.1 dB; MSE = 0.01–0		
EMG	[2] + DWT ( <i>sym7</i> )	2	Soft threshold all Dx.	SNRI = 9.3–5.7 dB MSE = 0.02–0.0005	C†	[154]
White				SNRI ≈ 10.3–5.9 dB; MSE = 0.011–0		
White	DWT ( <i>db8</i> )	10	Various thresholds.	RMSE ≈ 0.105	S	[140]
	DWT ( <i>sym4</i> )			RMSE ≈ 0.145		

**Legend:** Ax: Approximation coefficients of level x. Dx: Detail coefficients of level x. VH: Vaidyanathan-Hoang wavelet. † MIT-BIH Arrhythmia Dataset (not necessarily the only one). ‡ MIT-BIH Arrhythmia Dataset (for ECG) + MIT-BIH Noise Stress Test Dataset (for noises). [1]: Bandpass [1, 12] Hz IIR 3<sup>rd</sup> order. [2]: EMD gets IMFs 1, 2 and 3.

**Table 5.** Summary of adaptive algorithms to clean ECG.

Cleaning	Preprocessing	Algorithm	Action	Performance	Q	Ref	
EMG	PCA	NLMS	-	HR Acc = 98.5–99.3% (0.08 bpm bias)	W	[158]	
BW, MA	-	RLS	-	SNRI = 20.0–27.4 dB MSE = 0.0042	C†	[111]	
	Lowpass 40 Hz + Normalisation	RLS	Subtraction	Good quality	W		
White EMG	Moving average in flat segments	Stenlund-Gustafsson	-	SNRI = 2.5–13.2 dB SNRI = 10–14 dB	C†	[219]	
PLI	-	RLS or EKF	-	EKF outperforms RLS when PLI drifts	C† / NC	[156]	
BW, EMG, EN	-	LMS	Subtraction	MSE = 0.004, 0.002, 0.014	W (left arm)	[53]	
	-	Extended kernel RLS		MSE = 1.25, 1.75, 12.2			
	-	LMS	Subtraction	MSE = 0.004, 0.002, 0.016	W (chest)		
	-	Extended kernel RLS		MSE = 1.24, 1.75, 12.1			
PLI	-	Preconditioned Regularized LMS with dynamic step-size	-	Deviation norm = 2.13	C†	[98]	
	-	NLMS	-	Deviation norm = 2.80			
	-	LMS	-	Deviation norm = 3.00			
BW, MA	-	n.d.; Uses ACC as noise reference	-	Good quality	W	[160]	
White	Linear filter to remove BW	EKF	Subtraction	MSE = 0.003–0.023	C†	[159]	
Dynamic PLI	Bandpass [45, 55] Hz	LMS	Subtraction	SNRI ≈ 28.5 dB	C / S	[157]	
		RLS	Subtraction	SNRI ≈ 23.0 dB			

**Legend:** † MIT-BIH Arrhythmia Dataset (not necessarily the only one).

**Table 6.** Summary of machine learning models to clean ECG.

Cleaning	Preprocessing	Model	Output	Performance	Q	Ref
Colored noise	STFT	AE Convolutional	Denoised	SNRI = 6.5–17.4 dB SNRI = 7.4 dB	W C†	[164]
	–	AE 6 Conv, 7 DeConv	Denoised	SNRI = 10.5–15.5 dB RMSE = 0.044–0.063		
BW, EMG, EN	–	AE 6 Conv, 5 DeConv, 2 FC	Denoised	SNRI = 8.4–14.1 dB RMSE = 0.056–0.072	C‡	[162]
	–	NN 13 FC	Denoised	SNRI = 5.6–11.8 dB RMSE = 0.077–0.094		
EMG	Prepare [ECG, ACC]	AE 2 Conv, 3 DeConv	Denoised	SNRI = 18.3–22.5 dB	[C†, W]	[138]
BW, EMG, EN	Normalisation	AE 3 layers, 252 nodes	Denoised	MSE = 0.0029	C‡	[163]
PLI	Lowpass 35 Hz	–	–			
BW	Subtraction of Median filters (200 ms, 600 ms)	–	–	Arrhythmia Acc = 99.8%	C† / W	[103]
Others	(above)	AE 1 Conv, 1 DeConv, 1 FC	Features			
BW				SNR = 18.8 dB RMSE = 0.051		
EMG	Normalisation	AE Convolutional	Denoised	SNR = 18.6–19.1 dB RMSE = 0.051	C‡	[139]
EN				SNR = 18.7–18.8 dB RMSE = 0.051		
General	STFT	CNN Three 2D-Conv, Two FC	Features	A-fib and Noise F1-score = 1.00	C	[167]
BW	Bandpass [0.1, 30] Hz, Wavelet	CNN 3 Conv, 1 FC	Denoised	SNR = 12.36 dB	C†	[123]

**Legend:** Conv: Convolutional layer(s). DeConv: Deconvolutional layer(s). FC: Fully-connected layer(s) † MIT-BIH Arrhythmia Dataset (not necessarily the only one). ‡ MIT-BIH Arrhythmia Dataset (for ECG) + MIT-BIH Noise Stress Test Dataset (for noises).

**Table 7.** Summary of SWT wavelet thresholding techniques to clean EDA.

Cleaning	Wavelet	Distribution	APA (dB)	SNRI (dB)	MSE	Site (Q)	Ref.
MA	<i>haar</i>	Gaussian	6.32; 5.28*	–	–54.42 <sup>n</sup> ; –3.09 <sup>*n</sup>	Wrist (W)	[180]
BW	<i>db4</i>	Gaussian	–	26.98	0.0004	Wrist (n.d.)	[182]
	<i>db14</i>		–	27.42	0.0004		
	<i>brior 3.5</i>		–	26.88	0.0004		
	<i>sym4</i>		–	27.27	0.0004		
MA	<i>haar</i>	Laplacian	5.71	–	–3.68 <sup>n</sup>	Hand, Foot (NC)	[177]
	<i>db3</i>		4.81	–	–3.52 <sup>n</sup>		
	<i>coiflet3</i>		4.77	–	–3.67 <sup>n</sup>		
MA, BW	<i>db1</i>	Laplacian	–	–	3.2	Wrist (W)	[183]
	<i>db3</i>		1.62*	–	1.8; –11.63 <sup>*n</sup>		
	<i>db5</i>		–	–	2.4		

<sup>n</sup> Normalized version, NMSE, expressed in dB; \* When tested by Shukla *et al.* in [177].

**Table 8.** Summary of ML and optimization techniques for motion artifact detection in EDA.

Categories of Features	Model	Performance	Site (Q)	Ref.
Amplitude, 1 <sup>st</sup> and 2 <sup>nd</sup> derivatives, Wavelet coefficients	SVM	<i>Acc</i> = 95.67%	Wrist (W)	[188]
Amplitude, 1 <sup>st</sup> and 2 <sup>nd</sup> derivatives, AR, Wavelet coefficients (DWT, <i>haar</i> ), VFCDM	RF	<i>Acc</i> = 83.40%	Finger (C)	[186]
	SVM	<i>Acc</i> = 83.85%		
Amplitude, 1 <sup>st</sup> and 2 <sup>nd</sup> derivatives, Wavelet coefficients (DWT, <i>haar</i> )	kNN (k=3)	<i>Acc</i> = 97.83%	Wrist (W)	[169]
	NB	<i>Acc</i> ≈ 95%		
	SVM	<i>Acc</i> ≈ 90%		
Amplitude, 1 <sup>st</sup> and 2 <sup>nd</sup> derivatives, Wavelet coefficients (DWT, <i>haar</i> )	LDA	<i>Acc</i> ≈ 88%	Wrist (W)	[187]
	RF	<i>AUC</i> = 0.937		
	Logistic	<i>AUC</i> = 0.935		
	kNN distance	<i>AUC</i> = 0.930		
	MLP	<i>AUC</i> = 0.928		
	IF	<i>AUC</i> = 0.900		
	1-class SVM	<i>AUC</i> = 0.900		
	SVM	<i>AUC</i> = 0.898		
	kNN	<i>AUC</i> = 0.870		
Waveform dictionaries	Curve-fitting	<i>Acc</i> = 66.67 – 96.30%	Wrist (W)	[170]

## **Annex 2: Draft Proposal for the Acquisition of Noisy Biosignals in Mobility**

### **Goal**

To acquire digital timeseries of electrocardiography (ECG), photoplethysmography (PPG), electrodermal activity (EDA), and accelerometer (ACC), from (a) subject(s) performing three activities: (i) Running, (ii) Walking, (iii) Shaking hands, and (iv) Lifting objects. These activities are intended to introduce severe noise and motion artifacts that are natural in daily life scenarios, which should be able to be characterized by the ACC timeseries. The purpose of these biosignals is to serve as training examples for deep learning models to denoise them.

### **Procedure Details**

One subject (the author) or multiple subjects may participate in the acquisition of these biosignals, depending on the research needs. The activities of running should be performed outdoors, the activities of walking should be performed outdoors and indoors, and the activities of lifting objects should be performed indoors. Multiple (estimative: 20—100) collections of 5—30 minutes should be performed for each activity. During acquisitions, two timeseries capturing ECG and EDA should be collected: one from a wearable format with dry electrodes, one with better contact with the skin using wet electrodes that minimize the electrode-skin impedance variations. This later timeseries can serve as comparison versions for the models to target the desired denoised timeseries.

### **Hardware**

The wearable chest band developed by Instituto de Telecomunicações (IT), that uses a Bitalino board, and the Empatica E4 wristband should be used. These instruments are available at IT.

### **Software**

The software developed for Sicientisst Sense should be used to receive the biosignals through Bluetooth protocol and to store them in a smartphone that can be carried in the pocket of the subject during any of the activities.

### **Data Privacy**

All data should be stored offline. If more subjects, besides the author, participate in the acquisitions, then a formal proposal should be sent to the IST Ethics Commission, and every participant should voluntarily sign an informed consent. This written informed consent should guarantee that all data should be stored anonymously, be used only for the expressed finality, not be shared with anyone, and be deleted upon request of each subject, accordingly with the latest GDPR regulations. In the future, there is also the possibility of sharing these data in a public database for other researchers to use, in which case the informed consent should be written accordingly.

### **Duration**

The acquisition sessions should last no longer than one month, but it will depend on the frequency of sessions and the research needs.